REPORT

ON

NATURAL PRECIPITATION WASHOUT OF SULFUR DIOXIDE

M. T. Dana, J. M. Hales and M. A. Wolf

TO

ENVIRONMENTAL PROTECTION AGENCY
DIVISION OF METEOROLOGY

BNW-389

February 1972

ATMOSPHERIC SCIENCES DEPARTMENT
BATTELLE-PACIFIC NORTHWEST LABORATORIES
RICHLAND, WASHINGTON 99352

NOTICE

This report was prepared as an account of work sponsored by the United States Government. Neither the United States nor the United States Atomic Energy Commission, nor any of their employees, makes any warranty, express or implied, or assumes any legal liability or responsibility for the accuracy, completeness or usefulness of any information, apparatus, product, or process disclosed, or represents that its use would not infringe privately-owned rights.

PACIFIC NORTHWEST LABORATORY
operated by
BATTELLE
for the
U.S. ATOMIC ENERGY COMMISSION
Under Contract AT(45-1)-1830

REPORT

ON

NATURAL PRECIPITATION WASHOUT OF SULFUR DIOXIDE

M. T. Dana, J. M. Hales and M. A. Wolf

TO

ENVIRONMENTAL PROTECTION AGENCY
DIVISION OF METEOROLOGY

BNW-389

February 1972

ATMOSPHERIC SCIENCES DEPARTMENT
BATTELLE-PACIFIC NORTHWEST LABORATORIES
RICHLAND, WASHINGTON 99352

FOREWORD

This research was conducted by scientific and technical personnel of the Atmospheric Sciences Department of Battelle, Pacific Northwest Laboratories under related services agreement BNW-389 with the Richland Operations Office, U. S. Atomic Energy Commission for the Environmental Protection Agency. The Project Officer was Mr. Francis Pooler, Jr., Chief, Field Investigations Branch, Division of Meteorology, Raleigh, North Carolina.

The principal investigators were Mr. M. T. Dana, Dr. J. M. Hales and Mr. M. A. Wolf. Mr. D. W. Glover was responsible for the design and fabrication of the field generation and sampling equipment. Other personnel of Battelle, Pacific Northwest Laboratories who contributed significantly to the investigations were:

O. B. Abbey	M. C. Miller
A. G. Dunbar	J. W. Sloot
V. T. Henderson	S. L. Sutter
F. D. Lloyd	R. E. Wheeler

The authors especially want to acknowledge the contributions of the following persons to the success of the field investigation:

Mr. Ronald Pretti, Director, Washington State Aeronautics Commission, Seattle, Washington

Mr. Clarence Davis, Manager, Ouillayute State Landing Field, Forks, Washington

Mr. Donald Carte, Meteorologist-In-Charge, National Weather Service, Forks, Washington

TABLE OF CONTENTS

NATURAL PRECIPITATION WASHOUT OF SULFUR DIOXIDE

		Page
FOREWORD		i
LIST OF FIGURES		v
LIST OF TABLES		ix
NOMENCLATURE		xi
SUMMARY		xiii
CHAPTER I	INTRODUCTION	1
CHAPTER II	WASHOUT MODELING	3
CHAPTER III	SO_2 SOLUBILITY MEASUREMENT	23
CHAPTER IV	FIELD EXPERIMENTS IN WASHOUT	33
CHAPTER V	ANALYSIS OF RESULTS	55
CHAPTER VI	ISOLATED DROP EXPERIMENT	83
CHAPTER VII	EVALUATION AND CONCLUSIONS	89
REFERENCES		95
APPENDIX A	TABULATIONS OF MEASURED SO_2 CONCENTRATIONS IN PRECIPITATION	99
APPENDIX B	RESULTS OF PEAK-TO-MEAN ANALYSIS	111
APPENDIX C	COMPARISONS OF MEASURED WASHOUT CONCENTRATIONS WITH PREDICTIONS BY THE NONLINEAR, NONFEEDBACK MODEL	129

LIST OF FIGURES

FIGURE	TITLE	PAGE
2.1	Schematic of Volume Element in Space	5
2.2	Elements of Washout Rate Calculation	8
2.3	Simplified Schematic of Computer Program -- Nonlinear, Nonfeedback Model	15
3.1	Solubility Measurement Apparatus	26
3.2	Solubility Cell	27
3.3	Solubility of Dilute SO_2 in Water at 25.1 °C	29
4.1	Location of Field Experiment Site	34
4.2	Quillayute Grid System	36
4.3	Special Grid System	37
4.4	Composite of Field Study Equipment	40
4.5	Comparison of Observed and Calculated SO_2 Concentrations in Air	53
5.1	Comparison of Predicted and Measured Washout Coefficients as a Function of Rainfall Rate	58
5.2	Comparison of Observed Washout Rates with Those Predicted from Washout-Coefficient Analysis	59
5.3	Solubility Relationship for SO_2 in Water at 10°C, pH = 5.5	62
5.4	Time-Averaged SO_2 Concentrations in Rain Based Upon Equilibrium with Ground-Level Plume Concentrations -- Mean Plume on 15-Second Incremental Analyses	64
5.5	Time-Averaged SO_2 Concentrations in Rain Based on Equilibrium with Ground-Level Plume Concentrations -- Mean Plume and Peak-to-Mean Analyses	66
5.6	Comparison of Observed Washout Rates with Those Predicted from Peak-to-Mean Analyses	67
5.7	Comparison of Observed Washout Rates with Those Predicted on Basis of Equilibrium with Average Plume Concentrations at Ground Level	68
5.8	Comparison of Observed Washout Rates with Those Predicted by Nonlinear, Nonfeedback Model	73
5.9	Comparison of Observed Washout Rates with Those Predicted by Linear, Nonfeedback Model	74

FIGURE	TITLE	PAGE
5.10	Predictions by Nonlinear, Nonfeedback Model for Time-Average and 15-Second Incremental Analyses	76
5.11	Computed Concentrations in Drops as a Function of Vertical Position - Run 4WB, Gas-Phase Limited	78
5.12	Computed Ground-Level SO_2 Concentrations in Rain as a Function of Drop Size -- Run 4WB, Gas-Phase Limited	80
6.1	Schematic of Suspended-Drop Apparatus	88
7.1	Suggested Research Program	90
B.1	Comparison of Observed Values with Those Predicted by the Peak-to-Mean Analysis Run 1E	113
B.2	Comparison of Observed Values with Those Predicted by the Peak-to-Mean Analysis Run 1W	114
B.3	Comparison of Observed Values with Those Predicted by the Peak-to-Mean Analysis Run 2E	115
B.4	Comparison of Observed Values with Those Predicted by the Peak-to-Mean Analysis Run 2W	116
B.5	Comparison of Observed Values with Those Predicted by the Peak-to-Mean Analysis Run 3	117
B.6	Comparison of Observed Values with Those Predicted by the Peak-to-Mean Analysis Run 4E	118
B.7	Comparison of Observed Values with Those Predicted by the Peak-to-Mean Analysis Run 4W	119
B.8	Comparison of Observed Values with Those Predicted by the Peak-to-Mean Analysis Run 5E	120
B.9	Comparison of Observed Values with Those Predicted by the Peak-to-Mean Analysis Run 5W	121
B.10	Comparison of Observed Values with Those Predicted by the Peak-to-Mean Analysis Run 6W	122
B.11	Comparison of Observed Values with Those Predicted by the Peak-to-Mean Analysis Run 7E	123
B.12	Comparison of Observed Values with Those Predicted by the Peak-to-Mean Analysis Run 7W	124
B.13	Comparison of Observed Values with Those Predicted by the Peak-to-Mean Analysis Run 8E	125
B.14	Comparison of Observed Values with Those Predicted by the Peak-to-Mean Analysis Run 8W	126
B.15	Comparison of Observed Values with Those Predicted by the Peak-to-Mean Analysis Run 9E	127

FIGURE	TITLE	PAGE
B.16	Comparison of Observed Values with Those Predicted by the Peak-to-Mean Analysis Run 9W	128
C.1	Predictions of Nonlinear Model for Run 1E	131
C.2	Predictions of Nonlinear Model for Run 1W	132
C.3	Predictions of Nonlinear Model for Run 2E	133
C.4	Predictions of Nonlinear Model for Run 2W	134
C.5	Predictions of Nonlinear Model for Run 3E	135
C.6	Predictions of Nonlinear Model for Run 3W	136
C.7	Predictions of Nonlinear Model for Run 4E	137
C.8	Predictions of Nonlinear Model for Run 4W	138
C.9	Predictions of Nonlinear Model for Run 5E	139
C.10	Predictions of Nonlinear Model for Run 5W	140
C.11	Predictions of Nonlinear Model for Run 6E	141
C.12	Predictions of Nonlinear Model for Run 6W	142
C.13	Predictions of Nonlinear Model for Run 7E	143
C.14	Predictions of Nonlinear Model for Run 7W	144
C.15	Predictions of Nonlinear Model for Run 8E	145
C.16	Predictions of Nonlinear Model for Run 8W	146
C.17	Predictions of Nonlinear Model for Run 9E	147
C.18	Predictions of Nonlinear Model for Run 9W	148

LIST OF TABLES

TABLE	TITLE	PAGE
3.1	Solubility Parameters from Work of Johnstone and Leppla	25
3.2	Experimental Measurements of Solubility of SO_2 in Water Solution	30
4.1	Run Summary	44
4.2	Raindrop Size Frequency Distributions	46
4.3	Rainfall Characteristics Summary	47
4.4	SO_2 Washout Summary	49
4.5	Data Summary	52
5.1	Input to Nonlinear, Nonfeedback Model	71
6.1	Isolated Drop Experiments	86
A.1	Precipitation Sample SO_2 Concentration Run 1	101
A.2	Precipitation Sample SO_2 Concentration Run 2	102
A.3	Precipitation Sample SO_2 Concentration Run 3	103
A.4	Precipitation Sample SO_2 Concentration Run 4	104
A.5	Precipitation Sample SO_2 Concentration Run 5	105
A.6	Precipitation Sample SO_2 Concentration Run 6	106
A.7	Precipitation Sample SO_2 Concentration Run 7	107
A.8	Precipitation Sample SO_2 Concentration Run 8	108
A.9	Precipitation Sample SO_2 Concentration Run 9	109

NOMENCLATURE

a	Raindrop radius, ℓ
A	Bucket area, ℓ^2
c	Liquid-phase concentration, moles/ℓ^3
D	Diffusion coefficient, ℓ^2/t
f	Raindrop probability-density function
F	Fractional depletion of plume
H	Henry's-law constant for undissociated SO_2, ℓ^3/mole
h'	Functional form for partition coefficient
H'	Partition coefficient, ℓ^3/mole
J	Rainfall rate, ℓ/t
k_y	Liquid-phase mass-transfer coefficient, moles/$\ell^2 t$
k_y	Gas-phase mass-transfer coefficient, moles/$\ell^2 t$
K_y	Overall mass-transfer coefficient, moles/$\ell^2 t$
M	Downwind washout rate, moles/ℓt
m_i	Moles of SO_2 collected in individual sampler
m_o	Moles of SO_2 released during sampling period
N_A	Flux of SO_2 from drop surface, moles/$\ell^2 t$
N_o	Total raindrops in a unit volume element, drops/ℓ^3
Q	SO_2 release rate, moles/t or ℓ^3/t
r	Radius of collector, ℓ; also reaction rate, moles/$\ell^3 t$
t	Collection time, t
$\bar{u}$	Wind velocity at stack height, ℓ/t
$\bar{v}_A$	Velocity vector of pollutant in gas phase, ℓ/t
$\bar{v}_t$	Velocity vector of raindrop, ℓ/t

w	Volumetric washout rate, moles/ℓ^3t
x	Downplume distance, ℓ; also liquid-phase mole fraction
y	Crossplume distance, ℓ; also gas-phase mole fraction
z	Vertical distance, ℓ
z_o	Datum height, ℓ; taken to be infinite in this report
Δ	Difference operator
ΔY	Spacing between collectors, ℓ
Λ	Washout coefficient, 1/t
ρ	Density, m/ℓ^3
σ_i	Standard deviation in the i direction, units of i

SUBSCRIPTS

A	Pollutant A
b	Bulk
e	Equilibrium
x	Average value in total liquid phase
x_b	Average value in drop
y	Average value in gas phase

SUMMARY

This report presents recent results in the continuing investigation of SO_2 washout by precipitation from plumes of large, coal-fired power plants. The research consisted of three phases: a washout modeling effort, a laboratory investigation of solubility and mass-transfer behavior in the SO_2/water system, and an experimental field program.

The modeling effort resulted in the creation of two washout models. The first of these is based on linear theory and provides a relationship that can be used for hand-calculated estimates of washout provided that the implicit assumption of vertical rainfall is not violated significantly. The second model can account for nonlinear behavior and is not restricted to vertical rainfall, but necessitates computer calculation to predict washout values.

The general washout models reduce asymptotically two limiting cases. One of these describes washout totally in terms of rate processes (irreversible washout of the classical washout-coefficient approach); the other describes washout totally in terms of equilibrium phenomena (equilibrium washout). An additional derivation from the theory of reversible washout is the criterion for the approach of real systems to the limiting case of equilibrium washout. This criterion suggests that under the conditions of the recent experiments true equilibrium washout does not occur.

Both of the general washout models utilize the bivariate-normal plume equation for the description of airborne SO_2 concentration. Input data for the washout models are derived from field measurements. The extent to which these measurements are representative of the pertinent factors determines to a large degree the validity of the results.

The computer algorithm for the general nonlinear model computes the partition coefficient for SO_2 between air and water in accordance with

a previously derived solubility equation. Solubility experiments conducted in the laboratory show that the behavior of the SO_2/water system at low concentrations is predicted reasonably well by that solubility equation.

The field-study program was conducted on the Olympic Peninsula of Washington state to examine the washout of SO_2 in an unpolluted atmosphere. SO_2 from commercial gas cylinders was released at various heights on a 30.5 m tower during rainfall. Precipitation samples were collected on downwind arcs at distances to 122 m and analyzed for their SO_2 content. Support data were collected during the experiments to relate the washout to atmospheric parameters. Of the 20 experiments conducted, useful data were obtained from 16. The observed SO_2 concentrations and the derived washout rates, which are the arcwise integrated quantities of SO_2 deposited per unit time and unit distance, were compared with the washout models and with their asymptotic limits.

Irreversible washout was shown to be untenable, as was suggested earlier in the report of the SO_2 washout investigation conducted at the Keystone Generating Station. Although the asymptotic expressions of the general models do not necessarily correspond to extrema in washout rates, this limiting case does provide a virtual upper limit to washout rates observed at Quillayute. On the other hand, observed washout rates were found to fall close to those predicted on the basis of equilibrium behavior, noted exceptions being data from experiments conducted at short distances downwind from the source.

Predictions from the nonlimiting washout models were found to agree well with experiments in a majority of cases, including those corresponding to short downwind distances. In addition the models predict that the observed proximity to equilibrium of SO_2 in ground-level rain results more from a decrease of plume concentration with height at ground level than from fast mass-transfer responsiveness of the rain. This, therefore, resolves the apparent conflict between observation and the prediction of the equilibrium-washout criterion. The general-model ability to predict washout behavior at Quillayute suggests that these models will be useful in future analyses of SO_2

washout from power-plant plumes.

The possibility that the observed proximity to equilibrium behavior is caused by rapid absorption and desorption of SO_2 by rain on the sampler collection surfaces was considered. Although the present results indicate that this effect is minimal, additional experimentation will be required to resolve this question completely.

CHAPTER I

INTRODUCTION

Research described in this report was undertaken to elucidate several important aspects of SO_2 washout which were identified in a previous study.[1] The results of that study, conducted at the Keystone Generating Station in western Pennsylvania, indicated very low washout of SO_2 from the power plant plume. The nature of the source, however, raised doubt as to the amount of sulfur present in the plume as SO_2. An observed increase in sulfate washout beneath the plume suggested that chemical conversion of SO_2 had occurred. However, the high level of contamination in the atmosphere in the vicinity of the Keystone Station and the high background of sulfur dioxide from numerous sources in the area made the results inconclusive.

A concurrent development of gaseous washout theory indicated that reversibility of the process of SO_2 absorption in rain should be responsible for the low washout rates observed. It was recognized that certain properties of the SO_2, the precipitation and the atmosphere were necessary considerations in the washout determination. The need for detailed knowledge of their interactions led to the present work, which consists of model development, laboratory experiments and controlled field experiments.

This report documents the work performed during the latter half of FY-1971 and outlines the continuing effort to provide a general means for the calculation of sulfur dioxide washout. Chapter II describes the results of the washout-modeling effort. Solubility measurements, which are required to facilitate use of the models presented in Chapter II are described in Chapter III. Chapter IV describes the controlled field experiments which were conducted to clarify the washout behavior of SO_2. Data reduction techniques are discussed and the data are summarized.

The three phases of the research described in Chapters II through IV are brought together in Chapter V which is an analysis of the data resulting from the field experiments relative to irreversible and reversible theories. A remaining area of uncertainty in the washout model, SO_2 mass transfer rates, is discussed in Chapter VI. Chapter VII examines additional problems in the formulation of a general SO_2 washout model applicable to power plant plumes.

Dimensional units are expressed in the metric system throughout this report. Insofar as practicable the centimeter-gram-second-degree Kelvin system is used to provide a consistent set of units to facilitate the use of equations and computer routines described herein.

CHAPTER II

WASHOUT MODELING

The previous report[1] on SO_2 washout dealt extensively with microphysical aspects of gas-raindrop interactions, including the effects of mixing, solubility, and chemical reaction on washout by drops and ensembles of drops falling through pollutant clouds of arbitrary distribution. The present analysis will emphasize macrophysical aspects, combining microphysical factors into models to compute total washout from atmospheric plumes under stated conditions of rainfall, mixing, and pollutant release. Although rather general in nature, this analysis is devoted primarily to an examination of the March-April 1971 Quillayute field results, which will be described in a later chapter.

The present effort is initiated by a formulation of the general material balance relationships of importance to the overall scavenging process. Establishing these relationships is an essential first step in defining washout in the context of other, competing processes for transport and removal in the atmosphere. These relationships are important also in providing a standard of assessment for all scavenging models, which are necessarily based upon these more general equations of conservation.

Subsequent effort has been devoted to the creation of a progression of washout models in order of increasing sophistication. The first two of these models will be described in this chapter.

MATERIAL BALANCE RELATIONSHIPS

Pollutants may be transported through and removed from the atmosphere by a number of competing mechanisms. Because of such competition, any complete analysis of contaminant removal by scavenging must take stock of possible interactions with other processes. Such an analysis may be accomplished through the traditional approach of performing material balances about a

volume element, fixed in the atmosphere, as shown in Figure 2.1. The overall material balance for the element may be separated into individual balances for the gas and liquid phases. Thus:

Pollutant material balance for rain in volume element (liquid-phase):

time rate of change of mass of pollutant in rain (liquid-phase) within volume element =

time rate of gain of pollutant mass in liquid phase by flow of pollutant-containing rain through walls of volume element +

time rate of gain of pollutant mass in liquid phase by uptake from gas phase within the volume element +

time rate of gain of pollutant mass by liquid-phase reaction within the volume element. (2.1)

Pollutant material balance for air in volume element (gas-phase):

time rate of change of mass of pollutant in air (gas phase) within volume element =

time rate of gain of pollutant mass in gas phase by gas-phase input through walls of volume element +

time rate of gain of pollutant mass in gas phase by release from the liquid phase within the volume element +

time rate of gain of pollutant mass by gas phase reaction within the volume element. (2.2)

Total pollutant material balance for the volume element:

time rate of change of total mass of pollutant within volume element =

time rate of gain of pollutant mass in liquid phase by flow of pollutant-containing rain through walls of the volume element +

time rate of gain of pollutant mass in gas phase by gas phase input through walls of volume element +

time rate of gain of pollutant mass by liquid phase reaction within the volume element +

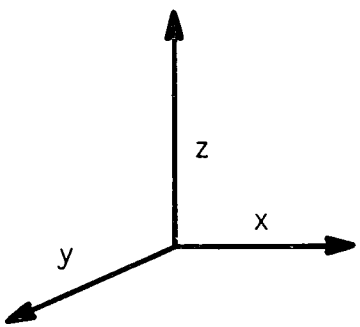

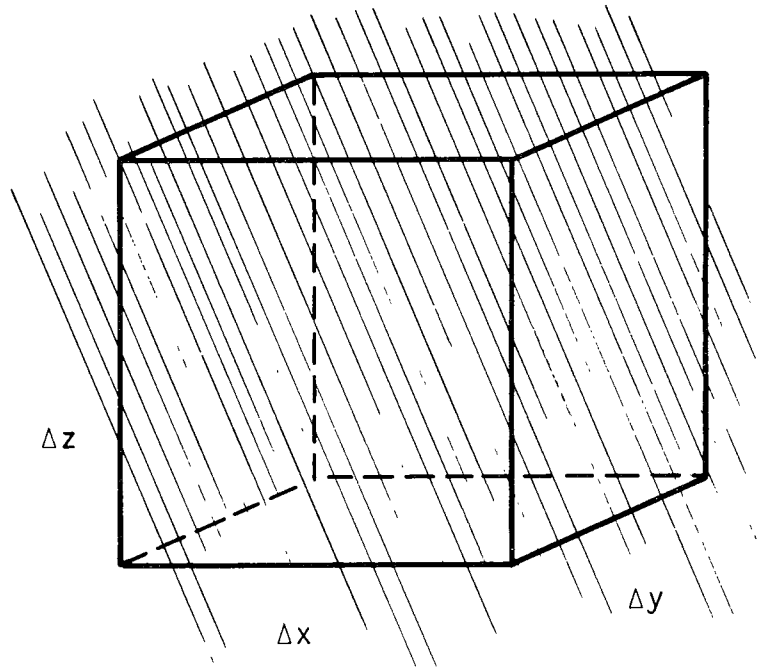

Figure 2.1 Schematic of Volume Element in Space

time rate of gain of pollutant mass by gas phase reaction within the volume element. (2.3)

Equations (2.1)-(2.3) form the basis for the partial differential equations of conservation of pollutant in the rain-air system. The restricted case wherein spherical, noninteracting raindrops fall with static size distribution may be represented by:

$$\frac{\partial \rho_{Ax}}{\partial t} = - \frac{4\pi N_o}{3} \left(\nabla \cdot \int_o^\infty a^3 f(a)\ \bar{v}_t\ \delta_{Ax}\ (a)\ da \right) + w + r_{Ax} \quad , \qquad (2.1a)$$

$$\frac{\partial \rho_{Ay}}{\partial t} = - (\nabla \cdot \rho_{Ay}\ \bar{v}_A) - w + r_{Ay} \quad , \qquad (2.2a)$$

and

$$\frac{\partial \rho_A}{\partial t} = - \frac{4\pi N_o}{3} \left(\nabla \cdot \int_o^\infty a^3 f(a)\ \bar{v}_t(a)\ \delta_{Ax}\ (a)\ da \right) - (\nabla \cdot \rho_{Ay}\ \bar{v}_A) + r_{Ax} + r_{Ay} \, . \qquad (2.3a)$$

w, for the stipulated conditions, is given in accordance with Reference (1) as:

$$w = - 4\pi N_o \int_o^\infty a^2 f(a)\ N_{Ao}\ da$$

$$= 4\pi N_o \int_o^\infty a^2 f(a)\ K_y(a)\ (y_{Ab} - y_{Ae})\ da \, . \qquad (2.4)$$

Other nomenclature is defined as follows:

a = drop radius

f = probability density function for drops existing in the volume element

K_y = overall mass transfer coefficient

N_o = number concentration of drops in volume element

t = time

$\bar{v}_A$ = velocity vector for pollutant A in gas phase

$\bar{v}_t$ = raindrop velocity vector

y_A = gas phase mole fraction of pollutant A

δ_{Ax} = mass of A in a drop/drop volume

ρ = density based on total space in volume element

subscripts

e = equilibrium

x = average value in total liquid phase

x_b = average value in drop

y = average value in gas phase.

One should note that Equation (2.3a) is simply the continuity equation for pollutant A in a "binary" solution,[2] including an additional term for depletion by washout. Formulation of general conservation equations such as the ones above may be viewed as somewhat academic, since in many washout situations a majority of the terms are negligible. For general purposes, however, the significance of each of the included terms must be considered, and such a breakdown is necessary to provide a meaningful definition of the washout process.

One should note in particular that Equation (2.3) is obtained by adding Equations (2.1) and (2.2): the uptake-release terms, which serve to couple the equations, simply cancel one another. Coupling of the differential equations constitutes a rather severe complication to their rigorous solution, and necessitates an iterative or "feedback" approach as shown schematically in Figure 2.2. The two models described in the following sections

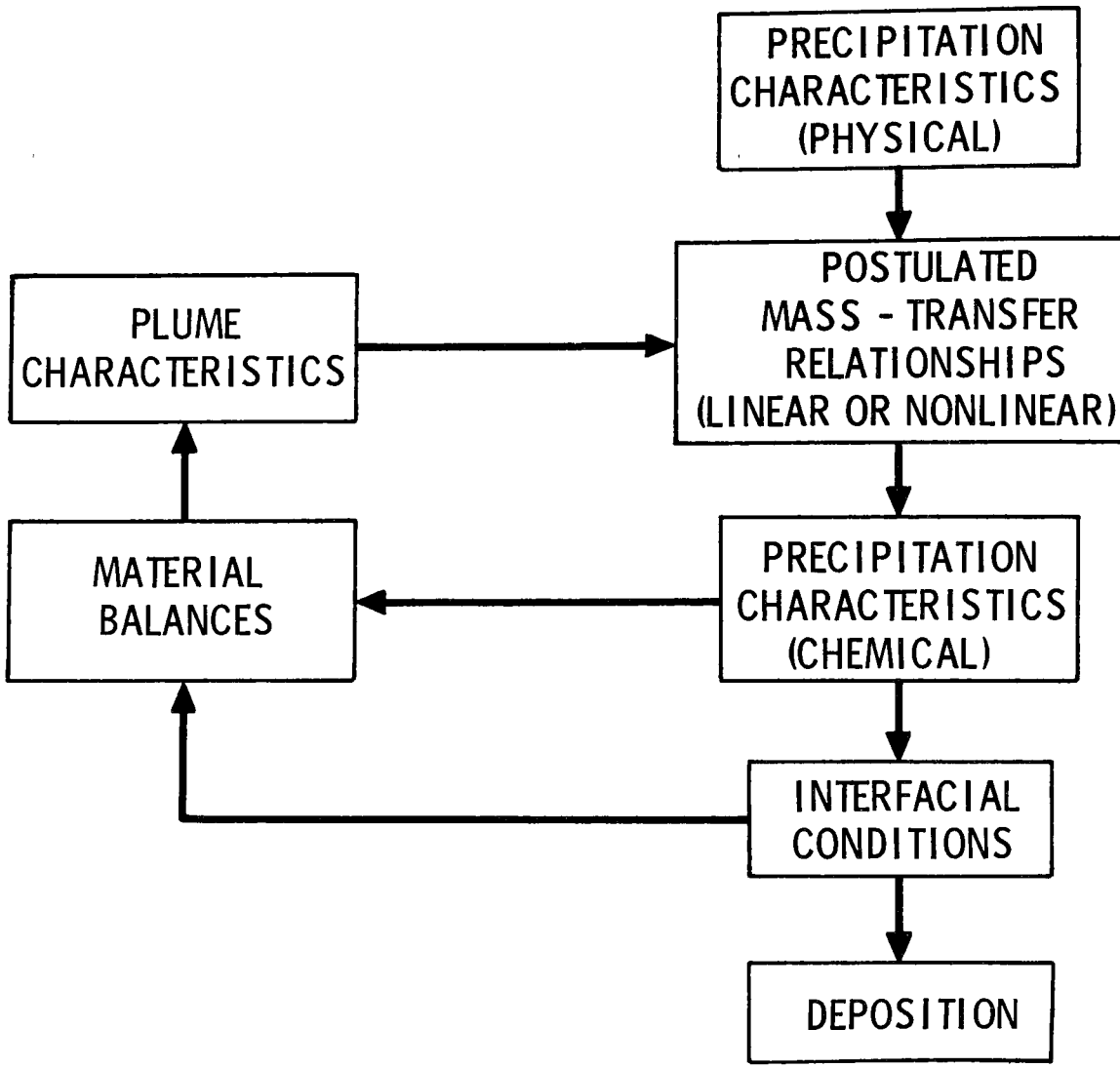

Figure 2.2 Elements of Washout Rate Calculation

attempt to overcome this problem by assuming that plume geometry under precipitation conditions is known; thus only Equation (2.1) (or a simplified version of it) need be solved. Future study, which will concentrate more directly on plume redistribution through washout processes, will involve solutions wherein this coupling is allowed to remain intact.

LINEAR, NONFEEDBACK MODEL

The objective of the initial modeling effort was to create a washout equation based upon linear solubility and transport relationships. This was accomplished in conjunction with a similar effort in the analysis of tritium washout.[3] Since SO_2 solubility and transport parameters are nonlinear, the result of this effort can be applied for SO_2 only after a suitable linearization is performed. Errors in this application, accordingly, will reflect the extent of deviation from linearity.

The assumptions employed by this model are summarized as follows:

1. Nonfeedback, i.e., the plume is defined under precipitation conditions, or alternatively, it is assumed that the precipitation has negligible effect on geometry of the plume.
2. Linearity; i.e., Henry's law is obeyed and the mass-transfer coefficient is independent of concentration.
3. Rainfall is vertical and of constant size-distribution and intensity.
4. Plume is expressible in terms of normal-distribution parameters.
5. The precipitation is composed of spherical, noninteracting elements.

Upon solving Equation (2.2) subject to these stipulations and to appropriate boundary conditions, one can obtain the well-known equation for a bivariate-normal plume. Equation (2.1) need not be solved completely, since the objective of this effort is simply to determine washout fluxes at ground level. This may be accomplished by performing material balances on drops of different sizes as they fall through the plume to determine their concentration at ground level, and then evaluating the fluxes after distribution over the drop size spectrum.

Material-balance considerations have been used previously[1] to show the ground level concentration in an a-radius drop to be given by

$$c_{Ao}(a) = \frac{3K_y}{v_t a} \int_{\infty}^{o} \exp\left(\frac{3K_y H' z}{v_t a}\right) y_{Ab}\, dz \quad . \tag{2.5}$$

When y_{Ab} is supplied by the bivariate normal equation this may be integrated to give

$$c_{Ao}(a) = -\frac{3QK_y F}{2\sqrt{2\pi}\,\sigma_y \bar{u} v_t a} \exp\left(-\frac{y^2}{2\sigma_y^2} + \frac{\sigma_z^2 \zeta^2}{2}\right)$$

$$\left\{ \exp(\zeta h)\left[1 - \operatorname{erf}\left(\frac{-\sigma_z^2 \zeta - h}{\sigma_z \sqrt{2}}\right)\right] + \right. \tag{2.6}$$

$$\left. \exp(-\zeta h)\left[1 - \operatorname{erf}\left(\frac{-\sigma_z^2 \zeta + h}{\sigma_z \sqrt{2}}\right)\right]\right\} ,$$

$$\zeta = \frac{3K_y H'}{v_t a} \quad . \tag{2.7}$$

Here the nomenclature is consistent with that used previously and that in the treatment by Gifford[4]. If units are expressed in the cgs system of measurement, then the "source strength" Q will have units of cm^3 SO_2/sec, measured at ambient conditions of temperature and pressure. The dimensionless variable F represents the fractional depletion of the plume at the downwind distance of interest. For the physical situations described in this report F is close to unity. F will be defined in terms of overall washout in the following development.

Computations for large distances from the source may be accomplished somewhat more conveniently using the following asymptotic approximation to (2.6);

$$c_{Ao}(a) = \frac{-3\ Q\ K_y\ \sigma_z\ F}{2\pi\ \sigma_y\ \bar{u}\ v_t a} \exp\left(-\frac{y^2}{2\sigma_y^2} - \frac{h^2}{2\sigma_z^2}\right)$$

$$\left\{ \frac{1}{-\sigma_z^2\ \zeta - h} \left[1 - \left(\frac{\sigma_z}{-\sigma_z^2\ \zeta - h}\right)^2\right] + \right.$$

$$\left. \frac{1}{-\sigma_z^2\ \zeta + h} \left[1 - \left(\frac{\sigma_z}{-\sigma_z^2\ \zeta + h}\right)^2\right] \right\} + 0\left(\frac{\sqrt{2}\ \sigma_z}{\sigma_z^2\ \zeta - h}\right)^4 . \quad (2.8)$$

The final term in (2.8) is a truncation-error estimate, 0 denoting "order of". Downwind washout rate, defined as the amount of material washed out per unit time per unit downwind distance can be calculated with the use of (2.6) or (2.8) by integrating over the crosswind distance and then distributing according to the rain spectrum. Thus the downwind washout rate is given by

$$M = \frac{J \int_0^\infty a^3\ c_{cross}(a)\ v_t(a)\ f(a)\ da}{\int_0^\infty a^3\ v_t(a)\ f(a)\ da} , \quad (2.9)$$

where J denotes rainfall rate and c_{cross}, defined by

$$c_{cross} = \int_{-\infty}^{\infty} c_{Ao}(a)\, dy \quad , \tag{2.10}$$

is obtained by formal integration of (2.6) or (2.8); thus

$$c_{cross} = \frac{-3\ Q\ K_y\ F}{2\ \bar{u}\ v_t a} \exp\left(\frac{\sigma_z^2\ \zeta^2}{2}\right) \left\{ \exp(\zeta h) \left[1 - \operatorname{erf}\left(\frac{-\sigma_z^2 \zeta - h}{\sigma_z \sqrt{2}}\right)\right] + \exp(-\zeta h) \left[1 - \operatorname{erf}\left(\frac{-\sigma_z^2 \zeta + h}{\sigma_z \sqrt{2}}\right)\right] \right\} \tag{2.11}$$

is the expression for c_{cross} corresponding to (2.6) and

$$c_{cross} = \frac{-3\ \sigma_z\ Q\ K_y\ F}{\sqrt{2\pi}\ \bar{u}\ v_t a} \exp\left(\frac{-h^2}{2\ \sigma_z^2}\right) \left\{ \frac{1}{-\sigma_z^2\ \zeta - h} \left[1 - \left(\frac{\sigma_z}{-\sigma_z^2\ \zeta - h}\right)^2\right] + \frac{1}{-\sigma_z^2\ \zeta + h} \left[1 - \left(\frac{\sigma_z}{-\sigma_z^2\ \zeta + h}\right)^2\right] \right\} \tag{2.12}$$

is that corresponding to (2.8).

In the event that there is appreciable depletion of the plume by washout F may be calculated from the expression

$$F = 1 - \frac{1}{Q\, c_y} \int_o^x M \, dx \qquad (2.13)$$

c_y denoting the total molar gas concentration at ambient conditions of temperature and pressure. Depending upon how the raindrop statistics are treated the previous equations may reduce to explicit forms upon incorporating (2.13), or they may be implicit in nature, necessitating iterative or numerical approximations to their solutions.

Although this linear, nonfeedback model is admittedly an approximate one, it is significant in that it is the first model to give a satisfactory qualitative description of some observed gas washout behavior, particularly the capability for desorption of pollutant from the rain. This model is also somewhat appealing because it is simple enough for hand calculation, if necessary. This model is evaluated by comparison with actual field results in a later chapter.

NONLINEAR, NONFEEDBACK MODEL

The second washout model developed as a part of this study differs from the previous model in that it allows for nonlinearities in both the mass transport and solubility parameters. It also allows for the downward passage of raindrops through arbitrary trajectories. This model is expected to provide a realistic calculation of washout from low elevation sources, and is intended primarily for use in analysis of the Quillayute results.

This model, in contrast to the one described previously, cannot be expressed in the concise mathematical form exhibited by Equation (2.6). Rather, it

takes the form of a general computer program, which solves the nonlinear differential mass-balance equation, (cf., [1]).

$$\frac{d\, c_{Ab}(a)}{dz} = \frac{3K_y}{v_t a}\, y_{Ab} - \frac{3K_y\, h'\, (c_{Ab})}{v_t a}\, c_{Ab}(a) \quad , \qquad (2.14)$$

$$(h',\ K_y \text{ variable}),$$

while calling on various subroutines to supply information concerning y_{Ab}, K_y, and h'.

Operation of the computer program is illustrated in Figure 2.3. It consists of a rather general calling program which coordinates subroutines, enabling a modular replacement should increased sophistication become desirable. Subroutines are listed as follows:

1. Terminal velocity routine (V) -- Computes fall velocity of radius-a drop from the equation

$$v_t = -8710.9\ a + 18029.7\ a^2 + 32184.5\ a^3 \quad , \qquad (2.15)$$

   which is a polynomial fit to the data of Gunn and Kinzer.[5]
2. Wind velocity routine (WIND) -- Computes wind velocity as a function of height (assumed to be constant at present).
3. Gas-phase concentration routine (CONC) -- Computes gas phase concentration over trajectory of drop as determined by the wind speed and the fall velocity.
4. Gas phase mass transfer coefficient routine (GK) -- Computes $K_y(a)$ using the Frössling equation (cf., [2]).
5. Solubility routine (HPRIME) -- Computes partition coefficient for SO_2 between air and water in accordance with the solubility equation derived in Chapter III and the parameters of Johnstone and Leppla.[8]
6. Differential-equation solving routine (ITER) -- Computes overall mass transfer coefficient and solves (2.14) for ground level concentration, c_{Ao}. Solves for gas phase limited, stagnant drop, linearized stagnant

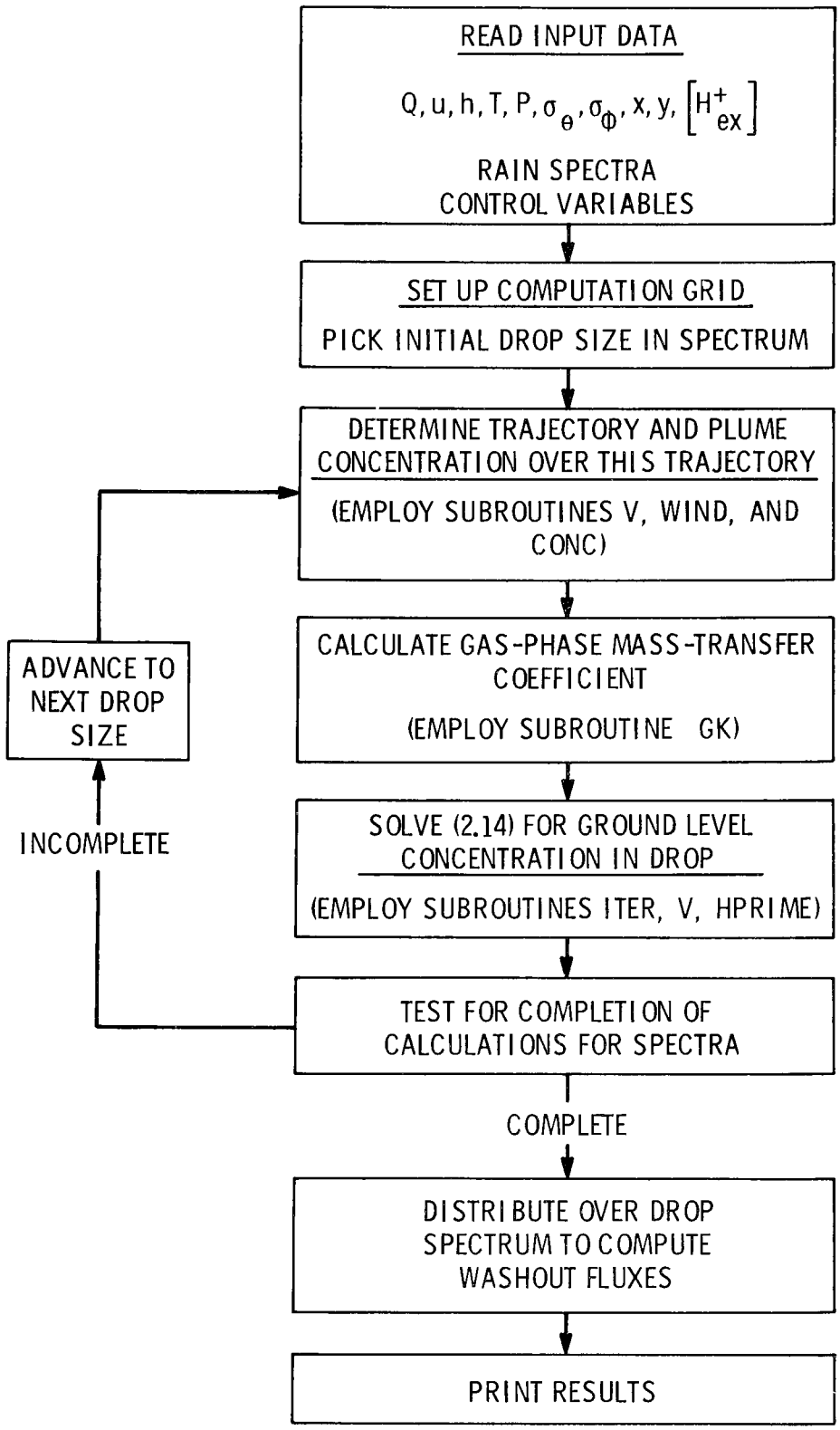

Figure 2.3 Simplified Schematic of Computer Program -- Nonlinear, Nonfeedback Model

drop, or arbitrary input values of K_y, depending upon control variables read in as data.

Euler's method[6] is used in ITER as the algorithm for approximating the solution to (2.14). This approximation is characterized by a truncation error of the order of the size of increment spacing chosen for the computational grid. This relatively simple algorithm was chosen over the more accurate and sophisticated techniques (higher-order Runge-Kutta methods) owing to the greater versatility that it offers for solving with various types of mass-transfer models. In addition Euler's method was judged to give results well within the limits of accuracy required by the present investigation.

Results from this nonlinear, nonfeedback model have been applied extensively in the analysis of field data and are presented with these data in Chapter V.

LIMITING BEHAVIOR OF WASHOUT EQUATIONS

It is emphasized that the general washout models presented in this chapter reduce asymptotically to limiting cases, which have been treated previously in more restricted theories of washout. Two cases of specific interest may be described as follows:

1) washout is describable totally in terms of rate phenomena; considerations of equilibria are of no importance, and
2) washout is describable totally in terms of equilibrium phenomena; rate processes are so fast that their consideration is unimportant.

The first of these cases has been referred to as "irreversible" washout, and has been treated previously using the classical washout-coefficient approach. The second limiting case occurs directly as a consequence of reversible behavior, and shall be referred to here as "equilibrium" washout.

The general linear washout Equation (2.6) can be used directly to illustrate the ability of the general models to describe asymptotically the above limiting types of behavior. This can be accomplished for the irreversible washout case by noting that "total solubility" corresponds to $\zeta=0$. In this event (2.6) reduces to

$$c_{Ao}(a) = \frac{3\ Q\ K_y\ F}{\sqrt{2\pi}\ \sigma_y\ \bar{u}\ v_t a} \exp\ (-\ y^2/2\ \sigma_y{}^2) \quad , \tag{2.16}$$

which is easily shown to be the product of $3K_y/v_t a$ and the integral exposure to a drop falling through a normally-distributed plume; i.e.,

$$c_{Ao} = \frac{3K_y}{v_t a} \int_o^\infty y_{Ab}\ dz \quad . \tag{2.17}$$

Equation (2.17) may be distributed over the drop-size spectrum to obtain the average concentration collected at ground level;

$$c_{Avg} = \frac{\int_o^\infty y_{Ab}\ dz \int_o^\infty 4\pi a^2\ N_o f(a)\ K_y\ da}{J} \quad . \tag{2.18}$$

Conventional definition of the washout coefficient, on the other hand, may be given by

$$w = \Lambda_i\ y_{Ab}\ c_y \quad , \tag{2.19}$$

c_y being the total gas concentration and w denoting, as before, the rate of removal of material from a unit volume of atmosphere by washout. Summing over all volumes encountered during passage to the ground, one may obtain the following expression for c_{Avg}:

$$c_{Avg} = \frac{\Lambda_i \; c_y \int_o^\infty y_{Ab} \, dz}{J} \quad . \tag{2.20}$$

From previous work [1, 10] in classical washout theory Λ_i may be shown to be given by

$$\Lambda_i = \frac{1}{c_y} \int_o^\infty 4\pi a^2 \, N_o f(a) \, K_y \, da \quad . \tag{2.21}$$

Applying this relationship to (2.20) results in an expression that is identical to (2.18) which was derived as a special case of the general linear theory; thus it is demonstrated that the washout-coefficient approach is simply a special case of the more general treatment discussed in this chapter, and may be derived directly from it.

Conditions leading to equilibrium washout are typified by large values of ζ. Applying $\zeta = \infty$ to Equation (2.8) results in the limiting form

$$c_{Ao} = \frac{QF}{\pi \, \sigma_y \, \sigma_z \, \bar{u} \, H'} \exp\left(- \frac{y^2}{2 \, \sigma_y^{\,2}} - \frac{h^2}{2 \, \sigma_z^{\,2}} \right) , \tag{2.22}$$

which is simply the expression for ground-level concentration of a bivariate-normal plume, modified by the solubility parameter, H'. One should note here in particular the lack of dependence of rain concentration on drop size, and also the independence of washout on plume concentrations other than those at ground level.

Criteria for equilibrium-washout conditions can be established by utilizing the linear theory to analyze behavior of a drop as it falls through a plume and approaches ground level. This can be accomplished describing a simple "plume" in terms of a concentration at ground level which increases steadily with vertical distance, thus

$$y_{Ab} = y_{Ab}\Big|_{\text{ground level}} + z \frac{d\, y_{Ab}}{dz} \quad . \tag{2.23}$$

Substitution of this into the material-balance expression (Equation [2.14]) for a single vertically falling drop and integration gives

$$c_{Ao} = \frac{y_{Ab}\Big|_{\text{ground level}}}{H'} - \frac{v_t a}{3K_y H'^2} \frac{dy_{Ab}}{dz} \quad . \tag{2.24}$$

Since the equilibrium state is represented by

$$c_{Ao} = \frac{y_{Ab}\Big|_{\text{ground level}}}{H'} \tag{2.25}$$

it follows directly that the criterion for equilibrium washout should be given by

$$-\frac{v_t a}{3K_y H'} \quad \frac{\left|\frac{dy_{Ab}}{dz}\right|}{y_{Ab}\Big|_{\text{ground level}}} \ll 1 \quad . \tag{2.26}$$

Inequality (2.26) may be used as a conservative criterion for equilibrium washout from plumes where concentration does not necessarily increase linearly with height by taking $|dy_{Ab}/dz|$ to be the <u>maximum</u> gradient experienced by the drop during its fall to the ground. For a bivariate-normal plume this maximum is given by

$$\frac{dy_{Ab}}{dz} = \frac{Q}{2\pi \bar{u} \sigma_y \sigma_z^2} \exp\left(-\frac{1}{2}\right) \tag{2.27}$$

which, in conjunction with (2.26) provides the following criterion for equilibrium washout from a bivariate-normal plume:

$$\frac{-3K_y H' \sigma_z e^{1/2}}{v_t a \exp(h^2/2\sigma_z^2)} \gg 1 \quad . \tag{2.28}$$

It should be emphasized that general application of (2.28) must pertain to the total ensemble of collected drops; hence the properties chosen for insertion into this criterion must be those corresponding to the largest drop of importance to the system. It also should be stressed that (2.28) is applicable to isolated, normally-distributed plumes only. If additional sources or background effects are present this criterion should not be employed.

Limiting behavior has been investigated here using the linear equations for washout, owing to their mathematical simplicity. It should be recognized, however, that the nonlinear model is simply a generalized version of the linear analysis. This model also, therefore, may be reduced to the limiting forms, and is capable of computation for either irreversible or equilibrium washout conditions. These asymptotic situations will be examined in more detail in Chapter V in the context of the field results.

CHAPTER III

SO_2 SOLUBILITY MEASUREMENT

The previous report on SO_2 scavenging[1] has emphasized the importance of solubility on washout behavior, and has indicated that rain acidity should be an important influence in this regard. The models presented in Chapter II provide an additional demonstration of how SO_2 solubility should affect its macroscopic washout behavior. Unfortunately there exist few data in the previous literature which pertain to the low concentration levels of interest, the only real contribution being the results of Terraglio and Manganelli,[7] which are rather limited in extent and give no specific information regarding the influence of acid-forming impurity.

Because of the need for knowing solubility behavior accurately prior to utilizing the models for washout calculations, a laboratory investigation was conducted to examine and quantify the relationships between SO_2 solubility, concentration, and hydrogen-ion impurity at levels normally encountered in the atmosphere.

The previous report[1] has suggested that if SO_2 dissolution progressed according to the scheme,

$$SO_{2g} + H_2O \rightleftarrows H_2O + SO_{2aq} \tag{3.1}$$

$$SO_{2aq} + H_2O \rightleftarrows H_3O^+ + HSO_3^- \tag{3.2}$$

(second ionization negligible) ,

then the concentration of dissolved SO_2 could be expressed in terms of airborne concentration and solution acidity by the form

$$c_{SO_2} = [SO_2]_{aq} + [HSO_3^-]$$

$$= \frac{[SO_2]_g}{H} + \frac{-[H_3O^+]_{ex} + \sqrt{[H_3O^+]_{ex}^2 + 4K_1[SO_2]_g/H}}{2} , \qquad (3.3)$$

where the bracketted terms denote concentrations in moles/liter and $[H_3O^+]_{ex}$ is the concentration in solution of hydrogen ions donated by sources other than Reaction (3.2). H and K_1 are the Henry's-law and dissociation constants, respectively, for Reactions (3.1) and (3.2):

$$H = \frac{[SO_2]_g}{[SO_2]_{aq}} , \qquad (3.4)$$

$$K_1 = \frac{[HSO_3^-][H_3O^+]_{total}}{[SO_2]_{aq}} . \qquad (3.5)$$

Precise measurements of H and K_1 have been obtained by Johnstone and Leppla[8]. The results of these authors, summarized in Table 3.1, were acquired under conditions involving gas-phase concentrations corresponding to 270 ppm and above. Use of these values in conjunction with Equation (3.3) to predict solubility under atmospheric conditions, therefore, represents an *a priori* extrapolation of over four orders of magnitude, and indicates a need for supporting experimental measurements.

TABLE 3.1

SOLUBILITY PARAMETERS* FROM WORK OF JOHNSTONE AND LEPPLA

Temperature °C	K_1 moles/ℓ	H
0	0.0232	0.0136
10	0.0184	0.0196
18	0.0154	0.0270
25	0.0130	0.0332
35	0.0105	0.0445
50	0.0076	0.0673

*Defined in Equations (3.4) and (3.5).

The apparatus employed herein to test solubility behavior and the validity of Equation (3.3) is shown schematically in Figures 3.1 and 3.2. Diluent gas from a regulated cylinder source was passed through a humidifier and a rotameter, and finally into a 25.1°C thermostatic water bath containing a heating coil, a permeation tube SO_2 source, and the solubility cell.

Upon emerging from the solubility cell the gas was passed through a wet test-meter for final accurate flow measurement.

The solubility cell is shown in detail in Figure 3.2. Constructed of Pyrex glass, this cell was designed so that the dilute gas stream was in contact with glass only, during its passage between the permeation tube and the absorbing liquid. Access ports were provided for optional insertion of pH and conductivity probes to monitor progress toward equilibrium.

An experimental run was initiated by charging the solubility cell with a given quantity of absorbing solution (usually 7 ml). The cylinder valve was then turned on and gas was allowed to bubble slowly through the solution until sufficient time had elapsed to bring the system to a point where it would be almost at equilibrium under the final flow conditions

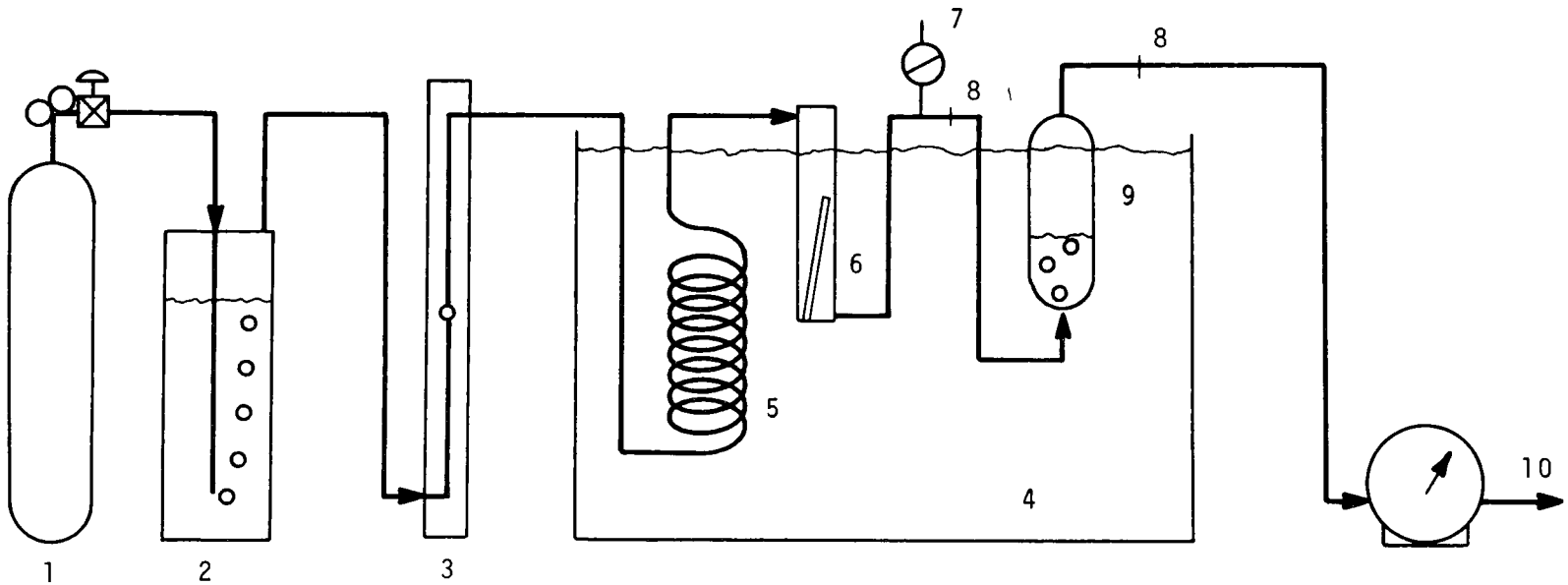

1. REGULATED DILUENT GAS SUPPLY
2. HUMIDIFIER
3. ROTAMETER
4. CONSTANT-TEMPERATURE BATH
5. STAINLESS STEEL HEATING COIL
6. SO_2 PERMEATION TUBE SYSTEM
7. BYPASS STOPCOCK
8. STANDARD TAPER JOINTS
9. TEST CELL
10. WET TEST METER

Figure 3.1 Solubility Measurement Apparatus

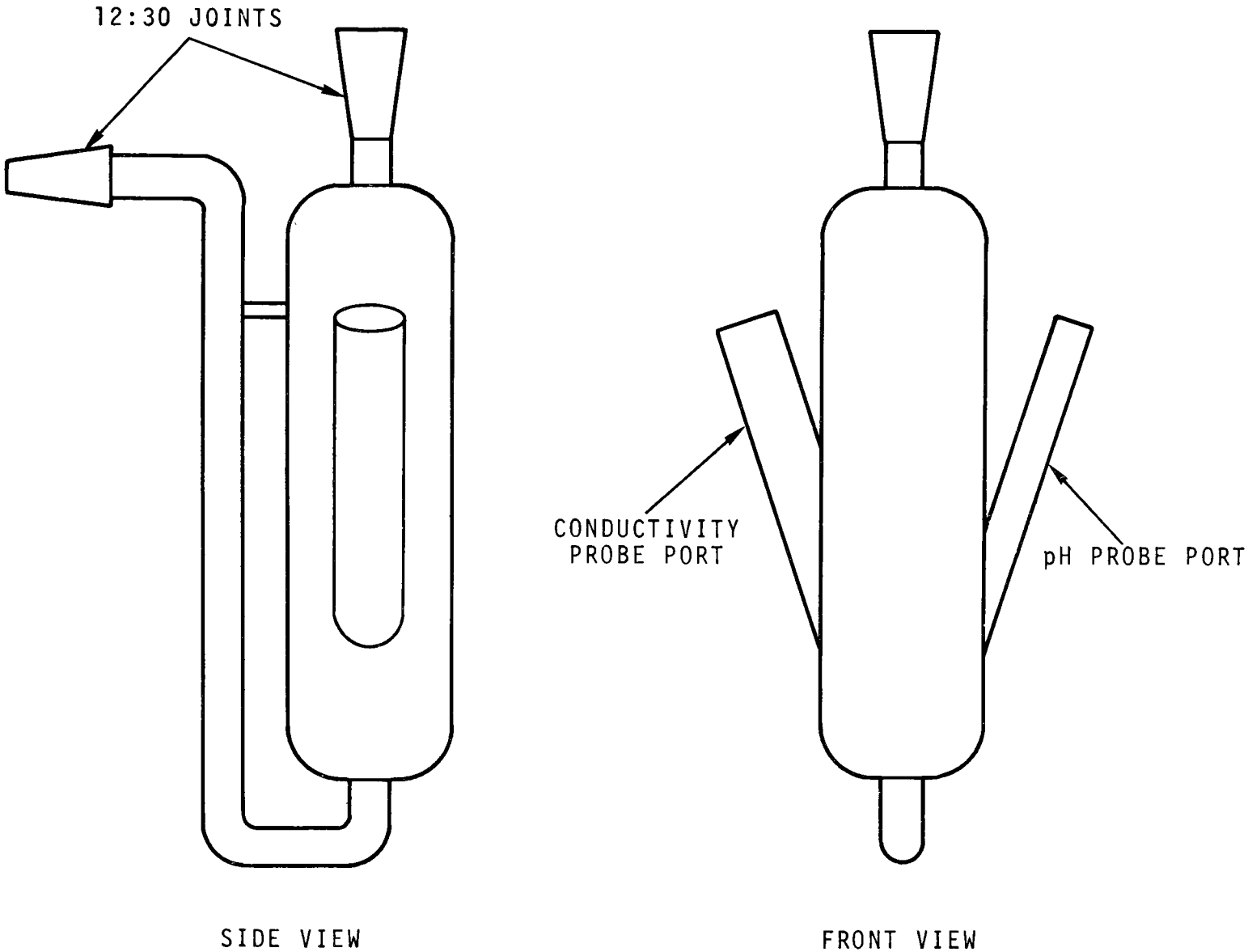

Figure 3.2 Solubility Cell

anticipated for the run. The gas flow was then turned up to a point where the desired gas concentration was attained, and the system was allowed to proceed to its final solubility equilibrium.

Gas-phase concentration was determined directly from known permeation rates of the calibrated permeation tubes, in conjunction with diluent flow measurements obtained from the wet test meter. Liquid-phase concentration was measured by removing aliquots from the solubility cell and analyzing them using the modified West and Gaeke method.[9] A Technicon Autoanalyzer was employed for this purpose. Approach to final equilibrium was noted by removing aliquots at various intervals of time which were comparable to the relaxation times expected for the system (usually 6 - 15 minutes). The few experiments for which equilibrium was not attained during the sequence of aliquot removal and measurement were discarded and then repeated to obtain more reliable results.

Grade A helium supplied by the Bureau of Mines was used as a diluent gas. Helium was ultimately chosen as a diluent after severe difficulties were encountered arising from impurities in the prepurified grade nitrogen employed during preliminary tests. Liquid absorbing solution was composed of water, triple distilled from permanganate solution, and adjusted to the desired pH by addition of standard HCl. Three types of absorbing solution, containing 0, 1.00×10^{-4}, and 1.00×10^{-3} moles HCl per liter (pH 7, 4, and 3), were employed.

Experimental results are shown in Table 3.2 and Figure 3.3, in conjunction with deviations from solubility behavior predicted from Equation (3.3) and the values of H and K_1 given by Johnstone and Leppla. These deviations, which range from 0.7 to 21.2 percent are noted to increase, in general, with decreasing SO_2 concentration. Such a trend should be expected, owing to the increasing errors of measurement as the lower limit of the analytical method (in the neighborhood of 2×10^{-7} moles/ℓ H_2O), is approached.

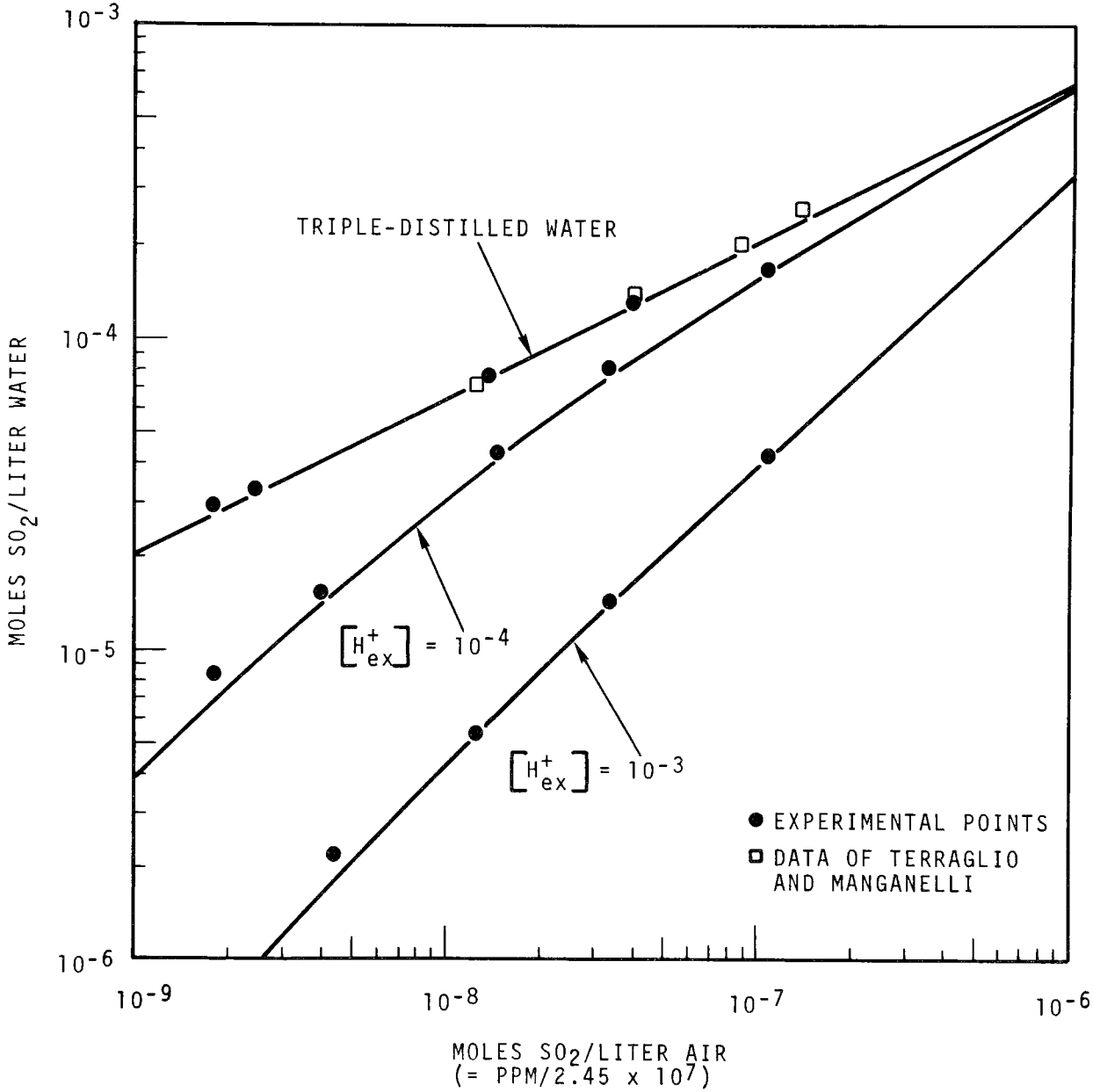

Figure 3.3 Solubility of Dilute SO_2 in Water at 25.1 °C

TABLE 3.2

EXPERIMENTAL MEASUREMENTS OF SOLUBILITY OF SO_2 IN WATER SOLUTION

Moles/ℓ HCl In Test Liquid	"Excess" pH	Moles/ℓ SO_2 In Gas x 10^6	Moles/ℓ SO_2 In Liquid x 10^6	Percent Deviation Above Predicted* Value
0	7	0.00178	29.4	10.2
0	7	0.00247	33.5	6.9
0	7	0.0135	74.0	1.4
0	7	0.0397	133.0	5.5
0.0001	4	0.00182	8.4	20.2
0.0001	4	0.00183	8.5	21.2
0.0001	4	0.00400	15.2	8.6
0.0001	4	0.0144	43.8	7.3
0.0001	4	0.0328	81.6	9.2
0.0001	4	0.1075	168.8	2.7
0.001	3	0.00437	2.2	18.2
0.001	3	0.0126	5.4	1.9
0.001	3	0.0333	14.5	4.1
0.001	3	0.1075	43.9	0.7

*Predicted using Johnstone-Leppla values for 25°C in Table 3.1 in conjunction with Equation (3.3).

The good reproducibility exhibited by the experiments in addition to the obvious high trend of the results, however, indicates that some nonrandom factor is present. This factor could have arisen either from a systematic error in the experiment or, more likely, from an increasing inability of Equation (3.3) to represent true behavior as concentration is lowered.

An analysis of the experimental procedure shows that a random error of about 3 to 7 percent (depending on concentration) should be expected, owing to individual errors in sampling and analysis. Systematic errors

could have arisen from a number of sources; these, however, were all considered to be too small to account for the effects observed. Permeation-tube characteristics were checked by both chemical and gravimetric analyses, and were known to within about $\pm$ 1 percent. Systematic errors arising from impurities in the diluent gas were severe during some of the preliminary tests using prepurified nitrogen; these, however, were shown to be inconsequential after the nitrogen was replaced with high-purity helium. The possibility of error arising from sparging of HCl from the absorbing solutions was checked by monitoring pH during the courses of several experiments. No loss of HCl could be measured in any of these tests, demonstrating this effect to be a negligible source of systematic error. Temperature depression of the absorbing solution by exposure to partially-humidified diluent was checked and found, under the most extreme circumstances, to be less than one degree centigrade. From Equation (3.3) and Table 3.1 one can predict that solubility will increase by about 3 percent per degree; thus this error source, while possibly approaching the expected random error under extreme conditions, cannot account for the total deviations shown.

The most plausible explanation of the nonrandom discrepancy between Equation (3.3) and the experimental results is simply the approximate nature of the equation itself, which neglects the effects of the second ionization,

$$HSO_3^- + H_2O \rightleftarrows SO_3^= + H_3O^+ \quad , \tag{3.6}$$

and the formation of other species such as pyrosulfites and hydrates. All of these effects could reasonably be expected to contribute to positive deviations from Equation (3.3), becoming increasingly significant as concentration is lowered.

In view of the large extrapolation from previous data and its approximate nature, Equation (3.3)'s ability to predict low-concentration solubility behavior is considered to be remarkable.

The positive trend of the deviation between experiment and Equation (3.3) might tempt one to adjust the values of H and K_1 to obtain a more satisfactory agreement. This should be discouraged, since the discrepancy is most likely to have arisen from the equation itself rather than from errors in the parameters. Adjusting these parameters, therefore, would amount to an empirical curve-fitting procedure wherein H and K_1 would be stripped of much of their theoretical significance. Any future endeavor to refine the agreement should begin, therefore, by attempting to formulate a more satisfactory solubility equation.

CHAPTER IV

FIELD EXPERIMENTS IN WASHOUT

OBJECTIVES OF FIELD STUDY

The necessity for controlled field experiments was recognized during the course of sulfur dioxide washout studies involving the Keystone Generating Station plume.[1] Here the apparent low washout of plume sulfur dioxide emphasized the influence of background sulfur dioxide in obscuring the experimental results. Uncertainties concerning the amount of sulfur as sulfur dioxide in the power plant plume further complicated the analysis. A revised theory of sulfur dioxide washout, which was developed in those studies, showed the importance of plume geometry and precipitation properties on the washout process. Adequate definition of these factors on the scale of the Keystone experiment was not feasible because of the plume height and the spatial and temporal nonuniformity of the atmosphere and precipitation on that scale.

A controlled field experiment at a properly selected site, it was reasoned, could circumvent the disadvantages of operation at the Keystone site while retaining the reality of natural precipitation in the actual atmosphere. Furthermore, suitable measurements could be taken to define adequately the plume and precipitation characteristics on this limited scale. Control would be exercised on the height, the rate, and the duration of the sulfur dioxide release and on the distance to the samplers. It was intended that a large number of experiments be conducted so that a variety of atmospheric and precipitation conditions could be sampled for each control configuration. It was therefore necessary to select a site with abundant rainfall. Such a site is the Quillayute State Landing Field near Forks, Washington, which has been utilized for washout studies by Battelle-PNL during recent years.

EXPERIMENT DESIGN

The Quillayute site, located west of the Olympic Mountains on the Olympic Peninsula of Washington, as shown in Figure 4.1, receives

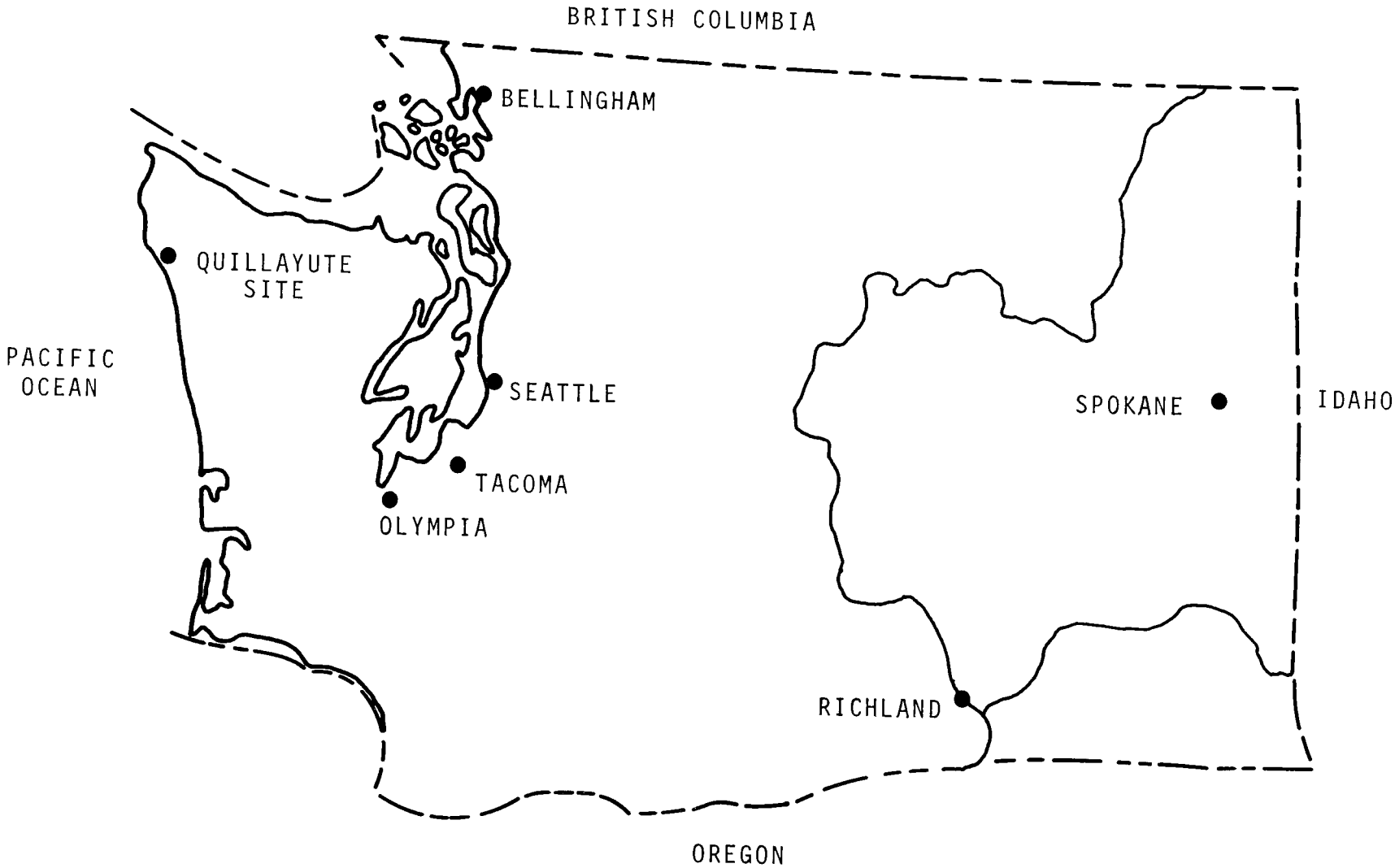

Figure 4.1 Location of Field Experiment Site

approximately 250 cm of precipitation per year. From October through March the precipitation, which is principally rain, falls during 20 or more days of each month for monthly totals in excess of 25 cm. The rainfall is usually continuous and of moderate intensity over periods of several hours. Wind speeds also are moderate and a southerly wind direction remains quite steady during most periods of precipitation. The southerly flow assures a low pollution background since the upwind trajectory is over the ocean or sparsely inhabited coastal regions.

The landing field is located 5 km inland from the coast on a broad plain and is relatively free of obstacles for extended distances. Winter closure of the field precludes interference from normal airport traffic. The National Weather Service has maintained a first class weather station at the site since 1966. Thus standard surface and upper air data are available for the site. Teletype circuits at the station provide information on the movement of storms.

At the Quillayute site, two trailer-mounted towers which could be extended from 7.6 to 30.5 m were installed approximately 215 m apart in a line roughly normal to the mean wind direction during precipitation. Three sampling arcs were established from 305° to 060° at distances of 30.5, 61 and 122 m from each tower. These arcs were staked out at 5° intervals for positioning of the precipitation and air samplers. These two grids, designated "East Grid" and "West Grid" are shown in Figure 4.2. Also shown in this figure is the location of a trailer-mounted 8.5 m tower, which was positioned about 150 m north of the West Grid tower to measure sulfur dioxide concentrations in the air with a vertical array of samplers. Figure 4.3 depicts the special grid that was utilized on one occasion when precipitation occurred with northerly flow.

The sulfur dioxide metering systems were located on the trailers at the tower bases. Each consisted of an insulated box containing two 9.1 kg manifold-connected cylinders of sulfur dioxide. The box temperature was regulated with a thermostatically controlled electric heater to maintain adequate

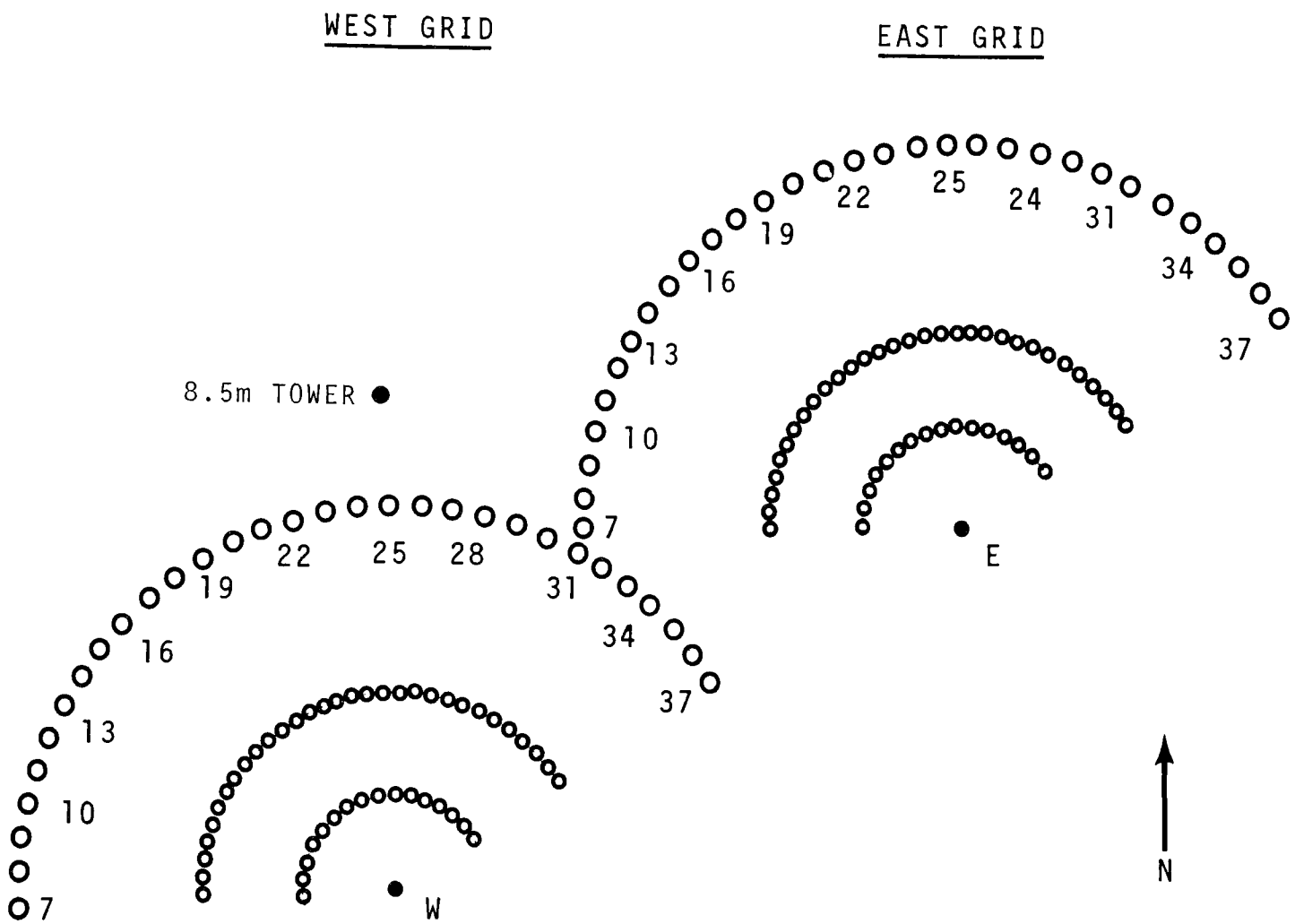

Figure 4.2 Quillayute Grid System

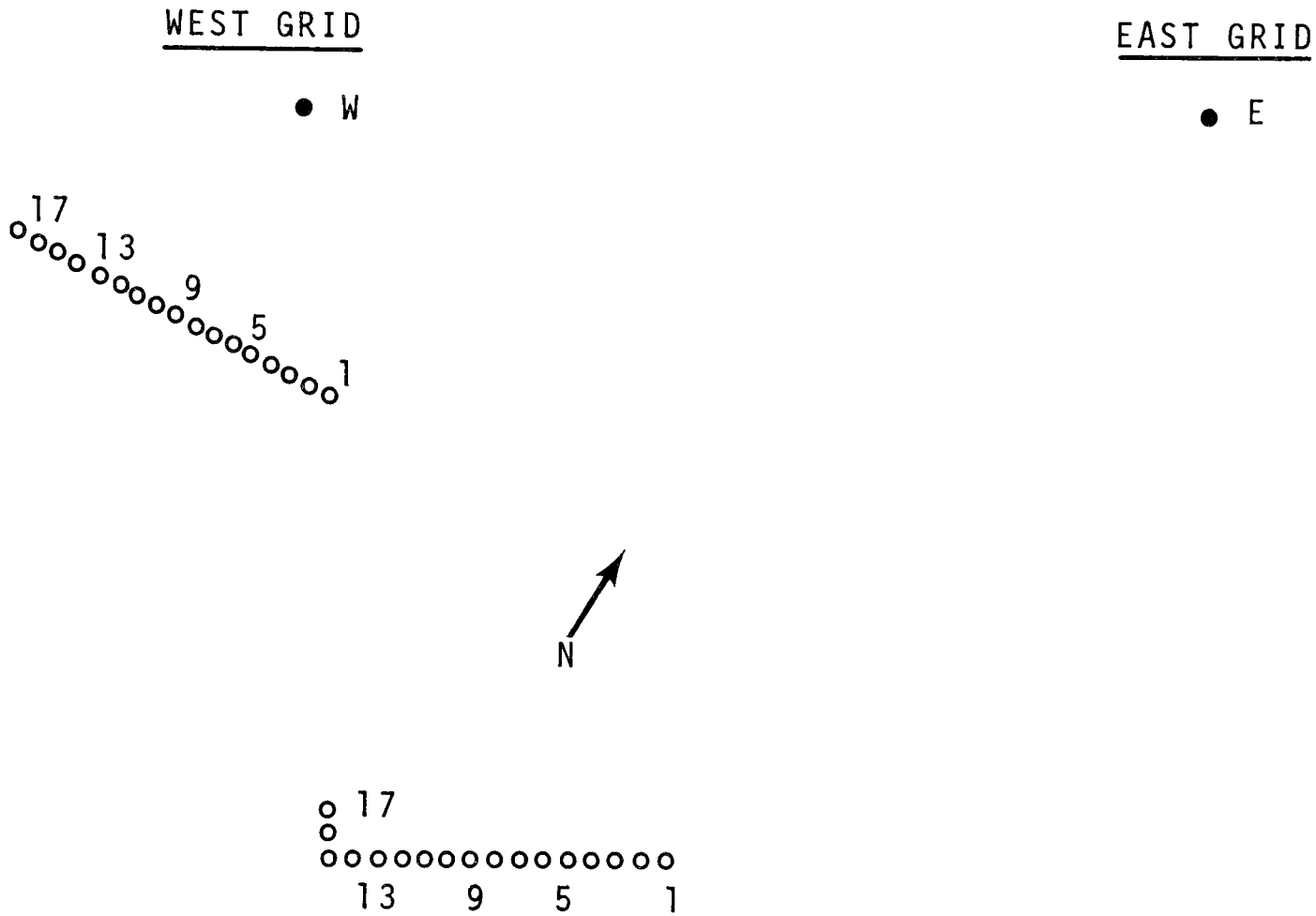

Figure 4.3 Special Grid System

cylinder pressure for constant emission rate. Valves and flowmeters on the box exterior permitted the operator to maintain a predetermined sulfur dioxide flow. Pressure and temperature sensors monitored the flowmeter conditions for accurate determination of the total emission. Polyethylene tubing carried the sulfur dioxide to the top of the tower where it was vented to the atmosphere.

Additional equipment at the top of each tower consisted of a three-dimensional Gill anemometer and a solenoid-activated device for the ignition of red smoke grenades. The Gill system was the primary instrumentation for documentation of both the mean and fluctuating wind conditions at the source. Additional detail concerning this system is contained in the discussion of the tape recorder, which follows. The smoke grenades were provided as a back-up system with time exposure photography to define the vertical plume spread.

Recording of the Gill system output was provided with a 20 channel digital magnetic tape recorder (Brush #DL 620 A). With 18 channels available for recording the u, v and w wind components from each tower (two channels were used for identification of the run and for timing), each parameter was sampled 7.2 times per second. Mean wind speed and direction and angular standard deviations, σ_θ and σ_ϕ, for the duration of the sulfur dioxide generation period were determined subsequently from these.

The recording system was housed in a 4.6 m house trailer located midway between the two towers. This trailer also housed recorders for a surface wind set and a fast response rain gauge. Operation control was exercised from this location by the field director who was in contact with the tower operators by citizen-band radio. The field director and his assistant had the additional duties of smoke plume photography and documentation of the raindrop size spectra using a Battelle-PNL developed ozalid image spectrometer.

Each precipitation sampler consisted of a rigid polypropylene funnel, supported by an ordinary office-type waste basket, with a polyethylene bottle attached at the neck by a perforated screw cap. The bottle contained 5 ml of tetrachloromercurate (TCM) solution to assure retention of the sulfur dioxide in the precipitation. Twenty-four samplers were spaced at 5° intervals on each of the active arcs. Except when the special grid was employed, two arcs were activated on each grid for all runs. Deployment or recovery of the sample bottles on the two arcs of each grid was accomplished in ten minutes or less with two men.

Five bubbler-type air samplers were operated at a sampling rate of 500 ml per minute on each active arc to ascertain the near-surface sulfur dioxide concentration in the air. One was located along the expected plume centerline and it was flanked by the others at angular distances of 15° and 45°. An additional five bubblers were logarithmically spaced in the vertical on the 8.5 m tower. These units, self-contained in plastic lunch boxes, are operated by minature, battery-pack powered pumps.

Chemical assay of the precipitation was performed in the Battelle laboratory trailer, which was located in a hanger at the air field. Complete analysis of the precipitation and air samples could be accomplished in about three hours using two Technicon Autoanalyzers. The sulfamic acid variation of the well-known West and Gaeke method was used. Precipitation volumes were measured prior to discarding the samples into carboys following the analysis. The carboys were returned to Battelle-PNL for safe disposal.

Figure 4.4 is a composite showing the various equipment described above.

CONDUCT OF EXPERIMENTS

The runs typically were conducted in the following manner. The field director determined the tentative run configuration, (i.e., release heights,

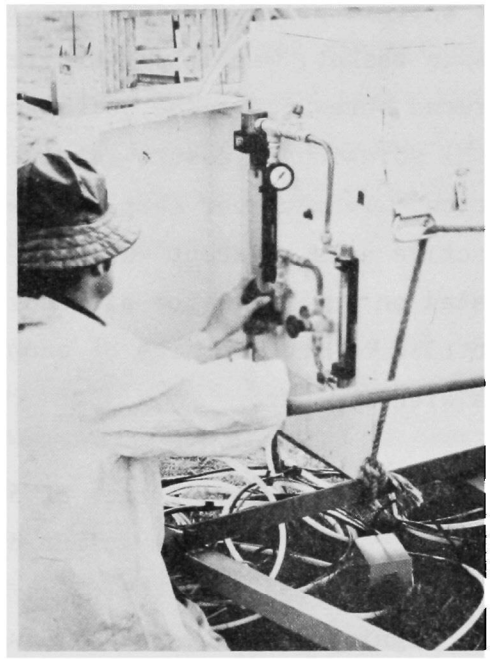

a

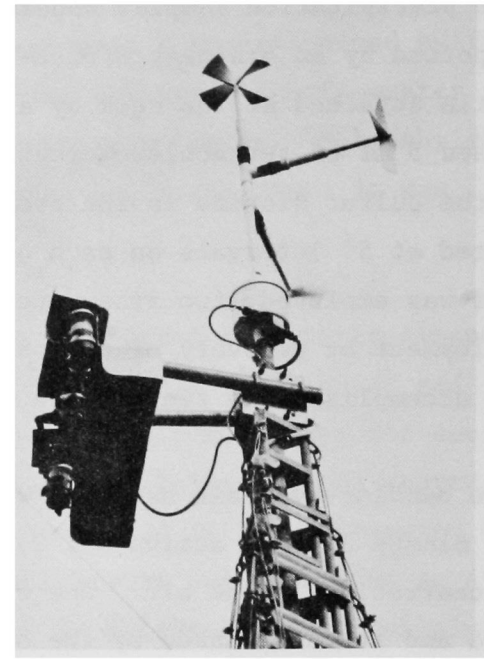

b

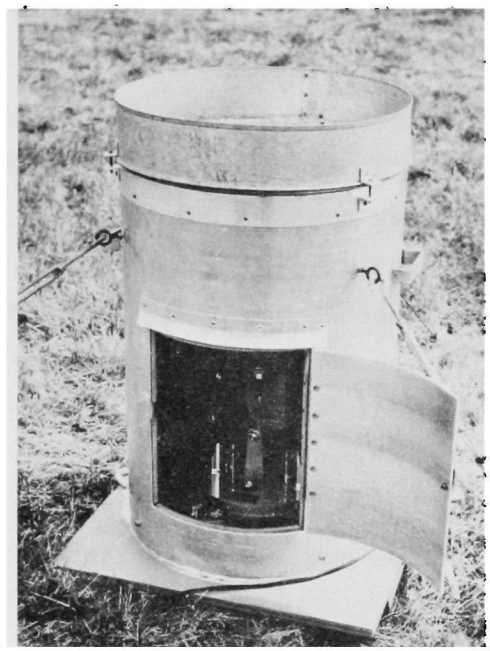

c

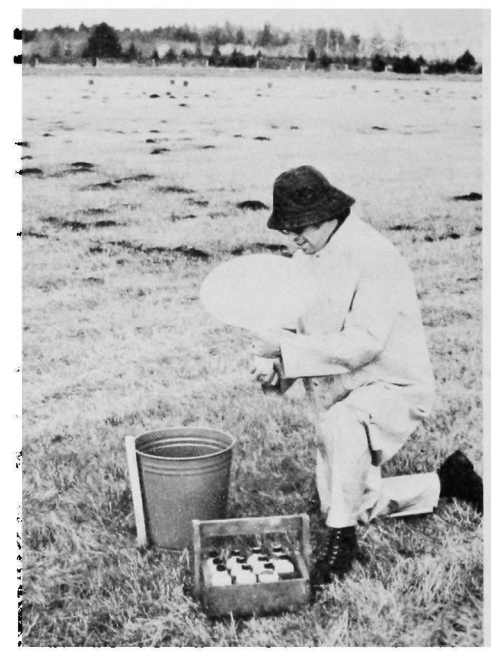

d

Figure 4.4 Composite of Field Study Equipment. (a) SO_2 release system, (b) Gill anemometer and smoke grenade rack on tower, (c) Fast-response rain gauge, (d) Precipitation collector.

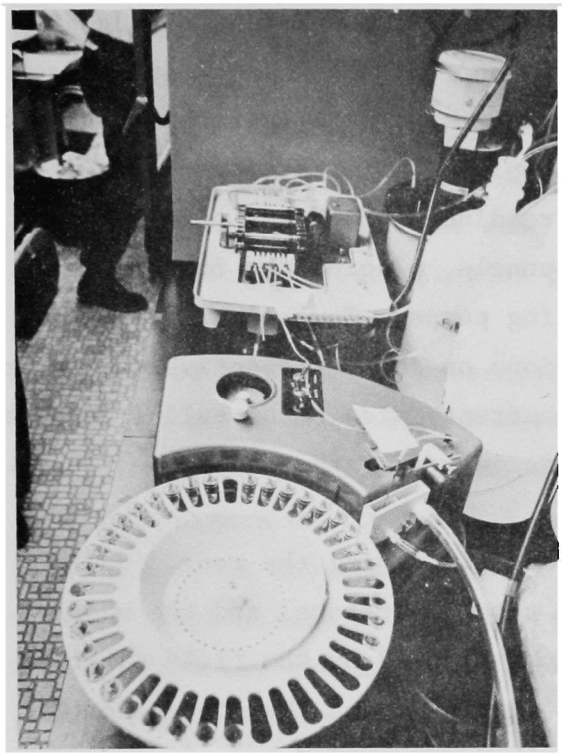

e

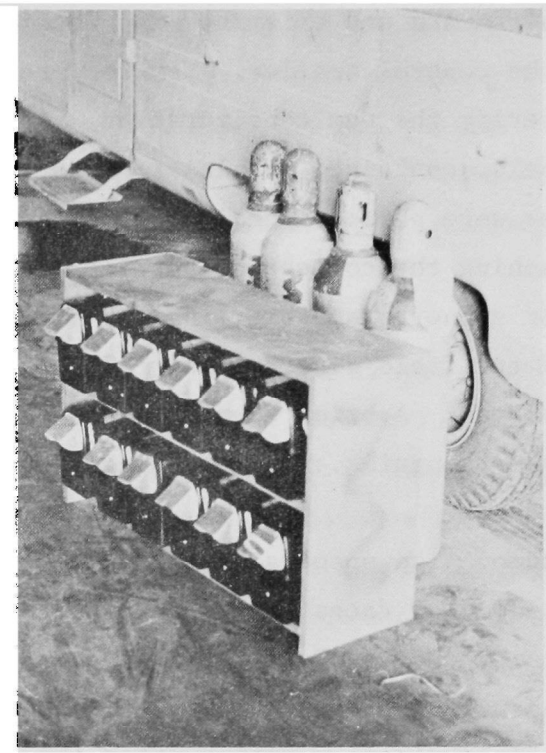

f

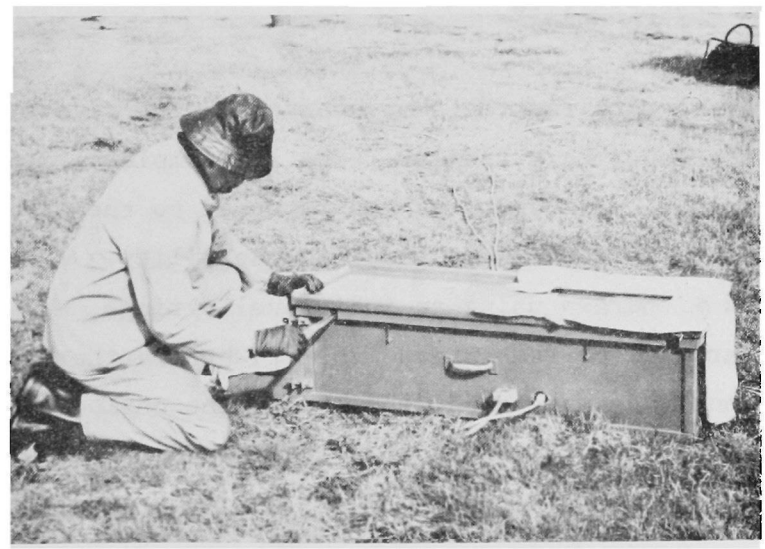

g

Figure 4.4 (continued). (e) SO_2 analysis system, (f) SO_2 bubbler boxes, (g) Raindrop size spectrometer.

release rates, and sampling arcs to be employed), based on preestablished requirements and existing wind conditions measured on a 3 m mast adjacent to the control trailer. Towers were raised and release height winds observed to verify the run configuration. Air samplers and the precipitation sampling funnels, contained in plastic bags, were deployed. Smoke releases from each tower were photographed before final run readiness which was completed by attaching the collection bottles to the funnels, placing the funnels in their supports and starting the air sampling pumps. Tower operators notified the field director when all preparations on their respective grids were completed. A brief countdown assured concurrent emission of sulfur dioxide on the two grids. The tape recorder was activated at the same time.

Raindrop size spectra were obtained periodically during the runs. Sulfur dioxide flow rates were maintained by the tower operators, and the wind velocity and rainfall rates were carefully monitored by the field director to assure run acceptability. The run was terminated at the discretion of the field director either after the prescribed run period had elapsed or when large changes in wind velocity or precipitation intensity threatened to compromise the acceptability.

Immediately following each run the sample bottles were recovered, capped, and returned to the laboratory trailer. The air samplers, deactivated during bottle recovery, were gathered and returned to the laboratory for sample removal and renewal of their sampling capability. A 2.5 ml aliquot of each sample was withdrawn using an individual syringe, and transferred to a cup on the carousel of the Autoanalyzer. When weather conditions were suitable, subsequent runs were conducted during the period of chemical analysis, which could be completed automatically upon loading the samples and activating the Autoanalyzer.

The field period extended from March 8 to April 9, 1971 with grid layout and equipment installation requiring about five days as a consequence of persistent, and often heavy, rains. The following week was dry and no runs were conducted until the third week in the field when 14 sulfur

dioxide releases were made. Another week went by before the weather became suitable for the final controlled releases. The extended dry periods and showery nature of the rain after mid-March were evidence that the ideal washout-studies weather, typical of Quillayute, had passed. As a consequence fewer runs were made than were planned, and there were few repetitive releases with the same configuration to observe the influence of atmospheric and precipitation parameters.

A summary of the runs is presented in Table 4.1. Rainfall ranged from 0.8 to 5.7 mm hr^{-1} and release-height wind speeds were between 2.2 and 7.6 m sec^{-1}. Rates of sulfur dioxide emission were between 0.38 and 5.66 moles min^{-1} at heights of 7.6 to 30.5 m. The selection of sampling arcs and release heights was tempered by the wind speed and the degree of atmospheric mixing. High mixing with a low release height was expected to result in high surface air concentrations of sulfur dioxide close to the source and, perhaps, give an erroneously high indication of washout as a result of SO_2 absorption on the wet funnels. A high elevation release in a high-wind condition could result in low observed washout on the inner arcs owing to sampled precipitation having blown in beneath the plume. Consequently, there is a bias toward release from midtower levels and sampling on the two outer arcs.

The plumes of sulfur dioxide were contained on the sampling arc (that is, they passed over active samplers) on 19 of the 20 releases. Data from all support instrumentation were complete. However, four of the releases did not result in meaningful washout distributions. Runs 1E and 1W did not result in SO_2 concentration measurements sufficiently above the analysis threshold to define the washout distribution. This was attributed to a loss of SO_2 from the samplers prior to analysis arising from insufficient TCM in the fixing solution. Runs 10E and 10W encountered an apparent malfunction of equipment during the analysis which resulted in only partial definition of the SO_2 distribution. Consequently, these four runs are omitted from further consideration.

TABLE 4.1

RUN SUMMARY

Run No.	Date	Time	Rainfall Rate ($cm\text{-}sec^{-1} \times 10^{4}$)	Temp. °K	Release Height ($cm \times 10^{-3}$)	Wind Speed ($cm\text{-}sec^{-1} \times 10^{-2}$)	Release Rate ($moles\text{-}sec^{-1} \times 10^{2}$)	Sampling Arc(1)
1E	3/22/71	1440-1455	0.28	282	2.14	5.2	4.96	B,C
1W					2.14	4.3	5.11	B,C
2E	3/23/71	1018-1027	0.42	282	1.68	6.2	9.44	B,C
2W					1.68	5.4	.63	B,C
3E	3/26/71	0954-1016	0.28	277	2.14	5.4	4.93	(2)
3W					1.22	4.9	4.86	(2)
4E	3/27/71	1011-1020	1.11	280	1.22	2.2	4.86	B,C
4W					3.05	2.3	5.31	B,C
5E	3/28/71	0812-0828	0.67	282	0.76	5.5	4.90	B,C
5W					1.68	6.3	5.40	B,C
6E	3/28/71	1028-1040	1.58	282	1.22	7.6	.95	B,C
6W					1.22	7.0	5.41	B,C
7E	3/28/71	1344-1410	0.42	282	1.22	6.4	2.70	B,C
7W					0.76	5.9	3.03	B,C
8E	4/06/71	0854-0901 0904-0911	0.22	282	0.76	3.5	8.17	A,C
8W					3.05	4.0	8.17	A,C
9E	4/07/71	0938-0952	0.75	279	1.22	3.0	4.41	A,B
9W					1.22	3.2	.97	A,B
10E	4/07/71	1450-1453	0.42	282	1.22	5.7	.63	A,B
10W					1.22	5.8	4.49	A,B

(1) Arc distances were: A, 100 ft; B, 200 ft; C, 400 ft.
(2) Special grid shown in Figure 4.3.

DATA REDUCTION

The basic field data consists of measurements describing the source and sampling configuration, the meteorology (including description of the precipitation), the concentration of SO_2 in the air and the SO_2 content of the precipitation; the former three being necessary in explanation of the latter. Many of the data can be utilized in initial form, but other data require additional processing. Such is the case with the raindrop size spectra, the SO_2 concentrations and the wind data from the three-dimensional anemometers.

Raindrop size spectra were determined from the raindrop images on ozalid paper which was exposed for a measured period during rainfall. Reduction of these data relies upon previous calibration of the images of various sized raindrops falling at terminal velocity. The frequency distribution of drop sizes for each run are presented in Table 4.2. A summary of other characteristics of the rainfall appear in Table 4.3.

Included are several raindrop spectrum parameters. Among the various runs, the number median raindrop diameter varied from 0.035-0.093 cm, and the flux varied over a factor of ten (.083-.87 cm^{-2} sec^{-1}). The quantity α is defined as π F $D_2^2/4$, where D_2 is the area mean raindrop diameter. This number is important in classical washout theory, where

$$\Lambda = \alpha E \quad , \tag{4.1}$$

E being the average collection efficiency of the raindrop spectrum for the material. Moreover, the great number of raindrop size spectra collected at Quillayute over the years has shown that α is proportional to the rainfall rate J, for prefrontal continuous rain - the proportionality constant being about 1.2. This parameter helps to indicate the type of rainfall experienced during the experiments noted in Table 4.3, the shower rain generally having a higher value for α/J. In this light, it is seen that the experiments included considerable variability in the rainfall character, and ostensibly in its washout ability.

TABLE 4.2

RAINDROP SIZE FREQUENCY DISTRIBUTION

Run No.	Diameter (cm)																
	.0249	.0299	.0360	.0430	.0515	.0615	.0740	.0900	.107	.129	.154	.169	.186	.209	.215	.229	.279
1		.007	.084	.122	.146	.092	.122	.240	.172	.014							
2	.030	.073	.253	.453	.161	.015	.015	.005									
3	.135	.184	.198	.090	.081	.062	.049	.186									
4	.093	.127	.211	.201	.083	.054	.030	.059	.059	.035	.040		.010				
5	.115	.082	.097	.094	.061	.097	.130	.106	.133	.058	.004		.010				
6	.085	.128	.191	.102	.045	.052	.056	.042	.045	.112	.095		.055				.009
7	.100	.123	.105	.241	.173	.073	.054	.023	.050	.027	.028	.005					
8	.101	.136	.169	.129	.154	.103	.125	.040	.011	.015	.015	.004					
9	.113	.117	.172	.140	.113	.091	.063	.046	.037	.045	.032		.032	.055			
10	.016	.082	.126	.121	.098	.099	.055	.077	.082	.121	.082		.038		.005		

NOTE: Tabulated values are the proportion of raindrops contained in the interval between the diameter of that entry and the preceding diameter.

TABLE 4.3

RAINFALL CHARACTERISTICS SUMMARY

Run No.	pH	Rain Type(1)	Raindrop Size Spectrometer Data					
			Sample No.	Median Diameter (cm x 10^2)	Raindrop Flux (cm^{-2} sec^{-1})	Rainfall Rate, J (cm sec^{-1} x 10^4)	α(2) (sec^{-1} x 10^3),	α/J (cm^{-1})
1	6.6	S	1	6.9	0.22	0.46	0.86	.186
			2	5.7	0.30	0.38	0.86	.227
2	6.4	S	1	3.7	0.87	0.28	1.03	.362
3	(3)	C	1	3.5	0.13	0.33	0.43	.130
4	5.3	S	1	3.8	0.27	0.52	0.81	.154
			2	4.7	0.33	0.54	0.93	.171
5	4.7	S	1	7.2	0.11	0.35	0.53	.151
			2	5.7	0.26	0.59	0.97	.163
6	5.0	C	1	9.3	0.19	1.12	1.41	.125
			2	4.2	0.25	1.21	1.39	.114
			3	3.8	0.62	2.34	2.80	.120
7	5.1	C	1	4.1	0.16	0.22	0.39	.174
			2	3.6	0.26	0.71	0.88	.124
8	5.1	S	1	4.0	0.21	0.22	0.45	.199
9	5.3	S	1	3.9	0.17	0.43	0.59	.137
10	5.4	S	1	5.5	0.08	0.36	0.46	.128

(1) Rain Type: S, shower; C, continuous (generally prefrontal).

(2) $\alpha = \pi F D_2^2/4$; D_2, area mean raindrop diameter.

(3) Not recorded.

pH of the rain was measured using a conventional pH meter. These results, however, were rather inaccurate owing to meter instability which was attributed subsequently to a faulty electrode. Fortunately, pH of the collected rain was in a region where its variations were insignificant in determining solubility behavior; thus these experimental errors were of no consequence to the related modeling effort. SO_2 concentrations of the collected precipitation samples were measured in the field laboratory and then corrected for dilution by precipitation which was collected before and after the period of SO_2 emission. Therefore, the precipitation concentration of SO_2 was calculated by dividing the quantity of SO_2 contained in a sampler by the precipitation collected during SO_2 emission, which was determined from the precipitation rate measured with the fast response rain gauge.

Table 4.4 shows the total amount of SO_2, Σm_i, recovered from the samplers of each arc and the total amount deposited in one cm of downwind distance during a one-second emission (downwind washout rate, cf. pg. 11). The latter quantity, M, is approximated by the relationship,

$$M = \frac{\Sigma m_i \ \Delta Y}{At} \quad , \tag{4.2}$$

(cf. Equation [2.9]) where ΔY is the sampler separation along the arc, A is the sampler collection area and t is the duration of SO_2 emission. A third column gives the washout per cm of downwind distance as the percent of SO_2 released. The maximum value is approximately 4 percent per kilometer. Precipitation concentrations of the individual samplers are tabulated in Appendix A.

Concentrations of airborne SO_2 were measured with bubbler-type samplers which were operated throughout the emission period. The recovered mass, determined in a manner similar to that for the precipitation samplers, was divided by the volume of air which was sampled during the emission period to give the average air concentration.

TABLE 4.4

SO_2 WASHOUT SUMMARY

Run No.	Arc	Σm_i (moles x 10^8)	Deposition, M (moles [cm sec]$^{-1}$ x 10^{10})	M/Q (percent cm^{-1} x 10^5)
1E *				
1W*				
2E	B	0.88	9.90	0.10
	C	2.04	44.40	0.47
2W	B	0.07	0.78	0.12
	C	0.18	4.00	0.63
3E		14.76**	65.10	1.30
3W		7.51	26.30	0.54
4E	B	14.00	153.00	3.20
	C	8.55	186.00	3.80
4W	B	5.23	56.80	1.10
	C	2.89	63.00	1.20
5E	B	13.61	83.40	1.70
	C	7.78	95.30	1.90
5W	B	0.29	2.19	0.04
	C	0.38	5.66	0.10
6E*				
6W	B	8.71	71.10	1.30
	C	9.23	150.80	2.80
7E	B	4.66	17.70	0.65
	C	4.63	34.90	1.30
7W	B	17.89	67.80	2.20
	C	9.77	73.60	2.40
8E	A	8.75	30.80	0.37
	C	8.82	127.50	1.50
8W*				
9E	A	7.98	28.00	0.64
	B	7.84	55.00	1.20
9W	A	2.19	7.70	0.79
	B	1.62	11.40	1.20
10E*				
10W*				

*Undefined
**Incompletely contained

The three-dimensional anemometers were oriented with their propellers facing upward, to the east and to the south. From the wind speed components thus obtained, mean and turbulent airflow parameters were calculated using the following relationships:

$$\bar{u} = \frac{\Sigma \left([u^2+v^2]^{1/2}\right)}{N} \tag{4.3}$$

$$\bar{\theta} = 180° - 57.3 \frac{\Sigma \left(\tan^{-1} \frac{u}{v}\right)}{N} \tag{4.4}$$

$$\sigma_\theta = \left\{ \frac{\Sigma \left([\tan^{-1} \frac{u}{v}]^2\right)}{N} - \left[\frac{\Sigma \left(\tan^{-1} \frac{u}{v}\right)}{N}\right]^2 \right\}^{1/2} \tag{4.5}$$

$$\sigma_w = \left\{ \frac{\Sigma w^2}{N} - \left[\frac{\Sigma w}{N}\right]^2 \right\}^{1/2} \tag{4.6}$$

$$\sigma_\phi = \frac{\sigma_w}{\bar{u}} \tag{4.7}$$

where u, v and w are the easterly, southerly and upward wind components, respectively. $\bar{u}$ and $\bar{\theta}$ are the mean resultant wind speed and direction, σ_w is the standard deviation of the wind speed in the vertical, and σ_θ and σ_ϕ are the standard deviations of wind direction and wind inclination, respectively. N is the number of data points contained in the summation.

With the exception of $\bar{\theta}$, all airflow parameters were used in the calculation of the concentrations of SO_2 in the near-surface air. These calculations were performed using the relationship

$$\chi = \frac{Q \exp - \frac{1}{2} [(h/\sigma_z)^2 + (y/\sigma_y)^2]}{\pi \bar{u} \sigma_y \sigma_z} \qquad (4.8)$$

where the concentration adjacent to the surface at a location displaced a lateral distance y from the plume axis is determined by the rate of SO_2 emission, the height of release, the mean wind speed at release height and the standard deviations of the plume in the lateral and vertical direction Evaluations of σ_y and σ_z at downwind distance x were accomplished using the relationships

$$\sigma_z = \sigma_\phi x \quad ; \quad \sigma_y = \sigma_\theta x \qquad (4.9)$$

which are appropriate when the standard deviation of wind inclination and wind direction are evaluated with sampling times equal to the duration of sulfur dioxide emission and averaging times which are equal to one-fourth the travel time from the source to the sampling arcs.[10] The standard deviations can be obtained by taking the square root of the difference of the squares of the standard deviations determined for sampling times equal to the emission duration and one-fourth the travel time.

The utilization of the airflow parameters for air concentration calculations, therefore, defined the manner in which the data were reduced. Table 4.5 contains the data appropriate to the Quillayute runs. Figure 4.5 shows the degree of agreement between observed and calculated values of SO_2 concentration in the near-surface air. While there is considerable scatter in the data pairs, it is markedly reduced when only the observed data for which

TABLE 4.5

DATA SUMMARY

QUILLAYUTE 3-D ANEMOMETERS

Run No.	Height ($cm \times 10^{-3}$)	Mean Wind Velocity Dir(Deg)	Mean Wind Velocity Speed ($cm\ sec^{-1} \times 10^{-2}$)	Turbulence Parameters 1st Arc (A or B) σ_θ	1st Arc (A or B) σ_ϕ	2nd Arc (B or C) σ_θ	2nd Arc (B or C) σ_ϕ
1E B,C	2.14	176.4	5.2	.1330	.1058	.1214	.0944
1W B,C	2.14	176.9	4.3	.1730	.1086	.1594	.0971
2E B,C	1.68	186.5	6.2	.1722	.0976	.1659	.0884
2W B,C	1.68	190.6	5.4	.1969	.1091	.1919	.0960
3E	2.14	008.6	5.4	.0997	.0582	-----	-----
3W	1.22	007.5	4.9	.1337	.0653	-----	-----
4E B,C	1.22	160.8	2.2	.3799	.1294	.3639	.1175
4W B,C	3.05	163.3	2.3	.3343	.2022	.3111	.1598
5E B,C	0.76	166.6	5.5	.1882	.0828	.1771	.0737
5W B,C	1.68	168.1	6.3	.2156	.1127	.1877	.1018
6E B,C	1.22	176.0	7.6	.1320	.0845	.1260	.0795
6W B,C	1.22	176.8	7.0	.1540	.0958	.1462	.0892
7E B,C	1.22	207.3	6.4	.2133	.0885	.2069	.0799
7W B,C	0.76	212.6	5.9	.2568	.0873	.2433	.0775
8E A,C	0.76	170.9	3.5	.1935	.0811	.1798	.0656
8W A,C	3.05	172.1	4.0	.1671	.1026	.1505	.0839
9E A,B	1.22	203.1	3.0	.2010	.1005	.1965	.0943
9W A,B	1.22	205.4	3.2	.2117	.0884	.2061	.0816
10E A,B	1.22	175.7	5.7	.1714	.0841	.1676	.0785
10W A,B	1.22	183.7	5.8	.2229	.1042	.2206	.0994

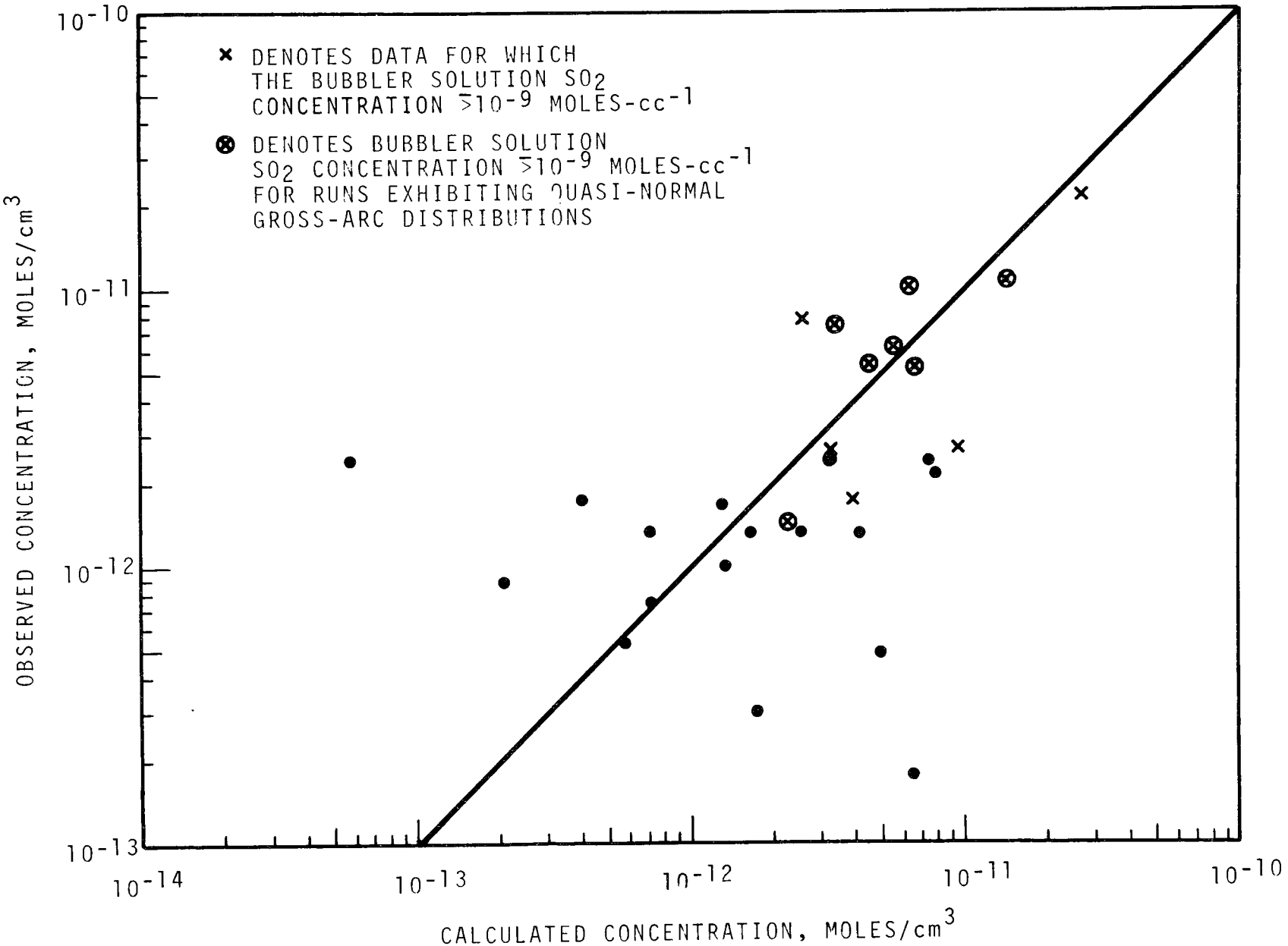

Figure 4.5 Comparison of Observed and Calculated SO_2 Concentrations in Air

the bubbler solution concentration of SO_2 exceeded 10^{-9} mole-cc^{-1} (those for which the analytical method is reasonably accurate) are considered. The scatter is further reduced by limiting these more reliable data to those runs for which the observed distribution of SO_2 concentrations in precipitation were approximately Gaussian. Finally, the even distribution around the line which denotes a one-to-one relationship, demonstrates the basic agreement of the calculated and observed values and establishes the validity of calculated SO_2 concentrations.

Although the concentration of SO_2 in the air apparently can be defined adequately in the preceding manner, it must be recognized that the resulting values are averages for the period of emission. It has been demonstrated previously[1] that washout is related directly to the time-averaged definition of a plume only when the process is linear. Chapter III has shown, however, that the solubility relationship between SO_2 and water is nonlinear under the conditions of interest. Consequently, long-period average air concentrations may be inappropriate for the definition of washout concentration. The influence of nonlinear behavior on the resultant washout is discussed in the following chapter.

CHAPTER V

ANALYSIS OF RESULTS

A large number of factors apparently influence the washout of SO_2. It is, therefore, extremely difficult to relate the observed washout variability to specific factors without the aid of some prescribed analysis technique which attempts to represent the influences of the pertinent variables to the total system. Accordingly it is convenient to evaluate the field observations by comparing them with predictions resulting from the analyses described in Chapter II. If these techniques are sufficiently valid to permit grouping of results they should enable greater insight into washout mechanisms and allow further refinement of the analysis.

It should be emphasized at the outset, however, that deviations between theory and experiment may arise from three basic causes, which are listed as follows:

1. intrinsic shortcomings of the analyses, for example, the use of an idealized plume model for mathematical description of the actual plumes;
2. utilization of input data that is not completely representative of the system, such as employing raindrop size spectra obtained over short time periods to represent conditions during an entire emission period;

and, to a lesser extent,

3. inadequate precision in measurements, for example, SO_2 measurements which, in some cases, were inaccurate because of sensitivity limits of the technique.

If deviations caused by the last two factors are significant, they will tend to mask systematic deviations caused by the first and thus reduce the effectiveness of the analysis.

This chapter will consider first the comparison of experimental results with predictions of the two simple asymptotic cases discussed in Chapter II (the washout coefficient and the equilibrium washout approaches). It is emphasized here that although these cases constitute opposing limits in the sense that they pertain, respectively, to transport-controlled and equilibrium-controlled behavior (ζ=o and ζ=∞) they do not necessarily define upper and lower limits of washout rates. Comparison of these limiting cases is followed by similar comparisons of the general models. Discussion of behavior exhibited by individual experiments is presented in the context of the examination of these techniques.

WASHOUT COEFFICIENT ANALYSIS

As shown in Chapter II, the traditional washout coefficient approach represents the limiting situation wherein washout is totally a kinetic phenomenon, and considerations of equilibria are unimportant to the analysis. This implies that the system is irreversible. Under such conditions it can be shown[1] that the washout coefficient, as defined by Equation (2.19), can be determined from experimental data using the relationship

$$\Lambda = \frac{\Sigma m_i \, \Delta Y \, \bar{u}}{m_o A} \quad . \tag{5.1}$$

Here Σm_i is the total amount of SO_2 recovered from the samplers on an arc, ΔY is the sampler spacing along the arc, $\bar{u}$ is the mean wind speed at release height, m_o is the total amount of SO_2 released, and A is the collection area of a sampler. Upon application of Equation (4.2), Equation (5.1) reduces to

$$\Lambda = \frac{M\bar{u}}{Q} \quad , \tag{5.2}$$

where Q is the SO_2 emission rate in moles/sec. From this it is observed that the M/Q values in Table 4.4 differ from Λ only by the factor $\bar{u}$.

As shown by Engelmann[11], the washout coefficient also may be estimated theoretically, assuming gas-phase limited behavior, by employing Equation (2.21) in conjunction with typical rain spectra. The curve for SO_2 washout coefficient as a function of rainfall rate defined by this relationship is plotted in Figure 5.1. The experimental points calculated by Equation (5.2) from the field data are also plotted on this graph. From this comparison it is seen that few data points approach the washout coefficients predicted by the irreversible washout theory. These data have been expressed as downwind washout rates and plotted versus values predicted from the Engelmann curve in Figure 5.2. This will be useful in comparing with predictions from other models later in this chapter.

It is apparent from Figures 5.1 and 5.2 that low elevation releases of SO_2 generally produce higher experimental washout coefficients. Also, higher coefficients tend to be observed at greater distances from the source. The Run 5 results demonstrate the effects of source elevation and sampling distance. Emission from 16.8 meters, on the west grid, results in coefficients that are more than an order of magnitude lower than the emission on the east grid from an elevation of 7.6 meters. In addition, the washout coefficient on Arc C of the west grid is more than double the value on Arc B. The smaller difference between washout coefficients on Arcs B and C of the east grid apparently results from more rapid diffusion into the near-surface layer from the lower-elevation emission. Consequently, there is a slight decrease in the air concentration of SO_2 between the arcs of the east grid, whereas a substantial increase occurs in concentration between the arcs of the west grid.

The washout coefficient determined theoretically for Run 5 from the measured raindrop size spectrum using the relationship by Engelmann[11] is shown as an asterisk in Figure 5.1 for comparison with the experimentally determined washout coefficients of that run. This point is

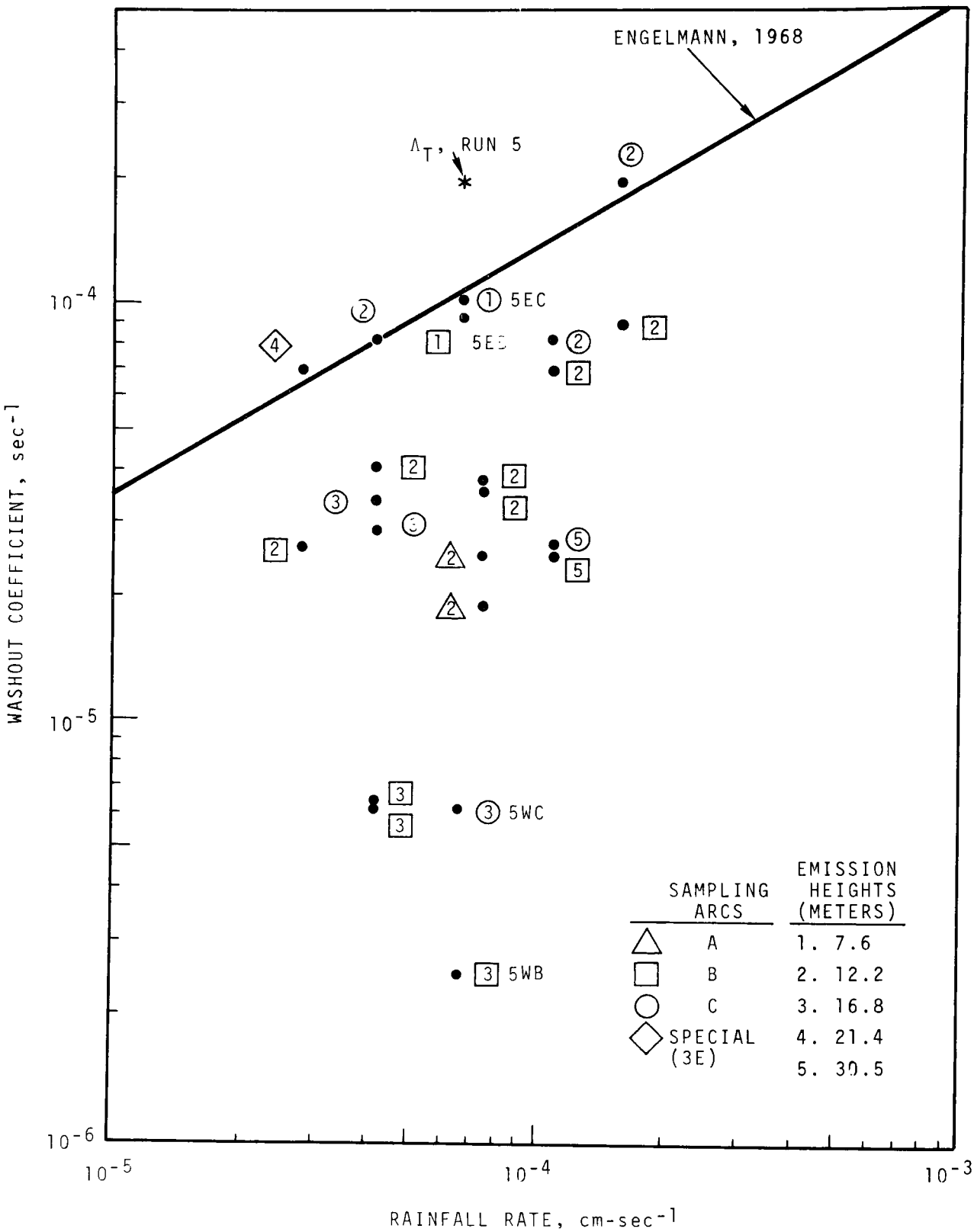

Figure 5.1 Comparison of Predicted and Measured Washout Coefficients as a Function of Rainfall Rate.

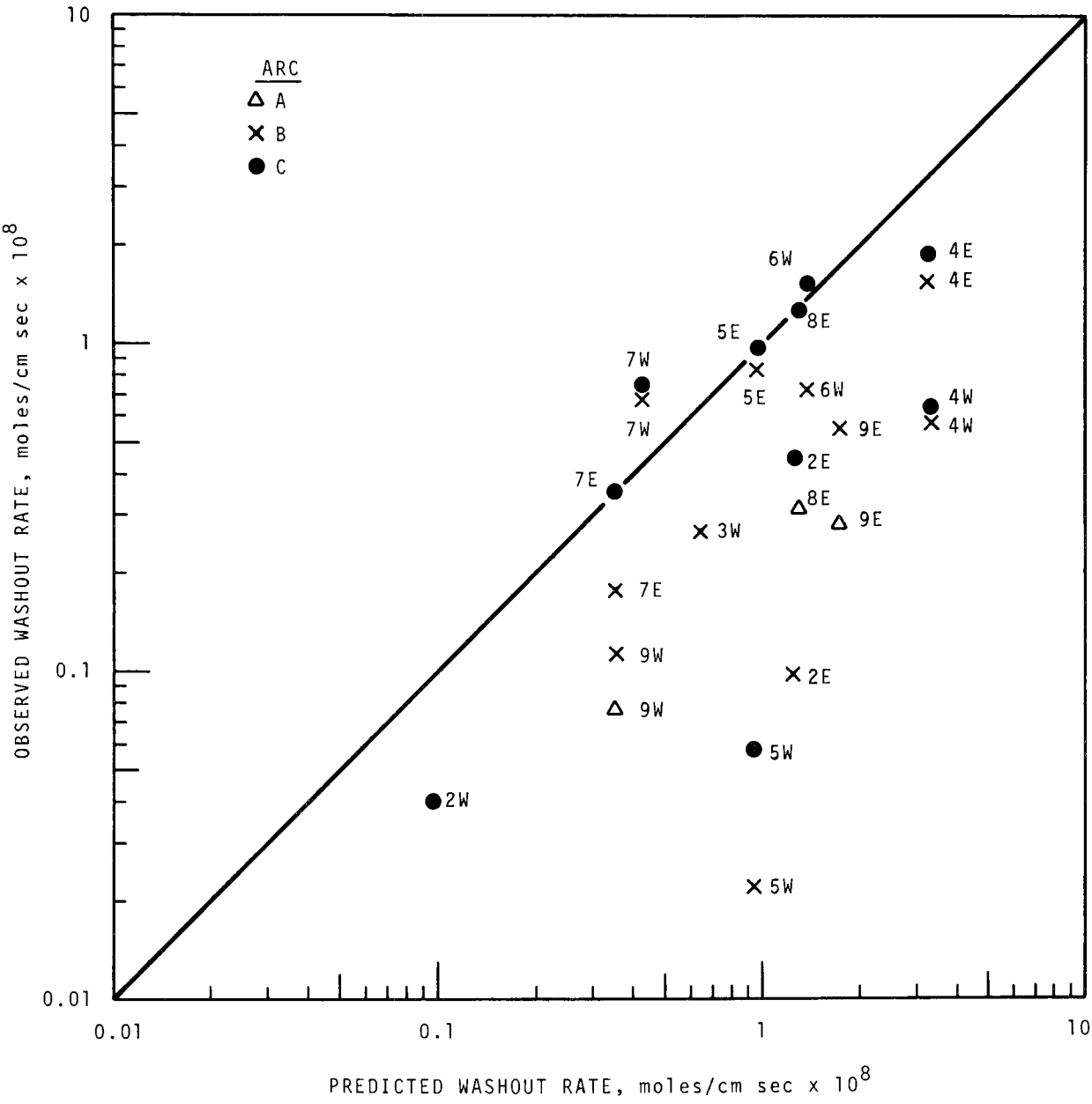

Figure 5.2 Comparison of Observed Washout Rates With Those Predicted From Washout-Coefficient Analysis

seen to lie above Engelmann's general curve, which was calculated with a generalized raindrop spectrum. The agreement within approximately a factor of two between the theoretical and experimental values for the 7.6 meter emission elevation emphasizes the importance of SO_2 desorption in the case of the higher elevation emission, where low concentrations of the gas occur beneath the plume centerline near the source.

The possibility that some of the collected rain passed into the system along trajectories below the SO_2 source was investigated. Obviously, such an effect would lead to the observance of lower washout for higher plumes and smaller downwind distances. An analysis of the rain trajectories for these experiments, however, has shown that such "blow under" effects were of small importance except for a few circumstances where rather severe conditions were encountered. These experimental results, therefore, are considered to be a strong confirmation of the occurrence of reversible sorption in SO_2 washout, and of the previous speculation that the washout coefficient is of reduced value for gases in general, which do not exhibit irreversible behavior except under rather specialized circumstances.

EQUILIBRIUM WASHOUT ANALYSIS

Chapter II has demonstrated that "equilibrium" washout poses a limiting case which is opposite to that characterized by washout coefficient theory. The usefulness of the limiting case can be tested, initially at least, simply by comparing measured SO_2 concentrations in rain with those predicted to occur if the rain were in diffusional equilibrium with SO_2 at the ground level plume concentrations present. In performing such a comparison, however, the question of the significance of plume fluctuations emerges as an important factor in the analysis. This question is a special case of a problem described previously[1], regarding errors arising from calculating washout in nonlinear systems on the basis of time-averaged concentrations of a fluctuating plume.* For the special case of true "equilibrium"

*It should be noted that this problem did not arise in the previous analysis using washout-coefficient theory, owing to the linear nature of this type of analysis.

washout this problem is simplified, since only the nonlinearities in the solubility relationship must be considered; furthermore, only the plume fluctuations at ground level are important to the analysis, since concentrations aloft have no direct bearing on SO_2 concentrations in rain at ground level, if equilibrium conditions prevail.

The effect of plume fluctuations on equilibrium washout may be demonstrated by referring to Figure 5.3, which is a solubility plot for SO_2 in water calculated for typical Ouillayute conditions from the relationships given in Chapter III. Since this plot is given on logarithmic scales, it is observed that any deviation from a slope of unity represents a nonlinear equilibrium relationship. To provide an example of this effect one can observe from this plot that a constant SO_2 concentration in air of 10^{-11} moles cc^{-1} will result in an equilibrium precipitation concentration of about 10^{-7} moles cc^{-1}. If the mean air concentration of 10^{-11} moles cc^{-1} were attained through precipitation exposure to an air concentration of 10^{-10} moles cc^{-1} for one-tenth of the sampling period and to clean air for the remainder of the time, however, the resultant SO_2 concentration in the sampled precipitation would be about 3.3×10^{-8} $moles^{-1}$ - a deviation that arises totally as a consequence of the nonlinear behavior shown by Figure 5.3. Consequently, time-averaged air concentrations are not totally appropriate in the determination of washout based on equilibrium with the surface air concentrations.

Owing to the complexities of actual plume fluctuations, an exact compensation for this effect would be extremely difficult. One way to partially correct for this behavior, however, is to break the description of the plume into individual descriptions for small time increments, thereby attempting to provide a more "instantaneous" definition of plume behavior. This was performed for conditions corresponding to one of the Ouillayute experiments (Run 4E) using anemometer data for consecutive 15-second intervals to compute ground-level plume and equilibrium rain concentrations. Average rain concentrations for the entire experiment were obtained by

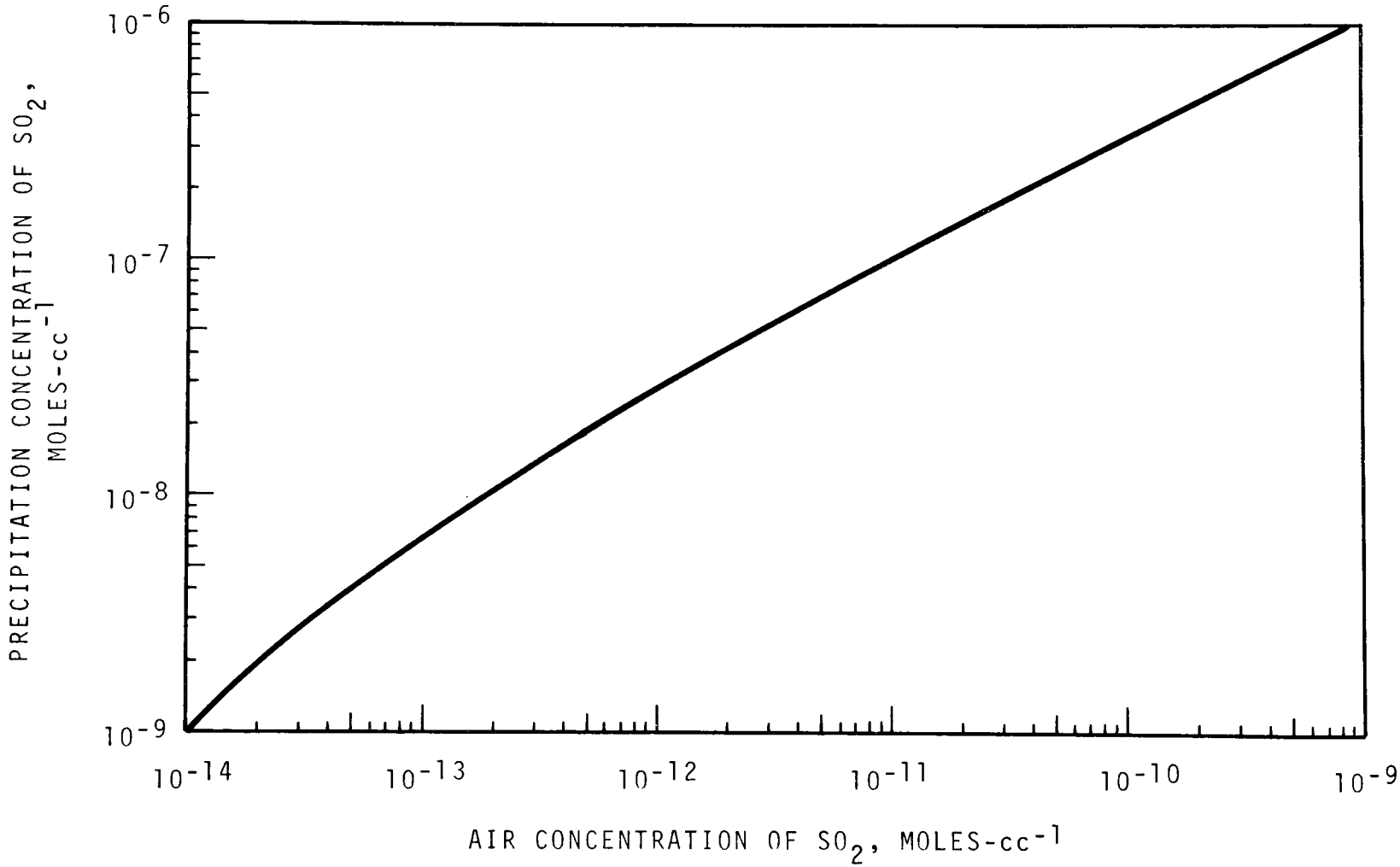

Figure 5.3 Solubility Relationship for SO_2 in Water at 10°C, pH = 5.5

adding the 15-second contributions distributed across the arc according to the individual 15-second mean wind directions.

These results are shown in Figure 5.4, which is a plot of ground-level rainborne SO_2 concentration as a function of crosswind distance. Here the equilibrium concentration predicted from the above incremental analysis, plotted as a solid line, is compared with that based on the simple time-averaged plume (plotted as circular points). Actual measured concentrations are shown as vertical bars for comparison. The magnitude of the deviation between predictions based on time-averaged and fluctuating plume models is striking; obviously plume fluctuations give rise to a first-order effect in this instance. It is interesting to observe that although the peak values are in close agreement, the predicted width of the washout distribution is greater than observed. The observed secondary peak is apparent in the calculated washout as well.

While there may be merit in this incremental analysis, it must be recognized as only a first-order approximation to instantaneous plume behavior. The associated calculations are rather laborious, and the choice of any fixed increment in time (e.g., 15 seconds) is arbitrary.

An additional technique for estimation of near-surface air concentrations appropriate for calculations of equilibrium washout in fluctuating plumes involves the use of "peak-to-mean" ratios. Some insight into the variability of instantaneous air concentrations relative to the mean concentration is provided by Hinds[12] and Ramsdell and Hinds[13] who measured short-term mean air concentrations (5 seconds and 38.4 seconds, respectively) during ground level emissions of 10 to 20 minutes. Their work indicates that the ratios of short-term to long-term mean air concentrations should vary from about 4 to 10 between the mean plume centerline and its edges. For elevated emissions, still greater rates are to be expected, owing to increased separation from the mean plume centerline. They show, furthermore, that short-term concentrations tend to be constant over a substantial crosswind region about the mean plume centerline. This suggests that the

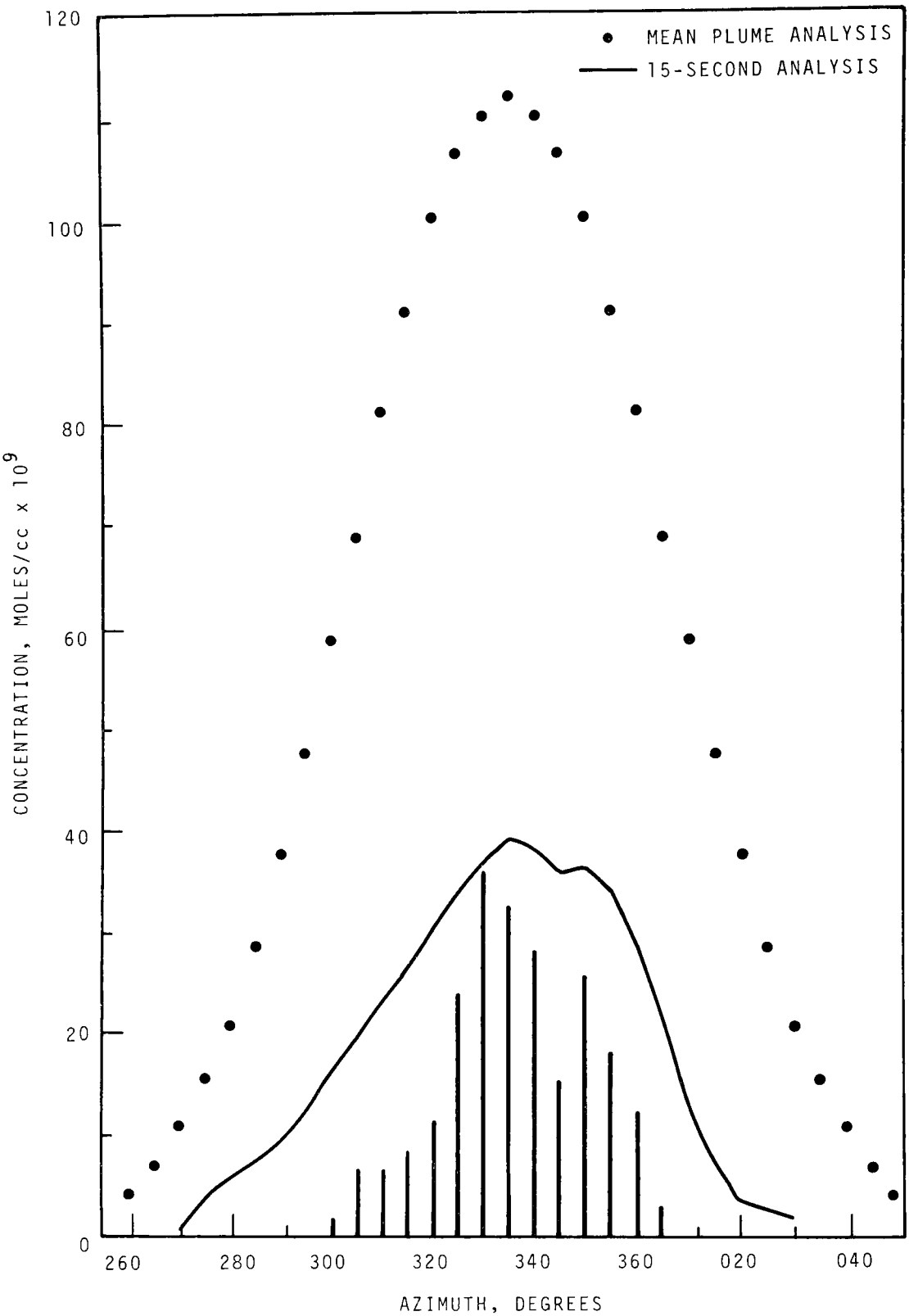

Figure 5.4 Time-Averaged SO_2 Concentrations in Rain Based Upon Equilibrium With Ground Level Plume Concentrations -- Mean Plume on 15-Second Incremental Analyses.

mean distribution arises largely from the frequency distribution of the instantaneous plume centerline location on the sampling arc. The peak-to-mean ratios, in conjunction with the mean air concentrations over the period of emission, can be used to define the peak concentrations in air at all crosswind arc positions and may be taken as the inverse of the probability of occurrence.

Peak-to-mean ratios extrapolated from the results of Ramsdell and Hinds[13] for short-term periods on the order of 5 seconds were applied to the calculated mean ground-level air concentrations for the periods of emission to obtain the peak air concentration values at each crosswind position. Equilibrium precipitation concentration values were then obtained using the solubility relationships of Chapter III (cf., Figure 5.3). These peak precipitation concentration values were divided, in turn, by the peak-to-mean ratios to obtain the mean precipitation concentrations of SO_2. Comparison of the results with observed values for Run 4EB is shown in Figure 5.5. The distributions are compared by superposing the peak values since this technique, unlike the previous one, does not account for the instantaneous wind direction. It is observed that the peak-to-mean analysis predicts equilibrium rain concentrations comparable to those predicted by the time-increment analysis, both analyses giving results that are close to those measured experimentally.

The peak-to-mean analysis was applied to all runs and the results are presented in Appendix B. These results are summarized in Figure 5.6, which is a comparison of observed washout rates with those that would occur if the rain were in equilibrium with the ground-level concentration as defined by the peak-to-mean relationship. It should be noted that the generally wider distribution of the predicted washout leads to calculation of washout rates higher than those observed, although predicted peak concentrations are generally lower than those measured experimentally. A similar plot, comparing observed washout with that which would occur with the rain in equilibrium with the time-averaged ground level concentration is given in Figure 5.7 for comparison. The measured washout rates are

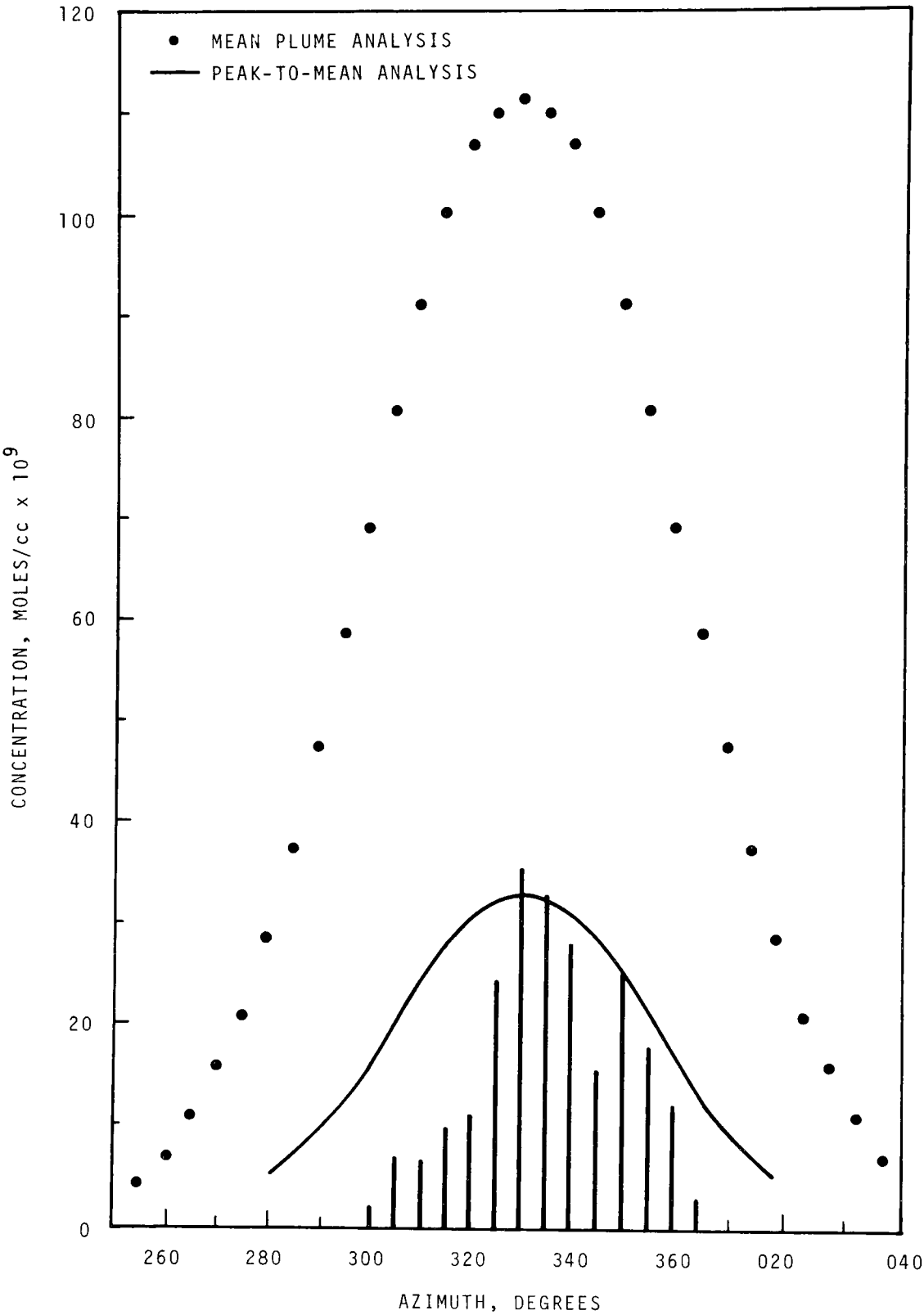

Figure 5.5 Time-Averaged SO_2 Concentrations in Rain Based on Equilibrium with Ground-Level Plume Concentrations -- Mean Plume and Peak-to-Mean Analyses

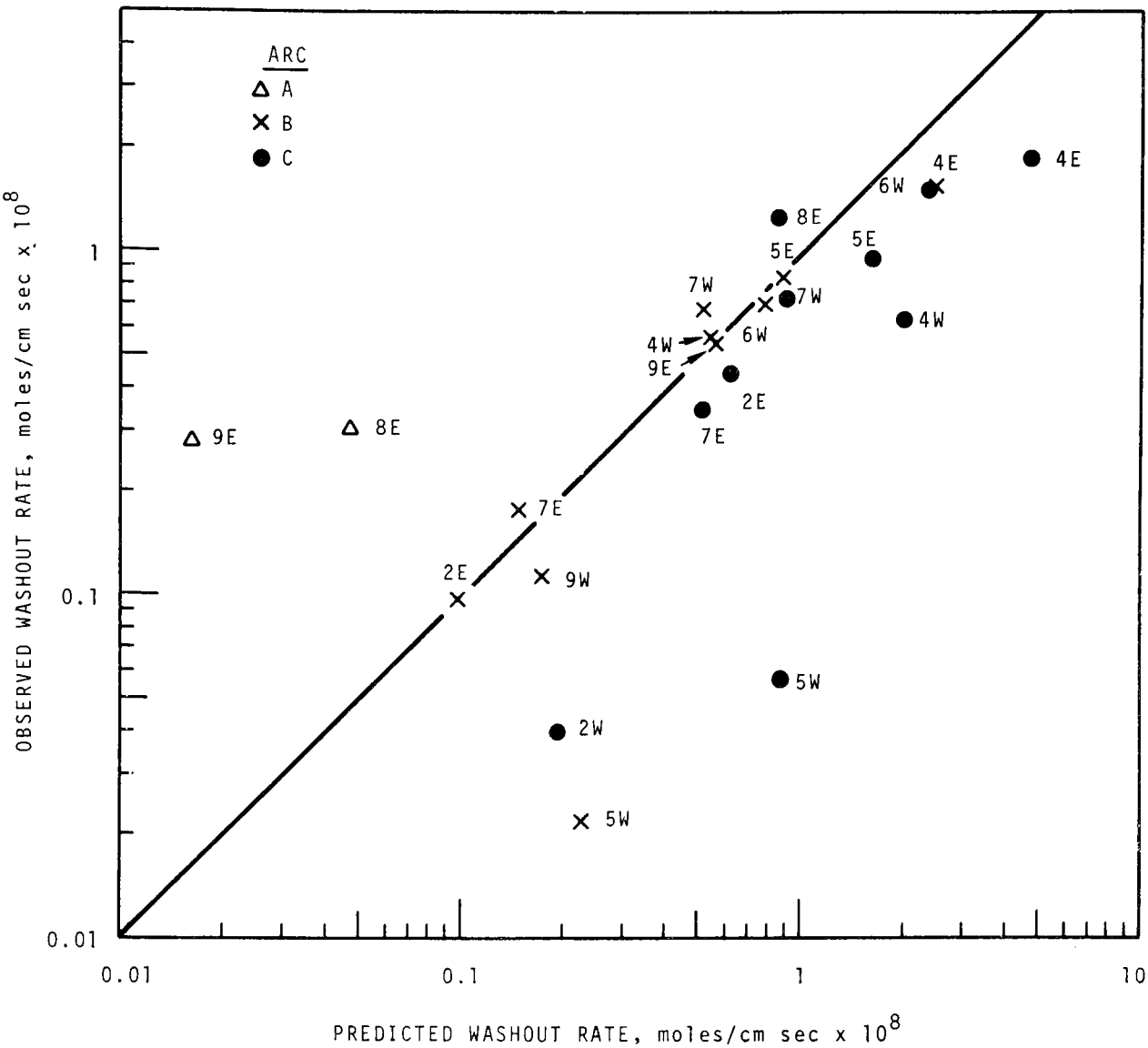

Figure 5.6 Comparison of Observed Washout Rates With Those Predicted from Peak-to-Mean Analyses

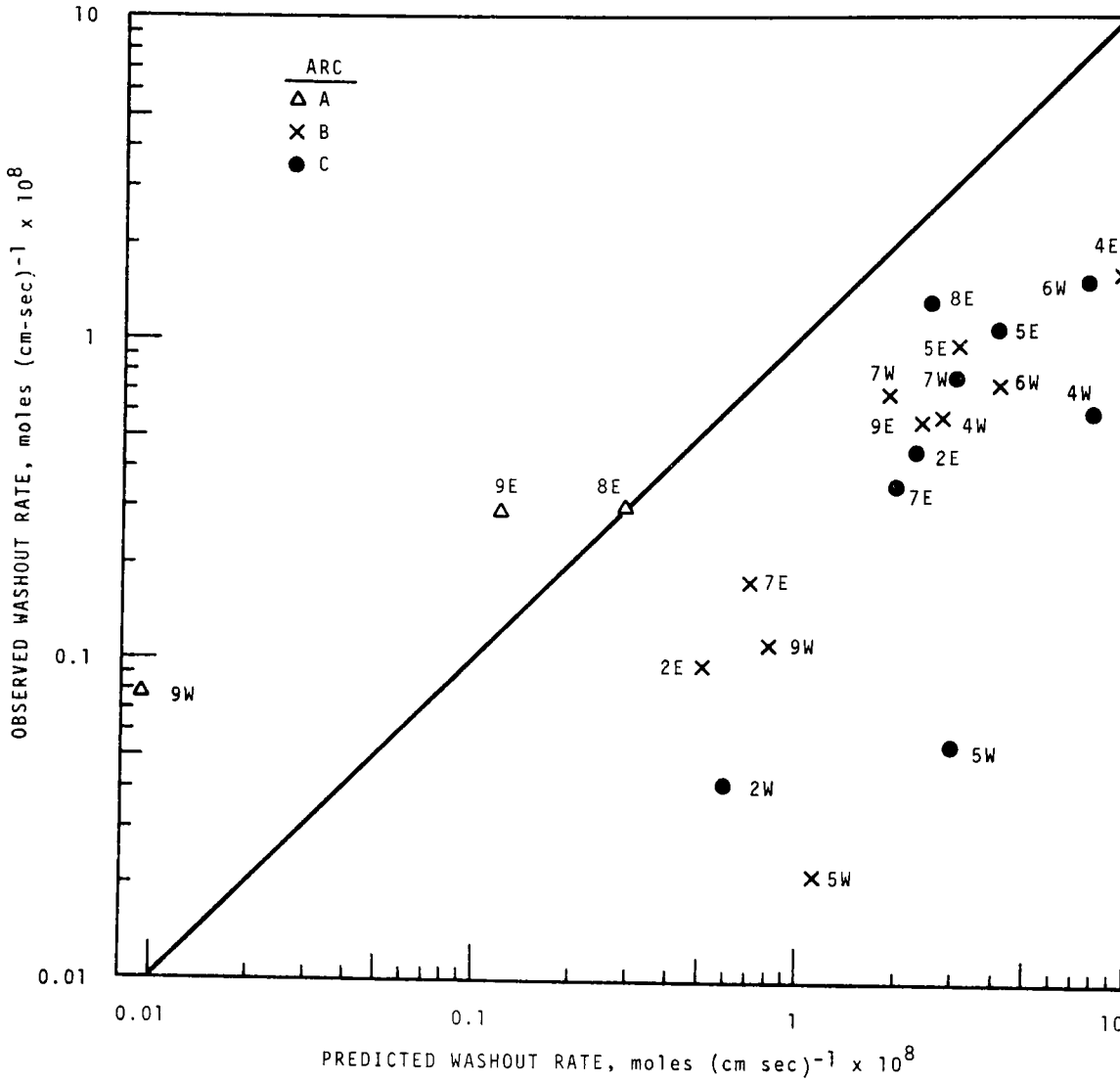

Figure 5.7 Comparison of Observed Washout Rates with Those Predicted on Basis of Equilibrium with Average Plume Concentrations at Ground Level

observed to fall much more closely to the peak-to-mean curve than to that obtained from the time-average analysis.

The criterion for equilibrium washout developed in Chapter II (Equation 2.26 and 2.28) predicts that for the conditions encountered at Quillayute, all falling raindrops should approach the ground at diffusional equilibrium only at downwind distances much greater than those at which sampling was performed. This apparent conflict with the findings of the peak-to-mean analysis requires further elaboration. Some possible explanations of this behavior are listed as follows:

1. The Chapter II criterion is in error, and mass transfer to and from the drops is much faster than has been assumed by this analysis;
2. The Chapter II criterion is not necessarily erroneous, but some artifact of the field sampling procedure (such as absorption or desorption of SO_2 by the fallen rain during its residence on the sampler-funnel surface) has distorted the measurements so that they tend to reflect some process other than washout; and,
3. The Chapter II criterion is essentially correct, but some effect not accounted for by these analyses occurs to make the observations coincide.

An example of the last explanation is simply that the rain is falling at diffusional disequilibrium, some drops being subsaturated with respect to the ground-level concentration while others are supersaturated. They then mix in the sample collectors to give an ensemble-average concentration close to the predicted equilibrium value. These possibilities will be examined in detail after presentation of results from the general models of SO_2 washout.

GENERAL MODELS OF GAS WASHOUT

The nonlinear model described in Chapter II has been utilized to calculate washout concentrations and downwind washout rates from input data corresponding to each of the Quillayute field tests. The input data and their

sources are summarized in Table 5.1. As discussed previously, the most important deficiencies of this model are:

1) time fluctuations in plume concentration are ignored,
2) time fluctuations in rainfall rate and direction are ignored,
3) redistribution of the plume is assumed negligible, and
4) the bivariate-normal plume distribution is assumed valid.

In addition it should be noted that this model accounts for SO_2 removal by washout only. Any dry deposition or reentrainment of SO_2, as mentioned previously, could alter the model's capability to predict natural behavior.

Predictions of the distributions of SO_2 concentrations in precipitation are compared in Appendix C with the observed results on each sampling arc for all runs (Figures C.1 - C.18). These curves pertain to the general model predictions based on gas-phase limited mass transfer and on the opposite limiting case of stagnant-drop behavior (cf., [1]). The predictions are compared with measured concentrations (represented by vertical bars) and with concentrations of SO_2 that would exist if the sample were in equilibrium with the calculated average ground-level gas phase concentration (denoted by circles). The results are "centered" by aligning the highest experimental values with the midpoints of the computed distributions. Stagnant drop mass-transfer coefficients for these computations were estimated using the linearized equation[16]

$$k_x = \frac{5\, D_{Ax}\, c_x}{a} \quad , \tag{5.3}$$

rather than solving the complete diffusion equation presented in the previous report[1]. This simplification was utilized in the face of excessive computation time required by the more exact alternative procedure. It is expected that this measure was of little consequence in influencing the final computed results.

TABLE 5.1

INPUT TO NONLINEAR NONFEEDBACK MODEL

Physical Parameters	Values Used in Model	Reference
Source Parameters: Height, Strength	Table 4.1	
Wind Parameters: Velocity, σ_ϕ, σ_θ	Table 4.5	
Precipitation Parameters: Rate, Size Spectra	Tables 4.1 and 4.2	
Receptor Parameters: x,y,z	Bucket Locations	
Solubility Parameters	Solubility Equation of Chapter III	
Transport Parameters:		
SO_2 Diffusivity in Air	.136 cm^2/sec	(14)
SO_2 Diffusivity in Water	9×10^{-6} cm^2/sec	(15)
Kinematic Viscosity of Air	.133 cm^2/sec	(14)

As discussed previously[1] limiting cases representing the extreme mass-transfer coefficients should bracket washout behavior. Limiting values of mass-transfer coefficients do not necessarily correspond to limiting washout concentrations; however, they should provide reasonable estimates of these limits under present circumstances. Provided the model and test data are valid, therefore, measured washout concentrations might reasonably be expected to fall somewhere between the solid and dashed lines in the figures.

Figures C.1 - C.18 provide point concentrations which may be integrated across the plume to obtain washout rates, as defined by Equation (2.9). A comparison of these values is shown in Figure 5.8, which is a plot of predicted versus observed washout rates. As in the previous integration of the equilibrium concentration distribution, the excessive width of the distribution tends to increase the calculated washout rate values. Here the limits on the tielines pertain to gas-phase limited and stagnant drop behavior as calculated using the nonlinear model.

It is also of interest to compare the results with the predictions of the simpler linear model, which was described in Chapter II. This model has the advantage of being amenable to hand calculation, provided that the raindrop size distribution is simplified in some acceptable manner. Here the mass-mean drop size was assumed, rather arbitrarily, to characterize the rain spectra. The linearized solubility parameter H' was chosen, again rather arbitrarily, as the mean between the centerline and ground level values beneath the plume axis at the downwind distance of the ground level receptor, as calculated using the procedures of Chapter III. The results are shown in Figure 5.9, a scatter diagram similar to that used previously to evaluate the more sophisticated nonlinear model. The results exhibited by this figure, as expected, are somewhat more scattered than those shown for the nonlinear model. The agreement is still rather good, however, in view of the related assumptions and the potential for uncertainty in the input data.

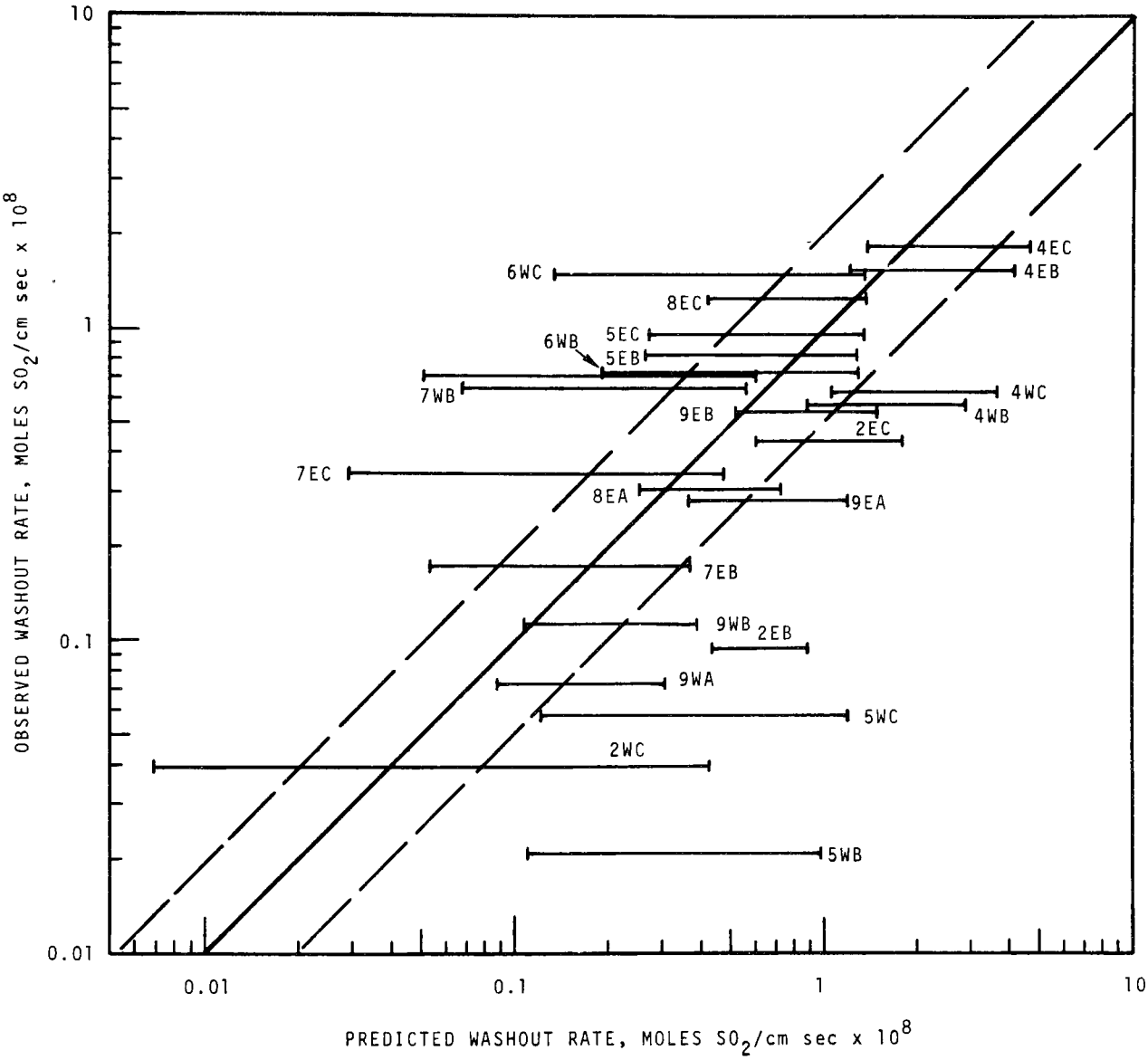

Figure 5.8 Comparison of Observed Washout Rates With Those Predicted by Nonlinear, Nonfeedback Model

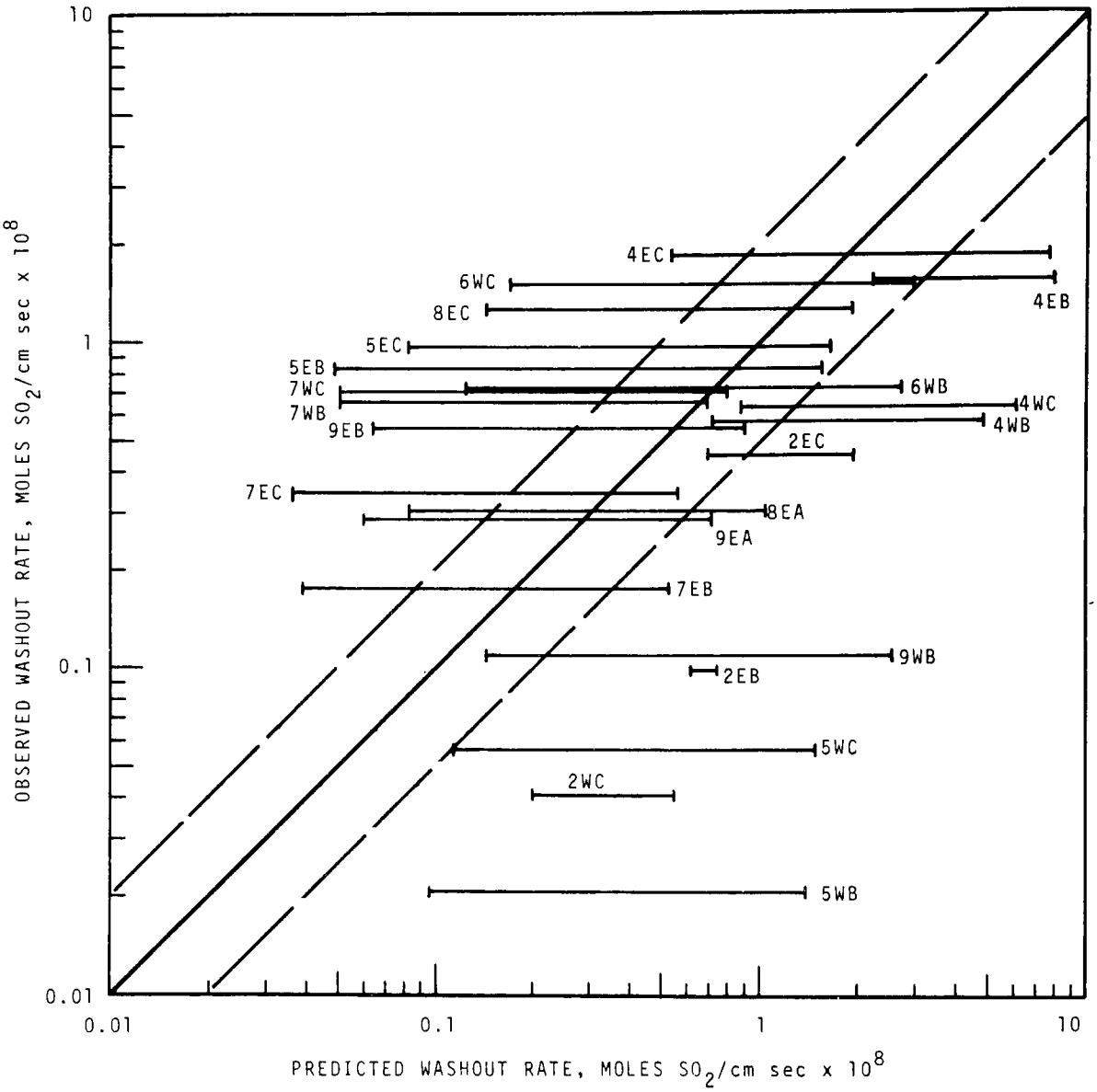

Figure 5.9 Comparison of Observed Washout Rates With Those Predicted by Linear, Nonfeedback Model

Comparison with Figures 5.1 and 5.6 indicates that the general model predictions show much better agreement than those of the washout-coefficient analysis, and in most cases agreement that is comparable to that given by the peak-to-mean analysis of equilibrium washout. In comparing with the equilibrium-washout analysis, however, it must be noted that this technique attempted to compensate for the effects of plume fluctuations. Since the general models are based upon time-averaged plume concentrations such a comparison is questionable, at least until some indication is given regarding the adequacy of the mean-plume assumption for modeling purposes.

Applicability of the mean-plume assumption to the general washout models was tested using the results for Run 4E, attempting to approximate instantaneous plume behavior by subdividing the experiment period into 15-second increments as described previously. Calculation for these individual time increments with subsequent recombination for the total run resulted in the predicted SO_2 concentration distributions shown in Figure 5.10. As shown by this diagram, the calculated concentrations based on the 15-second approximation to the fluctuating plume do not deviate markedly from those based on the average plume - a somewhat surprising outcome in view of the large deviations in the corresponding equilibrium curves (Figure 5.4). This undoubtedly is due in part to the complete dependence of the equilibrium analysis on air concentrations immediately above the sampler, whereas for the model the entire plume depth influences the washout. Thus while the lateral plume shift modifies the model prediction, it is less sensitive than the equilibrium analysis to large changes in the vertical distribution. Owing to the large amounts of computer time involved, similar analyses were not completed for the other Quillayute tests. It was concluded on the basis of Figure 5.10, however, that the mean-plume assumption was reasonably appropriate for comparison of the general models under present circumstances.

All computations presented thus far have pertained to ground-level elevations. For a general appreciation of the washout process it is of interest to observe also the predicted concentrations of pollutant in rain at different

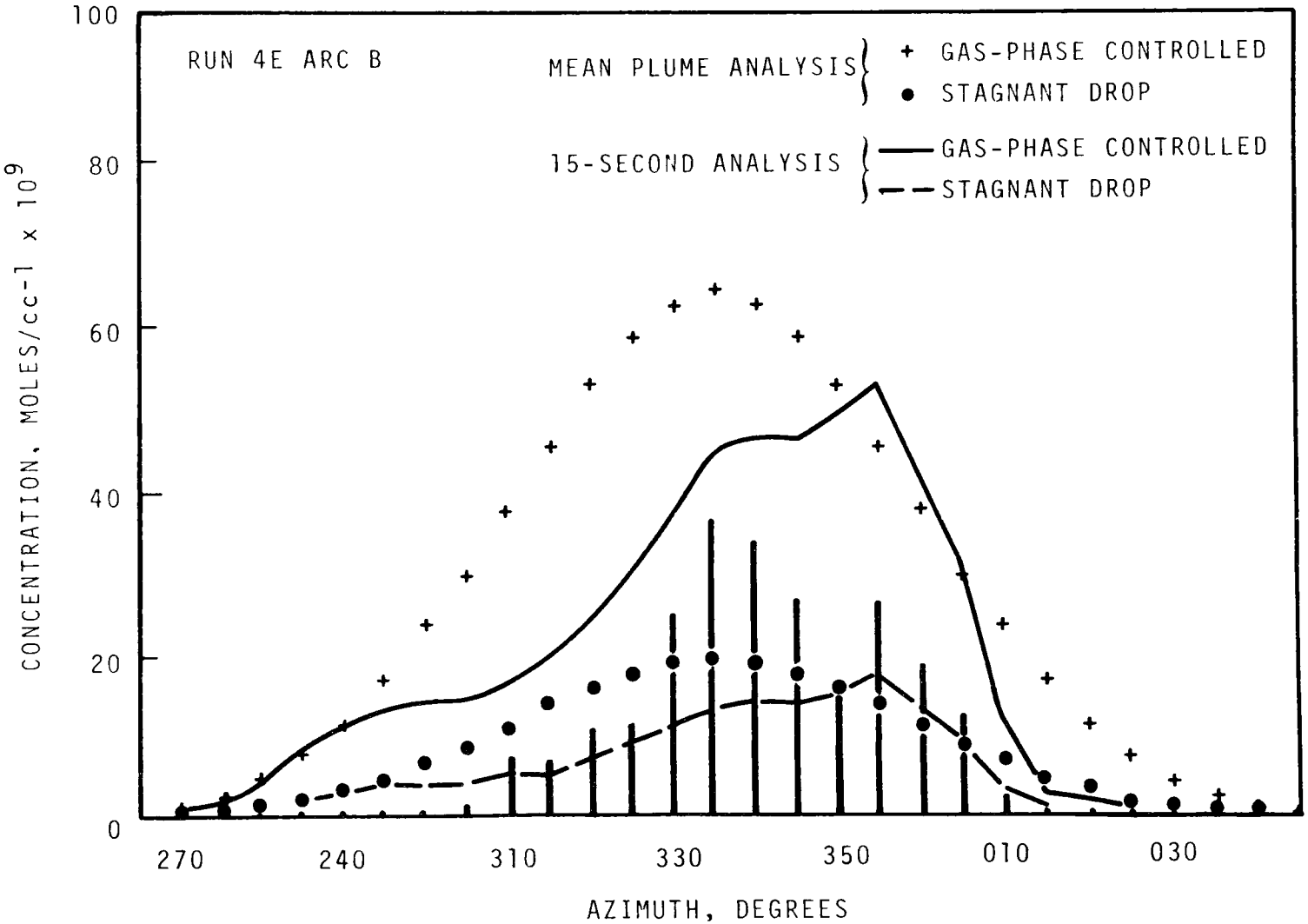

Figure 5.10 Predictions by Nonlinear, Nonfeedback Model for Time-Average and 15-Second Incremental Analyses

elevations during its fall through the plume. As mentioned in Chapter II, the algorithm for the nonlinear model computes these values enroute to obtaining final ground-level results. Such values, computed from the nonlinear model for Run 4WB, are shown for three different drop sizes in Figure 5.11. Here the SO_2 concentration in the drops is plotted (as solid lines) versus height of the drop above ground. The dotted lines denote the concentration that a drop would have if it were in continual equilibrium with the ambient mean gas-phase concentration, giving a representation of the gas-phase concentration experienced by the drop during its fall. The dotted lines are different for each drop size, of course, owing to the different trajectories of fall.

Observing the curves for the smallest (.0299 cm diameter) drop one should note the relatively rapid response of the drop as it attempts to approach diffusional equilibrium. During the drop's fall its concentration first increases with plume concentration (absorption) and then decreases (desorption) until it reaches the ground, almost in equilibrium with the ground-level plume concentration. The curves for the intermediate (.107 cm diameter) drop indicate considerable lag between the plume and drop concentrations; here, however, the drop has absorbed sufficient SO_2 so that is unable to lose enough by desorption to approach equilibrium conditions at ground level. It therefore approaches the ground appreciably supersaturated with respect to the ground level plume concentration.

The curve for the largest (.186 cm diameter) drop illustrates a prediction of the general washout models which is likely to be important in explaining some of the observations of the Quillayute experiments. Namely, this model predicts that a drop does not necessarily have to be highly responsive to mass transfer in order to approach the ground in a state close to equilibrium. As seen from the curve, the drop responds to the gas phase concentration in a sluggish manner, but the fact that the plume concentration decreases in the vicinity of the ground actually brings the two curves close together at ground level, that is, a near "psuedoequilibrium" washout condition is predicted.

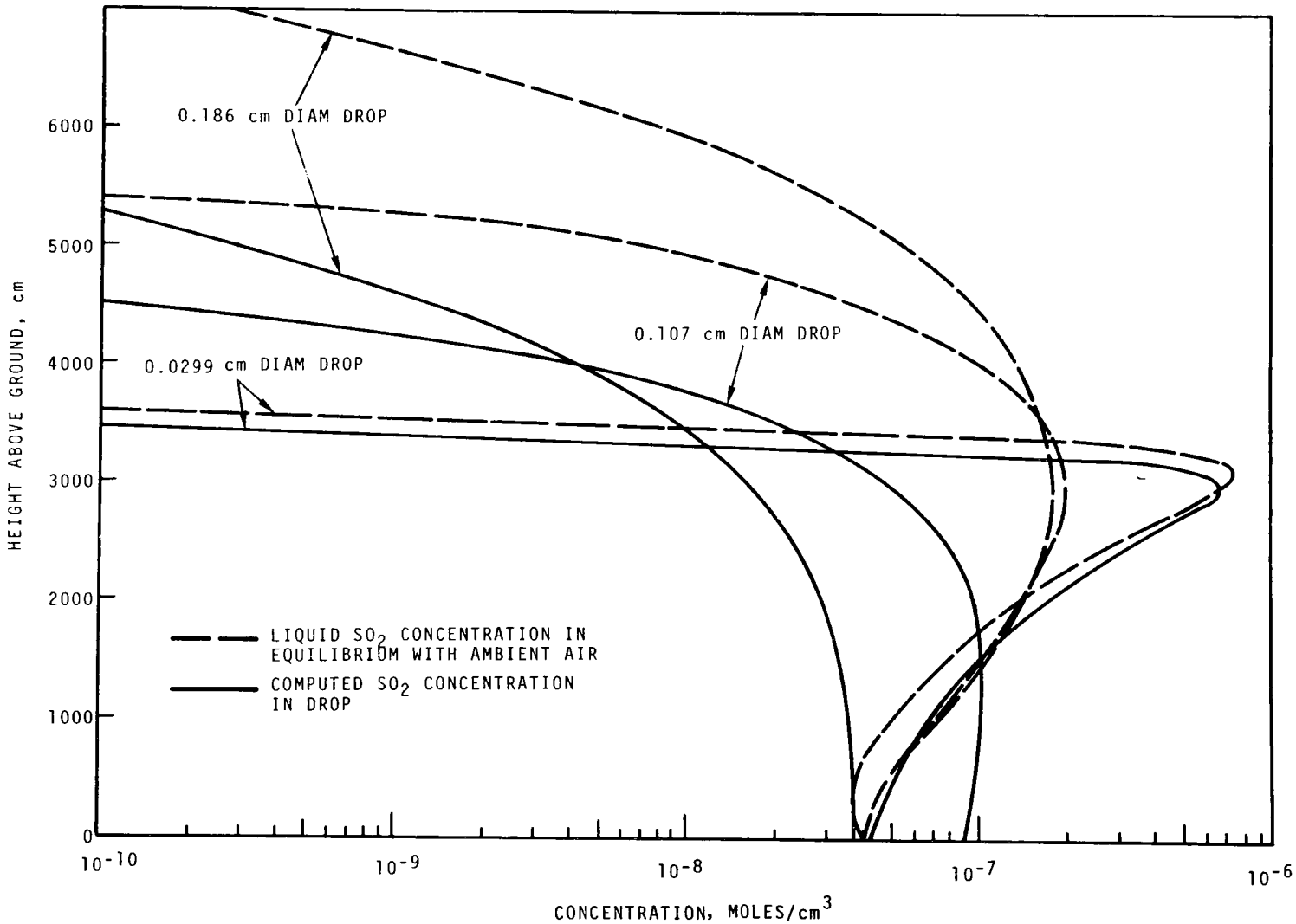

Figure 5.11 Computed Concentrations in Drops as a Function of Vertical Position - Run 4WB, Gas-Phase Limited

Predicted ground-level concentration is shown as a function of drop size in Figure 5.12, which pertains to gas-phase limited conditions for Run 4WB. From this it is seen that, according to the nonlinear model, the concentrations can vary considerably above and below the average of the ensemble, which may fall close to the equilibrium value. One can easily explain the reason for the maximum concentration value at intermediate drop size and the approach to equilibrium from Figure 5.10. The peculiar dip in concentration at small drop sizes occurs primarily because of the slight exposure to the plume by drops drifting in at small angles.

It is emphasized that the curves in Figures 5.11 and 5.12 pertain to specific hypothetical conditions, and curves for other rain-plume conditions may vary widely. In particular, the situation visualized to develop the equilibrium washout criteria (where all drops are sufficiently responsive to achieve true equilibrium conditions), would be characterized by a concentration curve lying exactly on the equilibrium line, rather than displaced above and below as shown in Figure 5.12.

An examination of the computer output for the experiments wherein both the nonlinear model and the peak-to-mean equilibrium analysis agree well with experiment shows that a combination of the above two effects contributed significantly in creating a prediction of near-equilibrium conditions in the mixed samples. Thus it may be concluded that, under conditions where this agreement exists, there is no real conflict between the final results and the precepts of the nonlinear model, or indeed, those of the equilibrium washout criterion.

DISCUSSION

The overlap in predictions by the general model and the equilibrium analysis limits the extent of any meaningful conjecture concerning the effects of absorption or desorption of SO_2 by rain on the collector surfaces. Obviously, if the incoming rain is close to equilibrium, little driving force will exist to encourage this process. Some information in this regard, however, may be

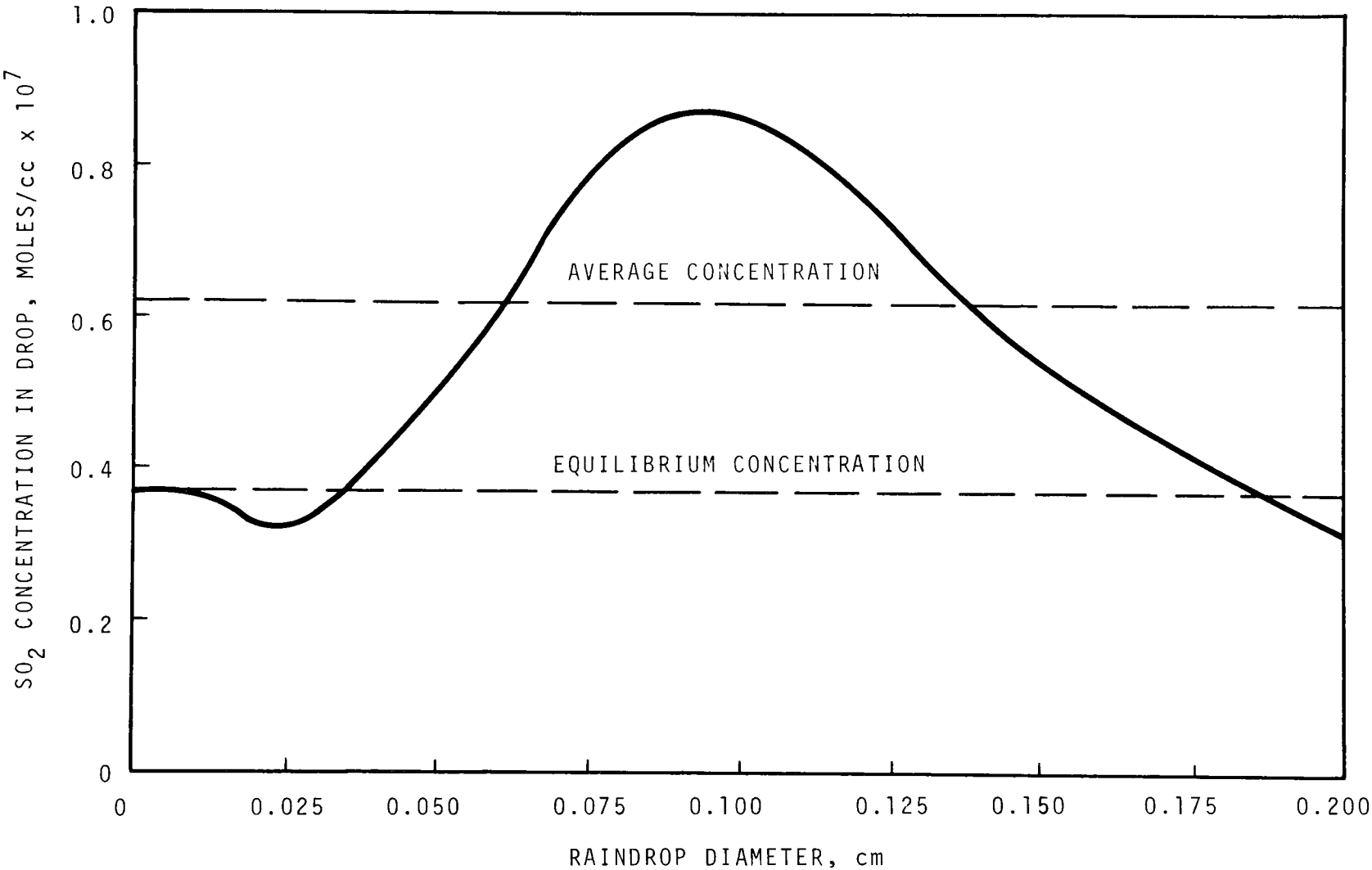

Figure 5.12 Computed Ground-Level SO_2 Concentrations in Rain as a Function of Drop Size -- Run 4WB, Gas-Phase Limited

obtained by examining the few data points in Figure 5.6 where poor agreement between the equilibrium analysis and experiment occurs. In particular, experiments 8EA, 9EA, and 9WA provide washout rates that are much greater than predicted by the peak-to-mean equilibrium analysis. Ostensibly this is explained by the short downwind distance of arc A, which results in relatively low ground-level concentrations. The drops entering the collectors apparently have brought down sufficient quantities of SO_2 from aloft to be substantially supersaturated at ground level. This conjecture is reinforced by noting that the general model (cf., Figure 5.8) predicts washout rates that are in reasonable accordance with those observed for these experiments. Apparently desorption of SO_2 at the funnel surfaces was not sufficient to cause an appreciable effect in these instances.

Experiments 5WB and 5WC provided results that agree poorly with both the general model and with the equilibrium analysis. The reason for this is unclear, although measured gas-phase concentrations were also low for this experiment, indicating a failure to describe the plume in a satisfactory manner. Regardless of this, the discrepancy appears to arise from a factor common to both analyses and cannot, therefore, be attributed to perturbations at the collector surfaces.

In a final analysis it is concluded that, for the most part, the field observations are predicted reasonably well by both the general models and the equilibrium analysis. The general models provide an explanation for this virtual overlap in prediction, and tend to give more satisfactory results for the few experiments where conditions leading to overlap did not exist. The relatively good agreement between the general models and experiment suggests that these models will be useful as basis for analysis of future experiments involving power-plant plumes.

The experimental results of the present study have enabled the conclusion that washout of SO_2 is indeed a reversible phenomenon, and that the washout-coefficient approach is generally invalid for these conditions. Although the results indicate that absorption and desorption on the collector surfaces

is an unimportant factor in most cases, these data are insufficient to resolve this question completely; direct experimental confirmation is needed prior to drawing final conclusions in this regard.

CHAPTER VI

ISOLATED DROP EXPERIMENT

Because of its basic importance to washout, an experiment has been designed to measure the overall mass-transfer coefficient, K_y. Such data, if available, could be used with the models to compute washout rates directly, rather than applying the presently used technique of "patching" solutions by definition of limiting behavior.

The major effort on this project so far has been the selection and design of the experiment. Experiments involving sprays and supported drops were ruled out immediately because of difficulties with unnatural perturbations in such systems. The decision between employing a falling drop experiment or an experiment wherein the test drop would be suspended by an upward flow of air was more difficult. Both types of experiments share the advantage of maintaining the drops under near-natural conditions; they do, however, have some rather critical disadvantages as well.

The major question concerning the suspended drop type of experiment is whether or not the upward flow of suspending air exhibits flow (particularly shear and/or turbulence) properties which may cause behavioral deviations between the experimental drop and a natural raindrop. Such effects apparently do occur if the drops are suspended in a vertical, tapered tube (a rotameter tube, for instance) wherein the dimensions of the drop and the tube diameter are similar. Kinzer and Gunn[17] found that water evaporation rates measured with such an experiment did not compare well with known values unless the ratio of the tube bore to the drop diameter exceeded two. This should obviously preclude any future use of tapered tube support columns under conditions where this ratio is low. Situations involving higher ratios are also suspect if liquid-phase phenomena are being observed. Kinzer and Gunn's study involved the transport of water from the drop surface to the ambient atmosphere, and was therefore essentially a gas-phase experiment. The present experiment,

which is devoted primarily to the investigation of liquid-phase phenomena, is expected to be more sensitive to distortions in gas-flow behavior. This may be seen intuitively by noting that there is a distinct velocity profile across the bore of a tapered support tube - if this is a small tube the profile will be nearly parabolic. A drop suspended on such a flow will tend to fall to one side of the tube to a region of lower velocity, resulting in a spin-inducing shear across the drop. By virtue of this spin, the Magnus effect will tend to counteract the force inducing the drop toward the wall, and ultimately a rather complex force equilibrium will exist.

Since internal circulation of the drop is dependent directly upon exterior flow behavior it is probable that liquid-phase mass-transfer coefficients measured in tapered tube experiments will tend to deviate markedly from natural values. This becomes especially apparent when it is observed that, owing to the low magnitudes of liquid molecular diffusion coefficients, any perturbation in convection behavior will have a marked effect upon modifying mass transfer rates. This contrasts to the gas-phase situation, where diffusion coefficients are usually about four orders of magnitude higher and reduce the relative effects of any changes in flow pattern.

Suspended drop experiments involving vertical wind tunnels of large cross sections are more attractive than the tapered tube type of experiment. These maintain the drop in the vertical flow of air by creating a "well" in the velocity profile near the center of the system. The shear field in the well region is much less intense than that in a small diameter tube, resulting in more nearly natural conditions. The question of perturbations to the drop by tunnel-induced turbulence is not completely resolved at present. It appears, however, that the turbulence can be maintained at levels low enough such that its effect is negligible, particularly if the spectra are not characterized by large powers at amplitudes of the order of the drop size or less. This has been substantiated in part through the work of Garner and his coworkers[18], who photographed oscillitory behavior of drops suspended in such systems.

A practical difficulty with suspended drop experiments is their small sample size, which makes the problem of analysis a rather difficult one. A 0.03 cm drop, for instance, has a volume of about 10^{-5} cm^3, and would necessitate an SO_2 concentration of 0.1 moles/ℓ to be detectable by conventional methods. Since concentrations of present interest range between 0 and 2×10^{-4} moles/ℓ, some rather elaborate means of measurement would be required.

Such a difficulty could be counteracted in part by catching multiple drops and combining them for analysis. Although this can be accomplished with a suspended drop apparatus, multiple drop samples can be acquired in a more natural way using an isolated, falling drop type of experiment. Falling drop experiments are attractive also because they allow the drops to fall under near natural conditions, avoiding the aforementioned problems with external flow conditions.

The major problem with falling drop experiments insofar as liquid phase measurements are concerned is simply their size. Because of nonlinear responses, measurements of gas mass-transfer coefficients must be acquired for all stages of concentration buildup; for the larger drops this may require fall distances of the order of hundreds of meters, not including the several meters of fall necessary to stabilize the drops and allow them to approach terminal velocity prior to their exposure to the test atmosphere.

The largest drop experiment reported in the literature is that of Kinzer and Gunn, which involved a vertical drop tube 200 meters in length. All other reported experiments have been smaller in scale, and, accordingly, have been of limited value insofar as liquid-phase mass-transfer measurements are concerned. A summary of the pertinent literature on suspended and isolated falling drop experiments is given in Table 6.1.

The preceding considerations indicate that a vertical wind tunnel suspended drop system, rather similar to the one employed in the studies by Garner and his coworkers, is most appropriate for present purposes. Shown

TABLE 6.1

ISOLATED DROP EXPERIMENTS

Type of Experiment	Drop Composition and Size Range	Gas Composition	Method Of Analysis	Author(s)
Suspended drop, in vertical wind tunnel. Suspension Times: 2 - 2000 sec	Water, Dekalin, Kerosene, Mentor 28 (fuel oil) Transformer oil,	0.5 mole-fraction CO_2 in air	Chemical	Garner and Lane [18]
	Glycerol, propylene glycol, ethylene glycol	Controlled H_2O vapor at 80 - 110°F in air.	Refractrometric	
	2.9 - 5.9 mm			
Suspended drop in tapered tube Suspension Times: 15 - 2500 sec	Water 1.2 - 1.5 mm	DHO - H_2O, saturated in air at room temperature	Mass-spectroscopic	Friedman, Machta, Soller [19]
Suspended drop, in tapered tube, and on "free" support.	Water 0.4 - 4.5 mm	Air	Gravimetric	Kinzer and Gunn [17]
Suspended drop in vertical wind tunnel. Suspension Times: 0 - 600 sec	Water	Air, THO	Scintillation counter	Mensing and Schügerl [20]
Drop Tube, Approx. 50 cm long	Water	NH_3	Chemical	Hatta and Babba [21]
Drop tube, 200 cm long	Water 4 - 6 mm	.95 mole fraction CO_2 in air	Chemical	Dixon, et al. [22, 23]
Drop tube, 165 cm long	Water 2.5 5 mm	Pure CO_2	Chemical	Hughes and Gilliland [24]
Drop tube, 200 cm long with 800 cm acceleration column	Water 2.2 4.2 mm	.06 mole fraction NH_3 in air, pure CO_2	Chemical	Shabalin [25]
Drop tubes, 200 cm long and 800 cm long	Water, saturated with CO_2	Air	Chemical	Guyer, et al. [26]
Drop tube, 70 cm long	Various amines and amine-water solutions, 1.3 - 1.6 mm	.05 to 1 mole fraction CO_2 in air	Differential pressure	Goodridge [27, 28]
Drop tube, 168 cm long	Solutions of H_2SO_4, NaOH, and NaOH H_2O_2 In Water 2.6 6.0 mm	.015 - .031 M.F. NH_3 .022 - .026 M.F. SO_2 .018 - .021 M.F. HCl .021 .048 M.F. CO_2 .021 - .029 M.F. H_2S In Air	Chemical	Johnstone and Williams [29]
Drop tube, 52 cm long	Water 2.7 2.8 mm	Pure CO_2 .43 .49 M.F. NH_3 in air .0007 .0030 M.F. H_2S in air	Chemical	Whitman, Long, and Wang [30]
Drop tube, 20,000 cm long (evaporation of drops)	Water .04 - 1.0 mm	Air	Gravimetric, photographic	Kinzer and Gunn [17]
Drop tube, 200 cm long with 1,000 cm adjustment height	Water 4 mm	Pure CO_2		Shabalin [25]

in Figure 6.1 this system utilizes a circulating flow driven by an internal blower. Temperature of the gas is controlled precisely by a compact heat exchanger, located just downstream of the blower. From this region the gas progresses through various turbulence control devices up to the tapered test section containing the drop formation and catching equipment. From this point the gas recirculates through flow control and metering devices, and finally back to the blower intake. SO_2 will be injected into the system through the ports as shown. Humidity will be controlled at saturation.

Experimental runs would begin by suspending a drop in clear air for a period of time until stabilization is complete. The SO_2 would then be turned on and the drop allowed to experience a simple function (e.g., a "step" or a "ramp") of concentration in time. Drops will be removed and analyzed after varying exposures to assess mass-transport behavior.

The most important problem involved with this experiment is that of analysis. It was first anticipated that this would be overcome by employing a radioactive tagging method; this, however, was discouraged because of severe associated difficulties including the large complexity and expense involved with the rather high levels of radioactivity required. Accordingly, it appears advantageous to employ a chemical microanalytical technique. At present the techniques of chemical conversion and analysis by microcoulometry or electron capture are under investigation, and it is expected that one of these will be developed for ultimate use with the experiment.

It was expected initially that construction of the experiment would be begun immediately. Recent findings from the modeling component of this project, however, suggest that it may be more beneficial to postpone this work until a later date, thereby allowing a total effort to be placed on field work and modeling in the immediate future. For this reason the isolated-drop experiment will be held at the present stage until future field tests are completed and interpreted.

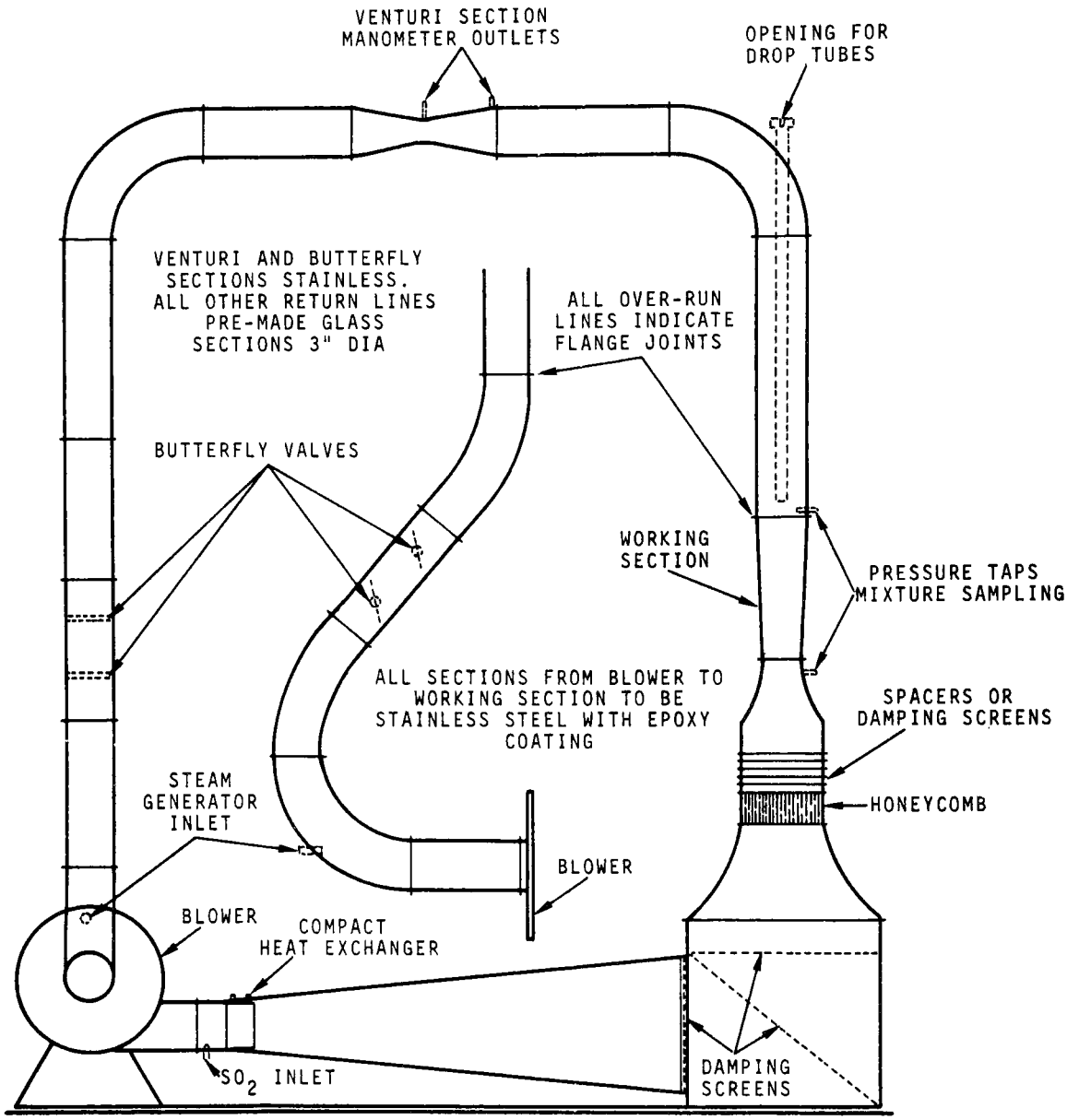

Figure 6.1 Schematic of Suspended-Drop Apparatus

CHAPTER VII

EVALUATION AND CONCLUSIONS

In evaluating the accomplishments described in this report it is appropriate to review the total washout program conducted to-date, indicating its direction and objectives, and describing briefly suggested plans for the continuing study. The perspective of the program is indicated by the chart in Figure 7.1, which shows portions of the program that have been completed as well as those that are in progress or suggested for the near future. As shown by the chart, each of these segments is related to the ultimate objective of establishing reliable models and correlations for calculating atmospheric scavenging of sulfur compounds under general atmospheric conditions.

The progress chart in Figure 7.1 begins with the initial Keystone washout study, which provided experimental results leading to a revision of the previously accepted theories of gas washout. This revised theory, while qualitatively in accord with experimental findings, indicated that interactions between various atmospheric phenomena were so complex that simpler studies were required for verification. For this reason, the current program consists essentially of three parts, including a modeling component, a laboratory component involving measurement of the basic physical parameters of interest, and finally, a field component consisting of controlled experiments conducted under natural atmospheric conditions.

Tentative plans for future work are shown schematically in the remainder of the chart. These are itemized in the following discussion.

1. The modeling program will continue in its development, and (at a later date), mass-transfer parameters will be measured using the single drop experiment.
2. A program will be initiated to investigate in more detail the significance to scavenging of the interaction between stack and cooling tower plumes.

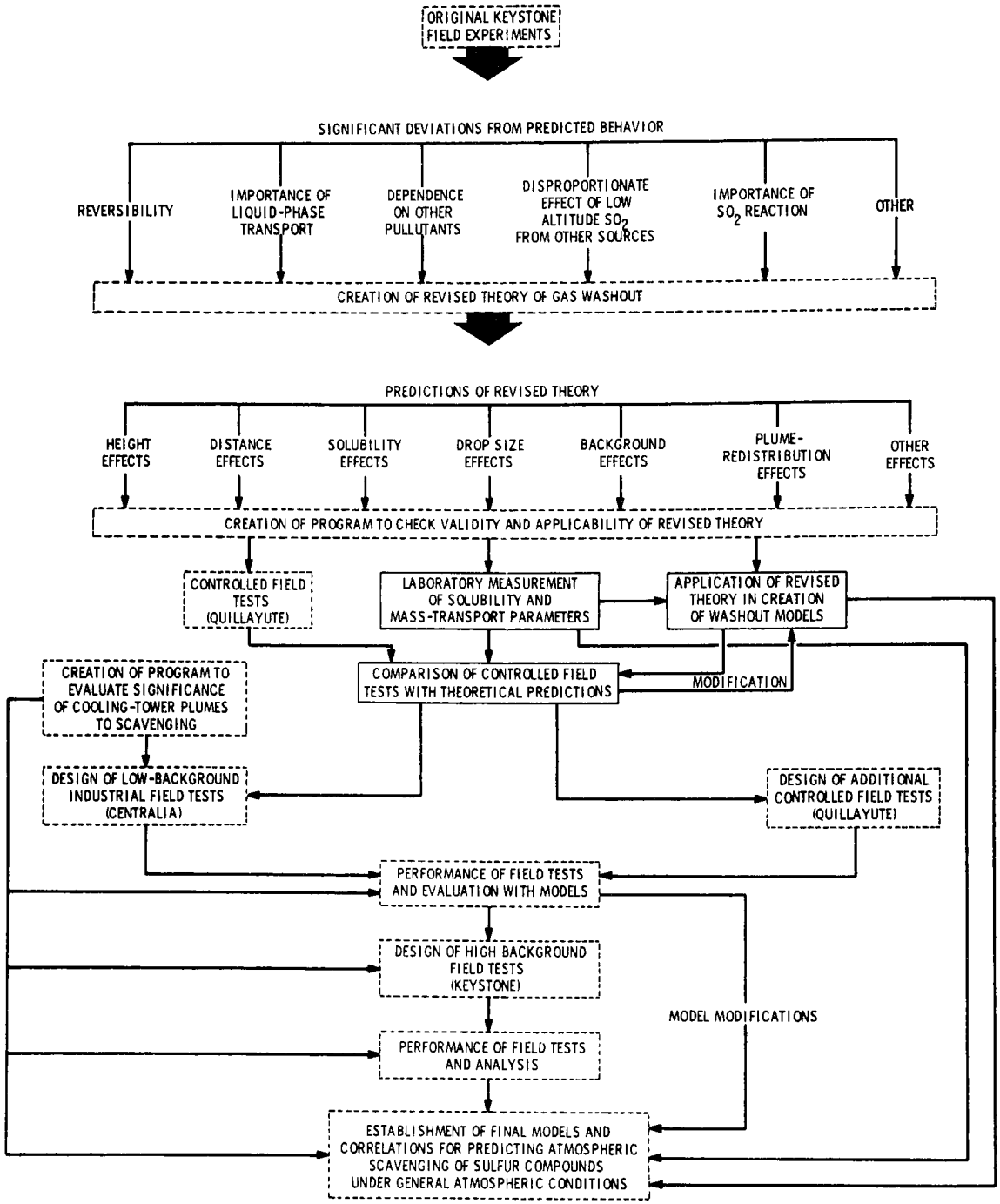

Figure 7.1 Suggested Research Program

3. Future field tests at Quillayute and at the Centralia, Washington power plant will be designed and conducted. The additional tests at Quillayute will be conducted for the purpose of increasing the volume and reliability of data and to obtain measurements at greater distances from the source. The Centralia experiments will be conducted for the following reasons:

   a. To measure washout from power plant plumes under low background conditions, and to compare the measurements with theoretical predictions.
   b. To evaluate in more detail the washout of sulfate and the rate of its formation. An automated means for sulfate analysis will be employed to facilitate this part of the study.
   c. To measure amounts of trace metals in the precipitation, and to attempt to relate these measurements to sulfate formation.
   d. To initiate investigations of the consequences to scavenging of the cooling tower plume interaction.

4. Results of the total Quillayute tests and those from Centralia will be analyzed, and the models and correlations will be revised accordingly. A first effort for incorporating sulfate formation in the scavenging model will be made.
5. The final field study of the Keystone Plant will be planned. These experiments will be conducted primarily for the following reasons:

   a. To verify and correct the refined model of sulfur compound washout.
   b. To examine sulfur dioxide washout in more detail at greater distances from the source.
   c. To examine sulfate formation in highly polluted atmospheres during precipitation as a function of

      (i) SO_2 concentration
      (ii) rain acidity
      (iii) background ammonia concentration
      (iv) trace metals concentration, and
      (v) cooling tower interactions.

d. To evaluate the significance of cooling tower-stack plume interactions to the problem of scavenging by post-emission precipitation.

6. The field study of the Keystone Plant will be conducted in accordance with the previously described plans.
7. Information from the total investigation will be compiled and evaluated to provide final models and correlations of sulfur compound scavenging rates.

The results described in this report constitute a significant contribution to accomplishment of the objectives shown in Figure 7.1. Measurements of SO_2 washout have been performed which confirm the existance of reversible sorption behavior. Two models of SO_2 washout have been formulated. Based on reversible absorption theory these models differ primarily in degree of sophistication, one being a linearized version of the other, more general treatment.

Utilization of these models in conjunction with average plume geometry calculated using the bivariate-normal distribution has shown encouraging agreement with measured values. The nonlinear washout model, when applied with a fluctuating plume analysis, gives somewhat different predictions for the conditions encountered at Quillayute. Optimism concerning the applicability of the general models to washout calculation is tempered somewhat by our present inability to provide a precise estimate of the mass-transfer coefficient. Measured washout rates, however, were generally observed to fall between those predicted on the basis of limiting conditions.

An additional factor tempering optimism is the rather close agreement between measured washout and that predicted on the basis of simple equilibrium with ground-level SO_2 in a fluctuating plume. This agreement is consistant with general-model predictions, but it also raises the question of the relative importance of factors such as dry deposition of SO_2 on collector surfaces. The field results suggest that these factors are of minor importance; more measurements are required, however, to confirm this completely.

Laboratory measurements of SO_2 solubility in water have been performed, and an equation has been presented which describes these measurements satisfactorily under the low concentrations of present interest. This solubility equation has been used extensively in formulation of the general washout models used for data evaluation.

It is expected that the solubility equation and the general washout models described in this report will be used extensively in the ongoing program, both as tools for evaluation of washout from industrial plumes and as bases for formulation of more refined expressions to be used as ultimate means for washout calculation.

REFERENCES

1. J. M. Hales, J. M. Thorp and M. A. Wolf. Field Investigation of Sulfur Dioxide Washout from the Plume of a Large Coal-Fired Power Plant by Natural Precipitation. Final report to Environmental Protection Agency, Air Pollution Control Office, Contract CPA 22-69-150, Battelle Memorial Institute, Pacific Northwest Laboratory, March, 1971.

2. R. B. Bird, W. E. Stewart, and E. N. Lightfoot. Transport Phenomena. Wiley Co., New York, 1960.

3. J. M. Hales and L. C. Schwendiman. "Precipitation Scavenging of Tritium and Tritiated Water," Pacific Northwest Laboratory Annual Report for 1970 to the USAEC Division of Biology and Medicine, BNWL-1551, Part 1, p. 82, Battelle, Pacific Northwest Laboratories, Richland, Washington, June, 1971.

4. F. A. Gifford. "An Outline of Theories of Diffusion in the Lower Layers of the Atmosphere," Meteorology and Atomic Energy 1968, D. H. Slade, Ed., U.S.A.E.C., 1968.

5. R. Gunn and G. D. Kinzer. "The Terminal Velocity of Fall for Water Droplets in Stagnant Air," J. Meteor., 6, 246, 1969.

6. B. Carnahan, H. A. Luther and J. O. Wilkes. Applied Numerical Methods. Wiley Co., New York, 1969.

7. F. P. Terraglio and R. M. Manganelli. "The Absorption of Atmospheric Sulfur Dioxide by Water Solutions," J. Air Poll. Control Assoc., 17, 403, 1967.

8. H. F. Johnstone and P. W. Leppla. "Solubility of SO_2 at Low Partial Pressures - Ionization Constant and Heat of Ionization of H_2SO_3," J. Am. Chem. Soc., 56, 2233, 1934.

9. F. P. Scaringelli, B. E. Saltzman and S. A. Frey. "Spectrophotometric Determination of Atmospheric Sulfur Dioxide," Anal. Chem., 39, 1709, 1967.

10. F. Pasquill. Atmospheric Diffusion, Van Nostrand Co., London, 1962.

11. R. J. Engelmann. The Calculation of Precipitation Scavenging, BNWL-77, Battelle-Northwest, Pacific Northwest Laboratory, Richland, Washington, July, 1965.

12. W. T. Hinds. "Peak-to-Mean Concentration Ratios from Ground Level Sources in Building Wakes," Atmospheric Environment, 3, 145, 1969.

13. J. V. Ramsdell and W. T. Hinds. "Concentration Fluctuations and Peak-to-Mean Concentration Ratios in Plumes from a Ground Level Continuous Point Source," Atmospheric Environment, 5, 483, 1971.

14. R. C. Reid and T. K. Sherwood. The Properties of Gases and Liquids, McGraw-Hill Co., New York, 1958.

15. S. Lynn, J. R. Straatemeier and H. Kramers. "Absorption Studies in the Light of Penetration Theory," Chem. E. Sci., 4, 49, 1955.

16. J. M. Hales. "Fundamentals of the Theory of Gas Scavenging by Rain," submitted to Atmospheric Environment, November, 1971.

17. G. D. Kinzer and R. Gunn. "The Evaporation, Temperature and Thermal Relaxation Time of Freely Falling Water Drops," J. Met., 8, 71, 1951.

18. F. H. Garner and J. J. Lane. "Mass Transfer to Drops of Liquid Suspended in a Gas Stream," Part II: Experimental Work and Results," Trans. Inst. Chem. Engrs., 37, 162, 1959.

19. I. Friedman, L. Machta and R. Soller. "Water Vapor Exchange Between A Water Droplet and its Environment," J. Geophys. Res., 67, 2761, 1962.

20. W. Mensing and K. Schügerl. " Stoffaustausch-Messungen an schwebenden Tropfen," Chemie. Ing. Techn., 42, 837, 1970.

21. S. Hatta and A. Babba. "The Absorption of Ammonia by a Water Drop," J. Soc. Chem. Inc., (Japan) 38, 546B, 1935.

22. B. E. Dixon and A.A.W. Russel. "Absorption of Carbon Dioxide by Liquid Drops," J. Soc. Chem. Ind., (London) 69, 284, 1950.

23. B. E. Dixon and J.E.L. Swallow. "Use of Liquid Films in the Study of Absorption of Gases by Drops," J. Appl. Chem., 4, 86, 1959.

24. R. R. Hughes and E. R. Gilliland. "The Mechanics of Drops," CEP Symp. Ser., 51, 16, 1955.

25. K. Shabalin. "Absorption of Gas by a Drop of Liquid," Zhur. Prikl. Khim., Leningr., 13, 412, 1940.

26. A. Guyer, B. Tobler and R. H. Farmer. "The Principles of Degasification," Chem. Fabrik., 9, 5, 1936.

27. F. Goodridge. "Kinetic Studies in Gas-Liquid Systems, I," Trans. Far. Soc., 51, 1703, 1955.

28. F. Goodridge. "Kinetic Studies in Gas-Liquid Systems, II," Trans. Far. Soc., 49, 1324, 1953.

29. H. F. Johnstone and G. C. Williams. "Absorption of Gases by Liquid Droplets," I.E.C., 31, 993, 1939.

30. W. G. Whitman, L. Long and H. Y. Wang. "Absorption of Gases by a Liquid Drop," I.E.C., 18, 361, 1926.

APPENDIX A

TABULATIONS OF MEASURED SO_2 CONCENTRATIONS IN PRECIPITATION

TABLE A.1

PRECIPITATION SAMPLE SO_2 CONCENTRATION RUN 1
(Values are in units of moles $cc^{-1} \times 10^9$)

EAST GRID

Arc B	Sampler No.	Arc C
.76	14	.16
.72	15	.44
1.36	16	.60
1.24	17	.32
.76	18	.32
1.40	19	.48
.42	20	0
1.20	21	.16
.40	22	.28
.92	23	.20
1.84	24	.20
1.04	25	.12
1.44	26	0
1.68	27	.04
1.08	28	.12
1.12	29	
1.08	30	.20

WEST GRID

Arc B	Sampler No.	Arc C
.16	20	
.24	23	

TABLE A.2

PRECIPITATION SAMPLE SO_2 CONCENTRATION RUN 2
(Values are in units of moles cc^{-1} x 10^9)

EAST GRID

Arc B	Sampler No.	Arc C
4.00	21	
1.42	22	
4.26	23	10.44
4.53	24	14.57
3.42	25	15.94
4.71	26	22.60
10.35	27	18.34
4.22	28	6.62
2.31	29	18.66

WEST GRID

Arc B	Sampler No.	Arc C
	14	.28
.19	17	.64
.23	20	.28
0	23	0
.24	24	0
.54	25	1.70
.22	26	2.42
0	27	.90
0	28	.18
.20	29	.69
.10	30	.44
0	31	.21
.32	32	.20
0	33	.24
.36	34	
.45	35	
.19	36	

TABLE A.3

PRECIPITATION SAMPLE SO_2 CONCENTRATION RUN 3
(Values are in units of moles $cc^{-1} \times 10^9$)

EAST GRID

Special Arc	Sampler No.
27.1	1
34.4	2
29.1	3
26.1	4
43.6	5
33.7	6
32.75	7
31.35	8
26.3	9
22.55	10
22.3	11
24.15	12
20.7	13
10.25	14
7.93	15
8.64	16

WEST GRID

Special Arc	Sampler No.
8.86	7
23.9	8
39.8	9
51.3	10
40.5	11
22.7	12
13.4	13
3.69	14

TABLE A.4

PRECIPITATION SAMPLE SO_2 CONCENTRATION RUN 4
(Values are in units of moles $cc^{-1} \times 10^9$)

EAST GRID

Arc B	Sampler No.	Arc C
1.07	13	
6.94	14	
6.65	15	
9.90	16	2.98
11.3	17	8.51
24.6	18	14.2
36.2	19	27.6
33.0	20	28.8
28.5	21	18.8
15.6	22	15.7
26.1	23	19.1
18.5	24	6.81
12.2	25	
2.78	26	

WEST GRID

Arc B	Sampler No.	Arc C
4.79	17	.23
6.89	18	.55
11.11	19	4.06
19.96	20	9.66
18.25	21	10.00
13.66	22	10.31
8.64	23	9.56
3.62	24	3.06
	25	.63

TABLE A.5

PRECIPITATION SAMPLE SO_2 CONCENTRATION RUN 5
(Values are in units of moles $cc^{-1} \times 10^9$)

EAST GRID

Arc B	Sampler No.	Arc C
16.1	19	2.74
37.4	20	30.3
58.6	21	41.1
56.5	22	31.9
28.8	23	15.5
14.4	24	
.83	25	

WEST GRID

Arc B	Sampler No.	Arc C
	17	.20
	20	.62
2.53	21	3.31
.23	22	.22
.19	23	.78
.20	24	missing
.47	25	.22
.23	26	.58
.19	29	
.47	32	

TABLE A.6

PRECIPITATION SAMPLE SO_2 CONCENTRATION RUN 6
(Values are in units of moles $cc^{-1} \times 10^9$)

EAST GRID

Arc B	Sampler No.	Arc C
.46	14	0
.30	17	.12
0	20	0
0	21	0
.45	22	0
0	23	.17
0	24	0
0	25	0
0	26	.13
0	29	.22
.084	32	0
0	35	0

WEST GRID

Arc B	Sampler No.	Arc C
7.72	21	3.58
14.9	22	13.8
19.2	23	17.8
16.25	24	32.2
18.3	25	13.6
	26	

TABLE A.7

PRECIPITATION SAMPLE SO_2 CONCENTRATION RUN 7
(Values are in units of moles $cc^{-1} \times 10^9$)

EAST GRID

Arc B	Sampler No.	Arc C
	27	2.04
1.00	28	3.60
4.25	29	5.43
13.0	30	14.0
17.1	31	16.1
16.0	32	17.1
14.8	33	9.87
5.65	34	6.50

WEST GRID

Arc B	Sampler No.	Arc C
5.98	28	
19.5	29	8.24
21.5	30	22.7
43.8	31	26.0
49.4	32	31.4
58.8	33	33.8
36.5	34	17.4
38.4	35	10.7
1.20	36	

TABLE A.8

PRECIPITATION SAMPLE SO_2 CONCENTRATION RUN 8
(Values are in units of moles $cc^{-1} \times 10^9$)

EAST GRID

Arc A	Sampler No.	Arc C
0.9	17	0
0.7	18	0.5
3.5	19	9.3
16.1	20	10.8
30.8	21	26.9
32.3	22	50.2
56.7	23	46.7
48.4	24	66.8
54.0	25	74.9
54.5	26	61.0
50.1	27	25.7
22.4	28	

WEST GRID

Arc A	Sampler No.	Arc C

TABLE A.9

PRECIPITATION SAMPLE SO_2 CONCENTRATION RUN 9
(Values are in units of moles $cc^{-1} \times 10^9$)

EAST GRID

Arc A	Sampler No.	Arc B
.63	26	.86
3.40	27	5.02
9.70	28	12.4
28.2	29	16.5
34.5	30	27.2
27.5	31	26.1
13.0	32	18.6
9.72	33	15.4
	34	2.37
	35	

WEST GRID

Arc A	Sampler No.	Arc B
3.40	28	
9.52	29	6.43
11.4	30	4.71
7.58	31	5.98
1.64	32	6.45
1.19	33	2.21

APPENDIX B

RESULTS OF PEAK-TO-MEAN ANALYSIS

Plots of measured concentrations (vertical bars) versus those predicted from peak-to-mean analysis (dots).

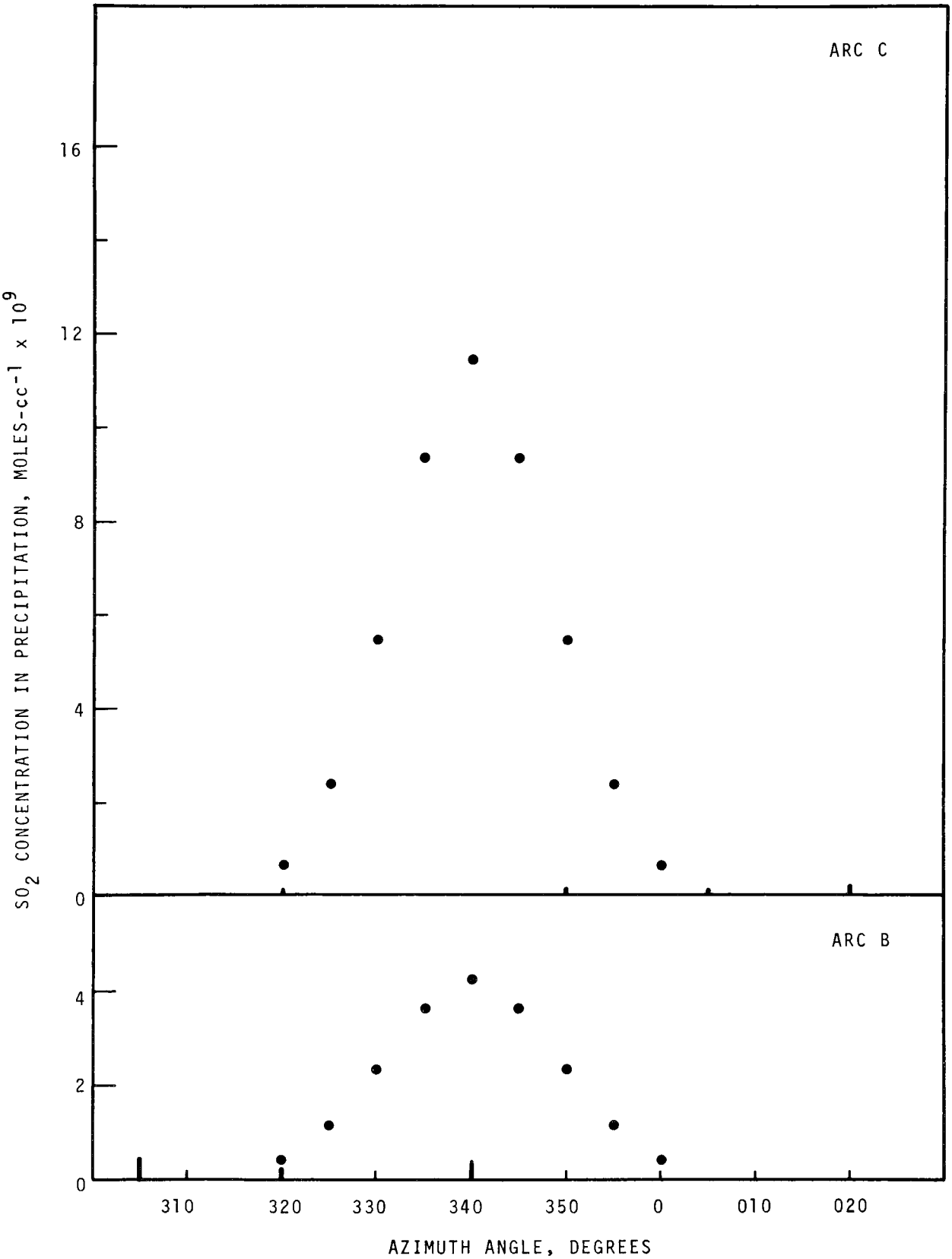

Figure B.1 Comparison of Observed Values with Those Predicted by the Peak-to-Mean Analysis Run 1E.

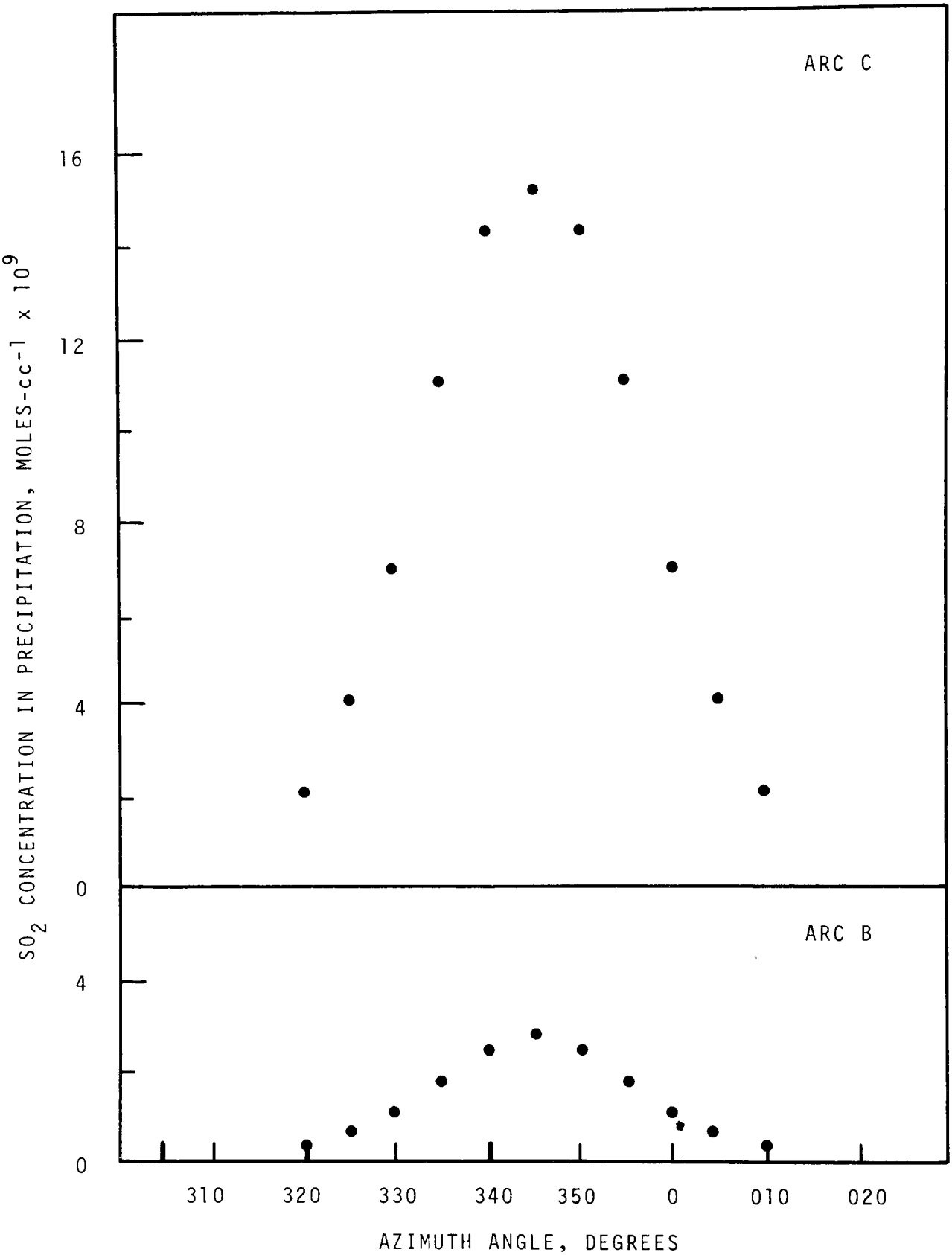

Figure B.2 Comparison of Observed Values with Those Predicted by the Peak-to-Mean Analysis Run 1W.

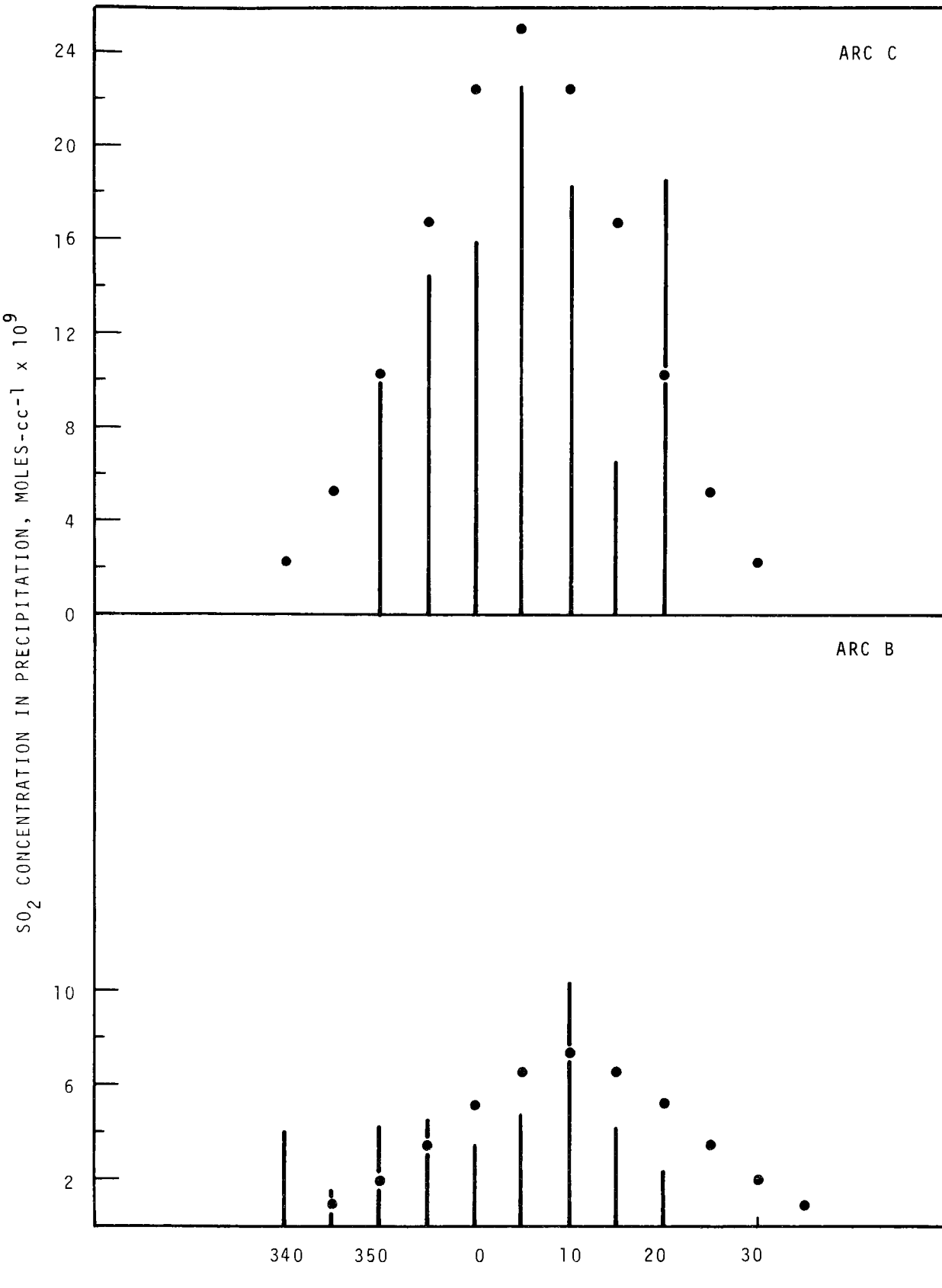

Figure B.3 Comparison of Observed Values with Those Predicted by the Peak-to-Mean Analysis Run 2E.

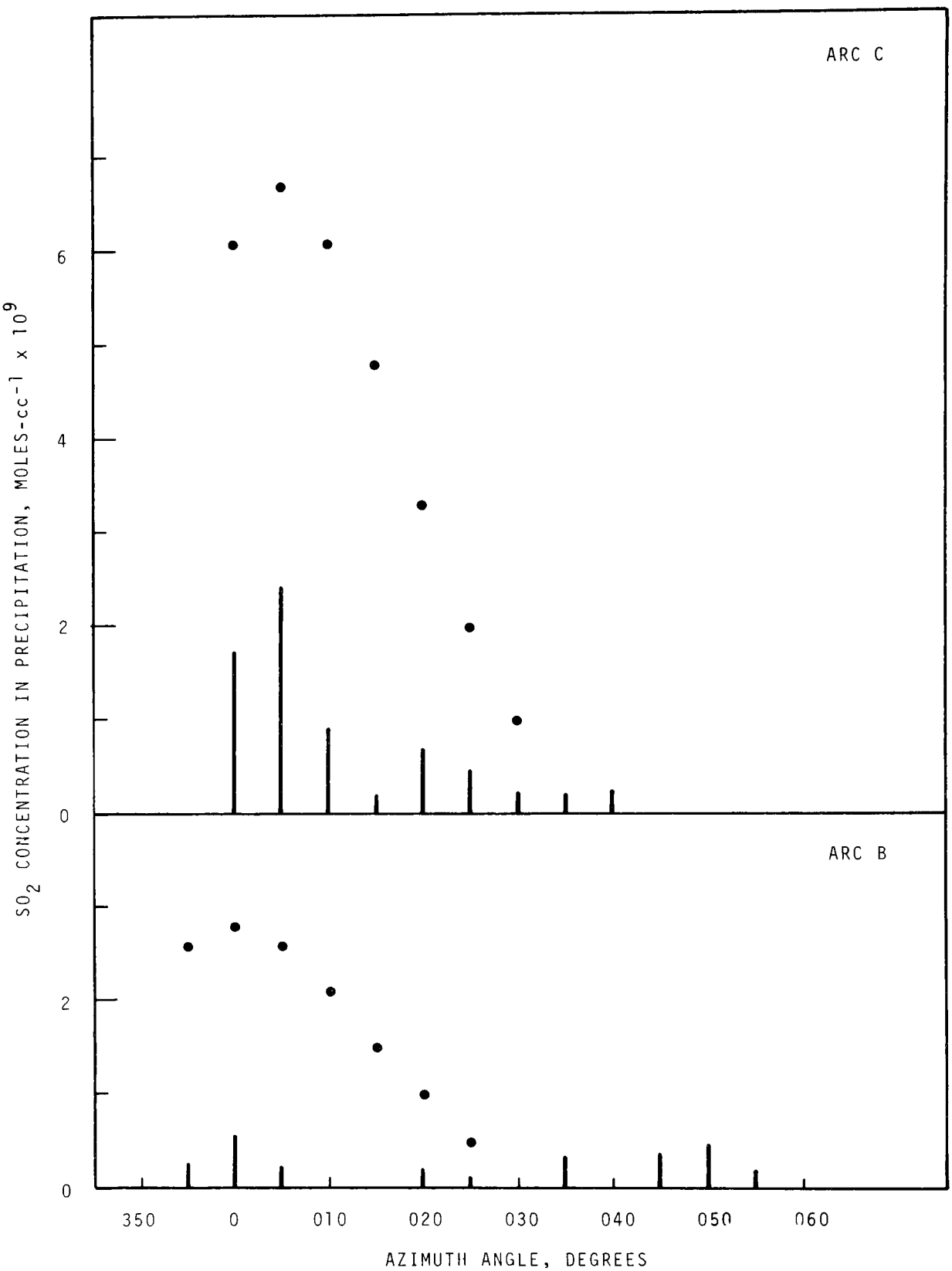

Figure B.4 Comparison of Observed Values with Those Predicted by the Peak-to-Mean Analysis Run 2W.

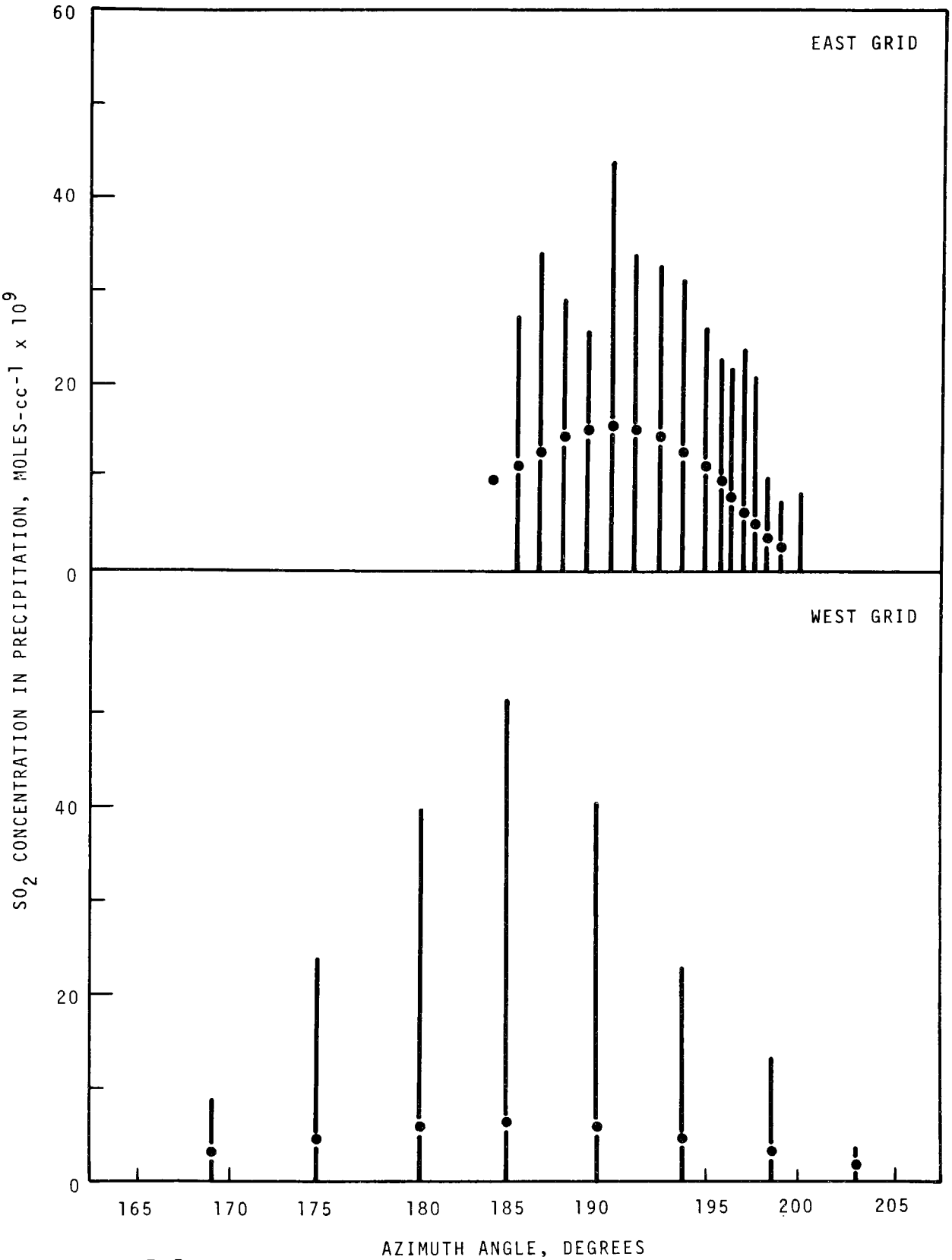

Figure B.5 Comparison of Observed Values with Those Predicted by the Peak-to-Mean Analysis Run 3.

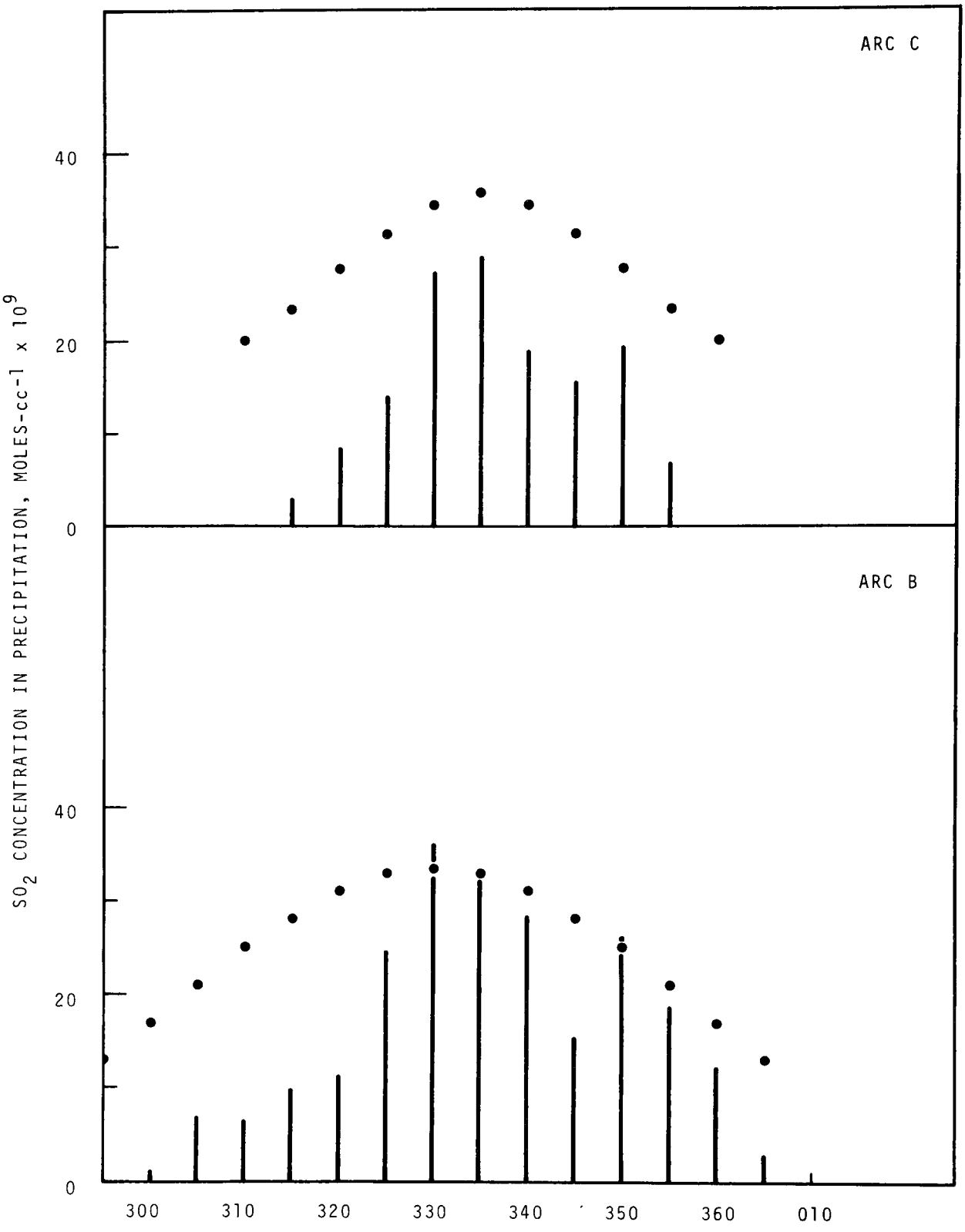

Figure B.6 Comparison of Observed Values with Those Predicted by the Peak-to-Mean Analysis Run 4E.

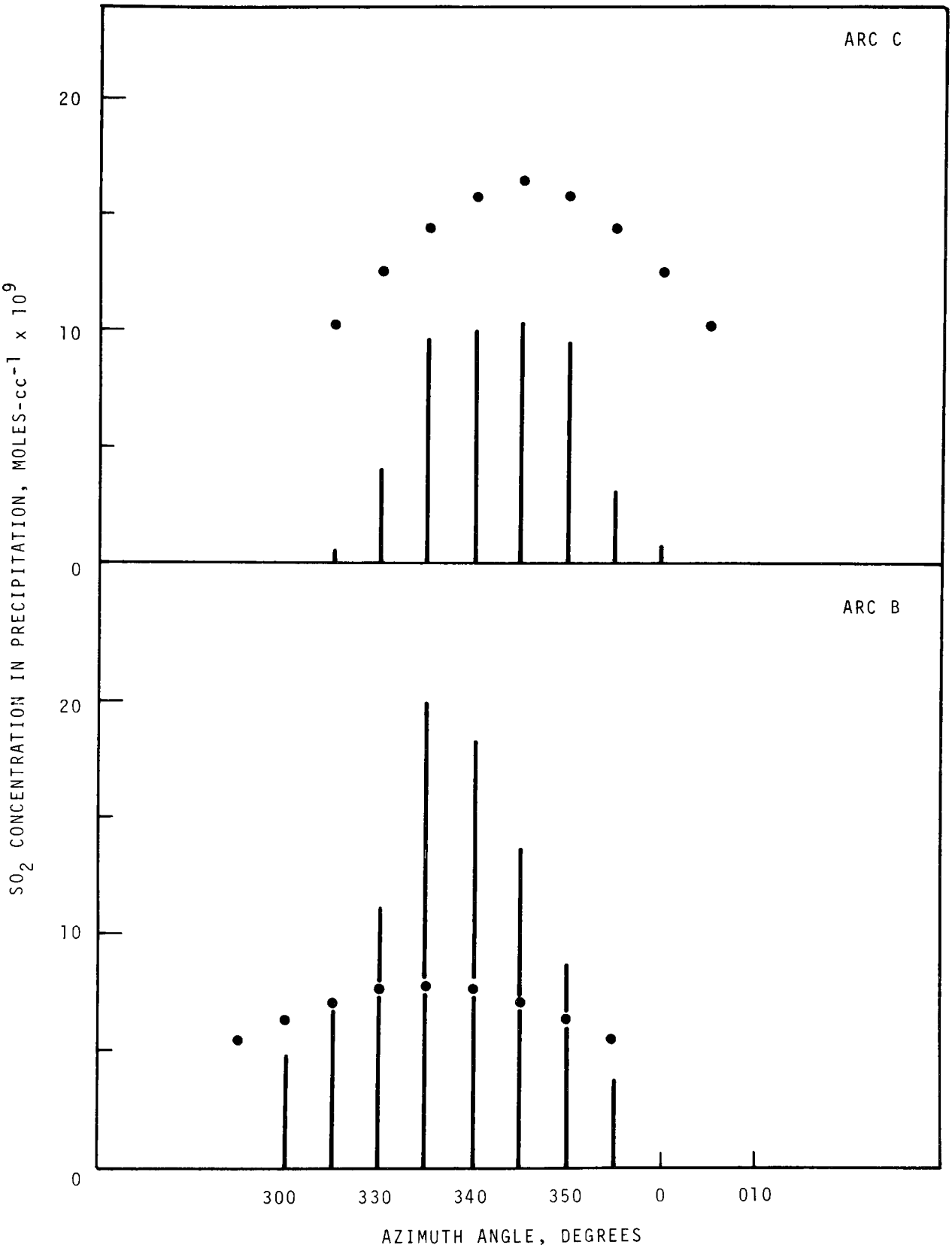

Figure B.7 Comparison of Observed Values with Those Predicted by the Peak-to-Mean Analysis Run 4W.

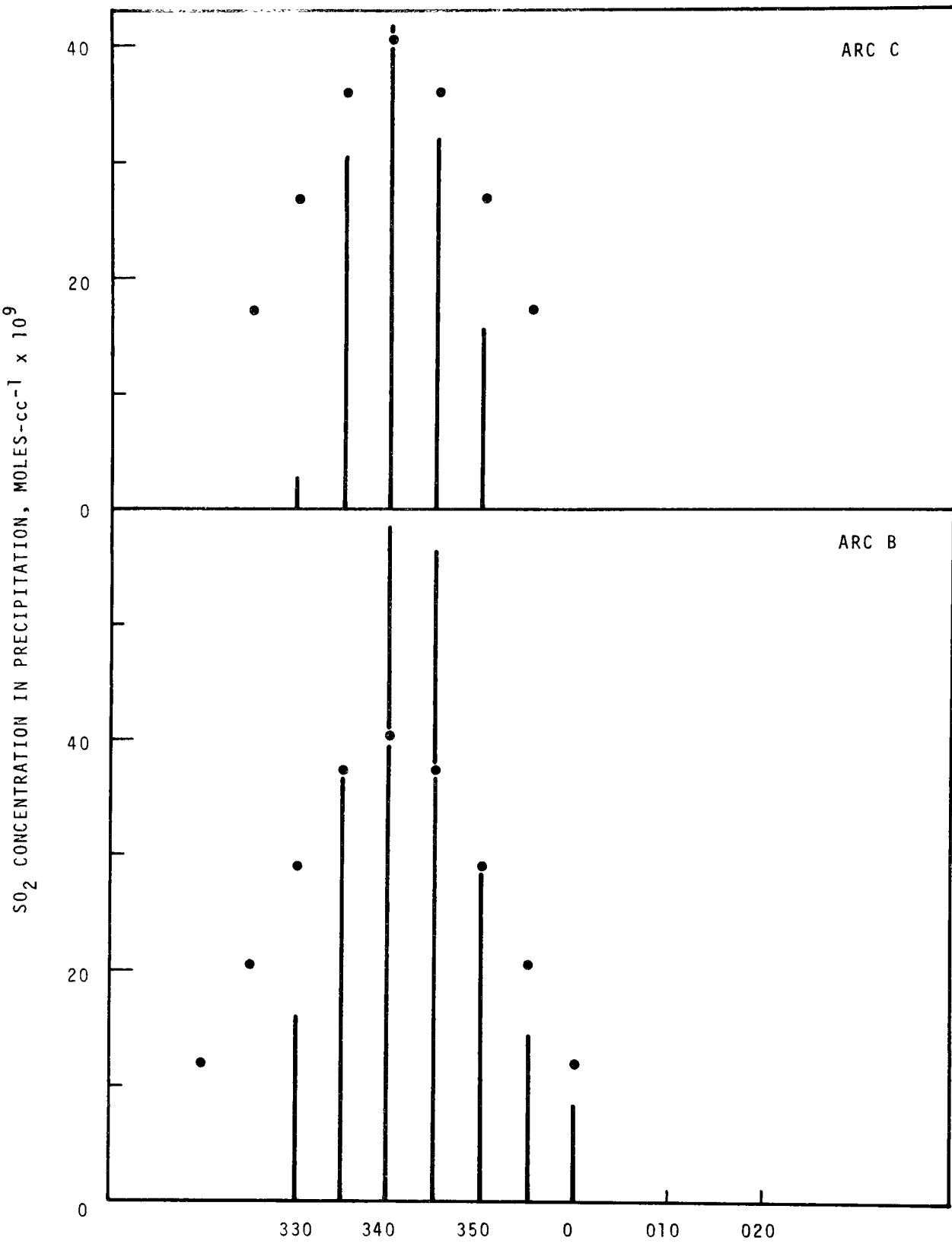

Figure B.8 Comparison of Observed Values with Those Predicted by the Peak-to-Mean Analysis Run 5E.

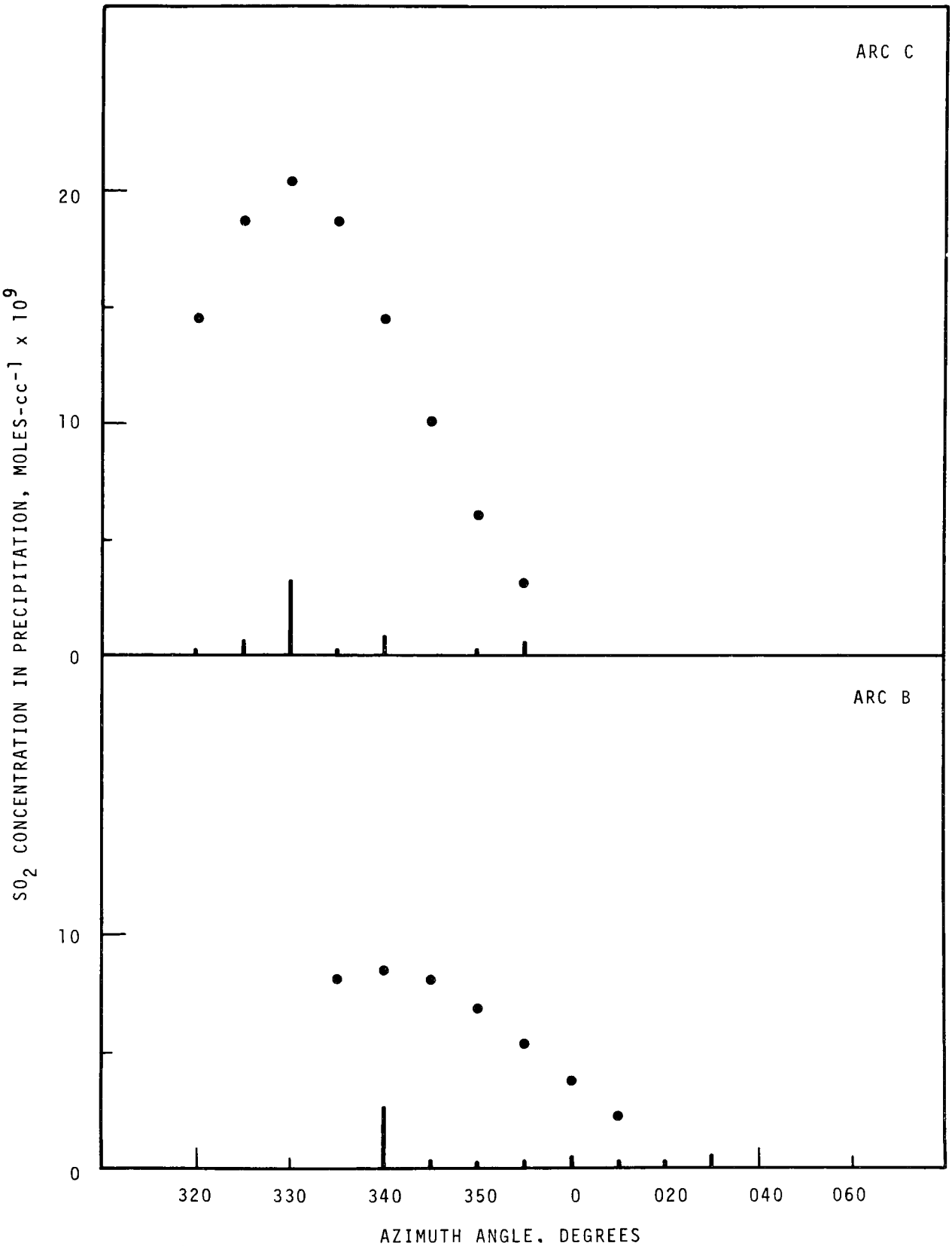

Figure B.9 Comparison of Observed Values with Those Predicted by the Peak-to-Mean Analysis Run 5W.

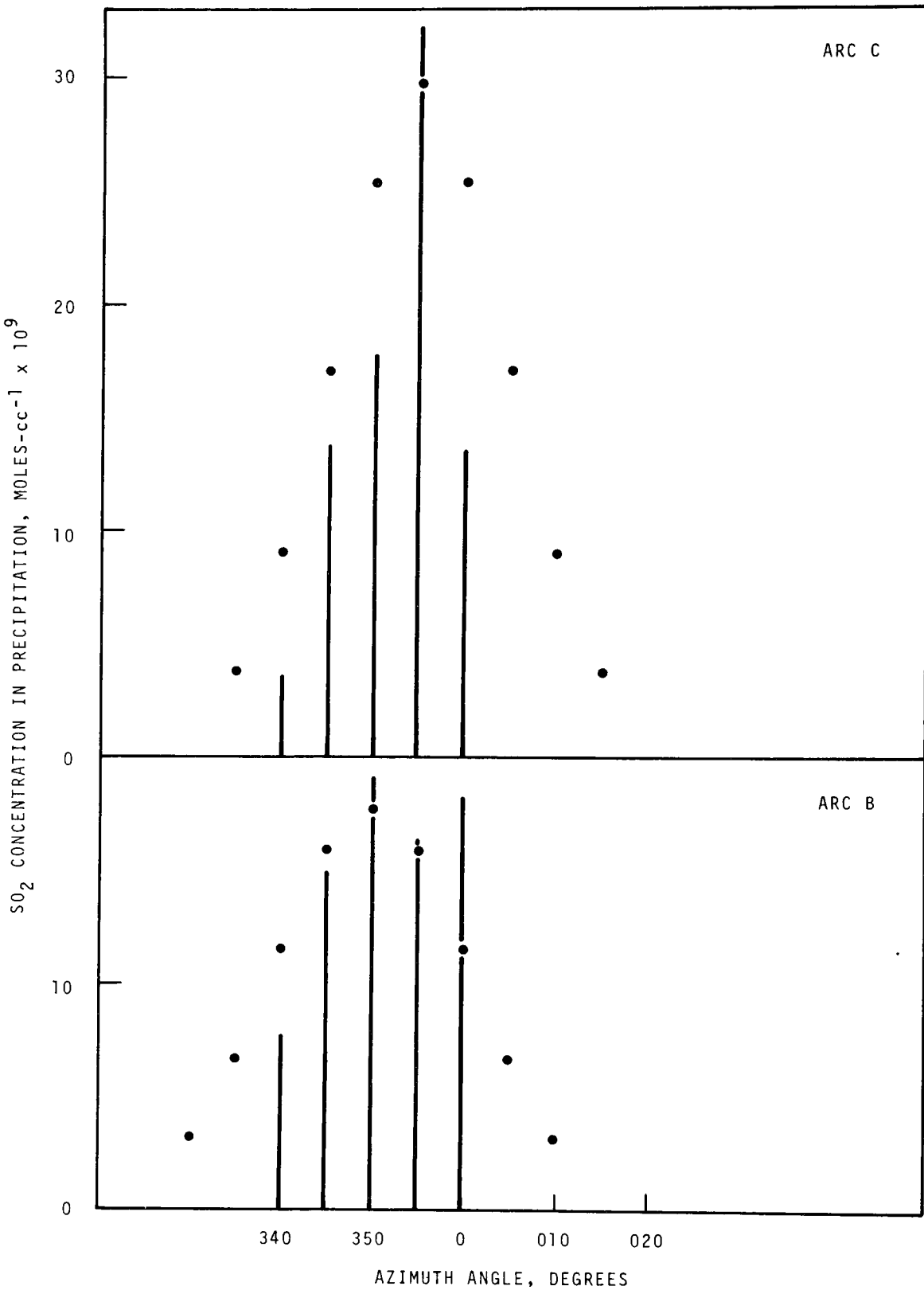

Figure B.10 Comparison of Observed Values with Those Predicted by the Peak-to-Mean Analysis Run 6W.

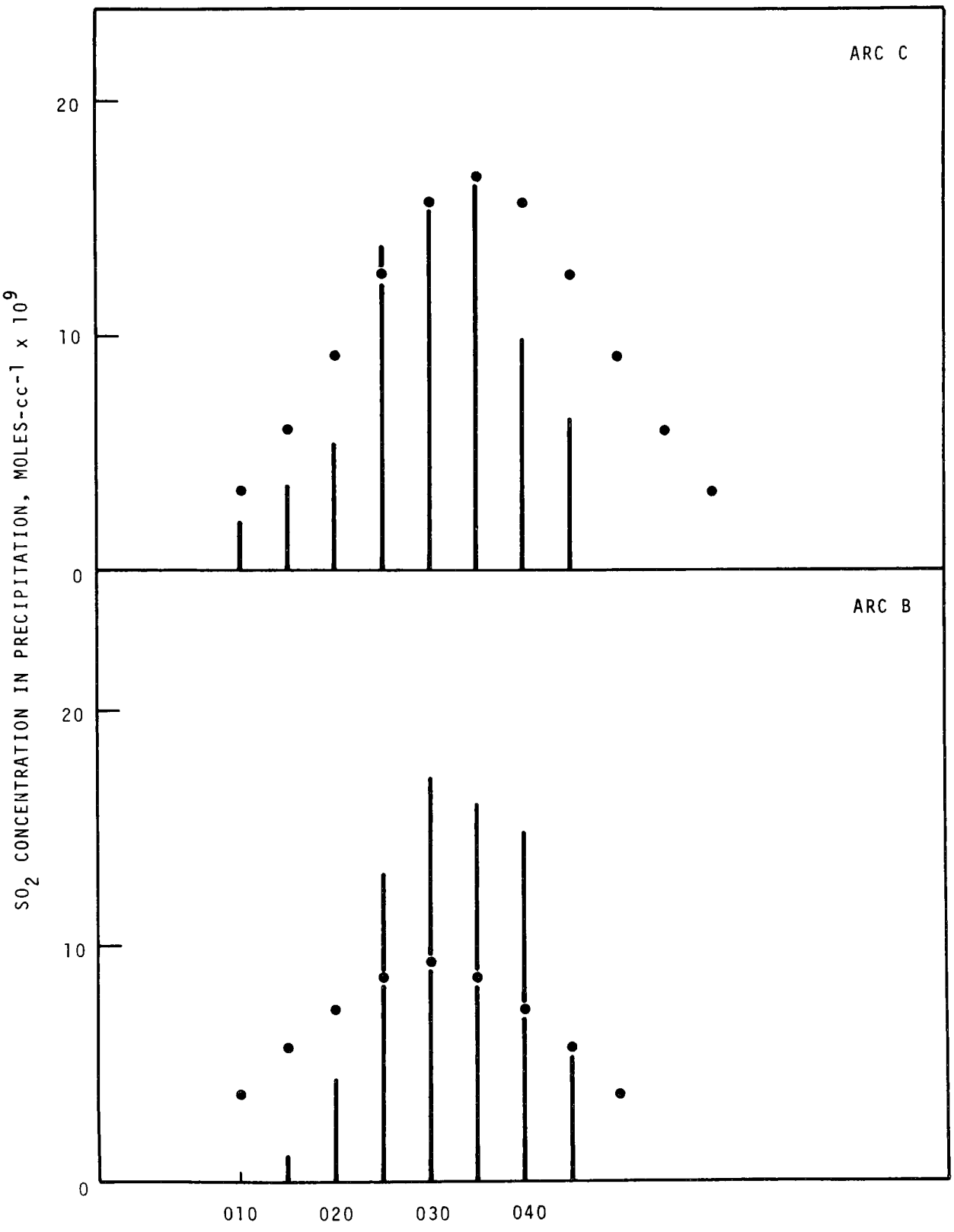

Figure B.11 Comparison of Observed Values with Those Predicted by the Peak-to-Mean Analysis Run 7E.

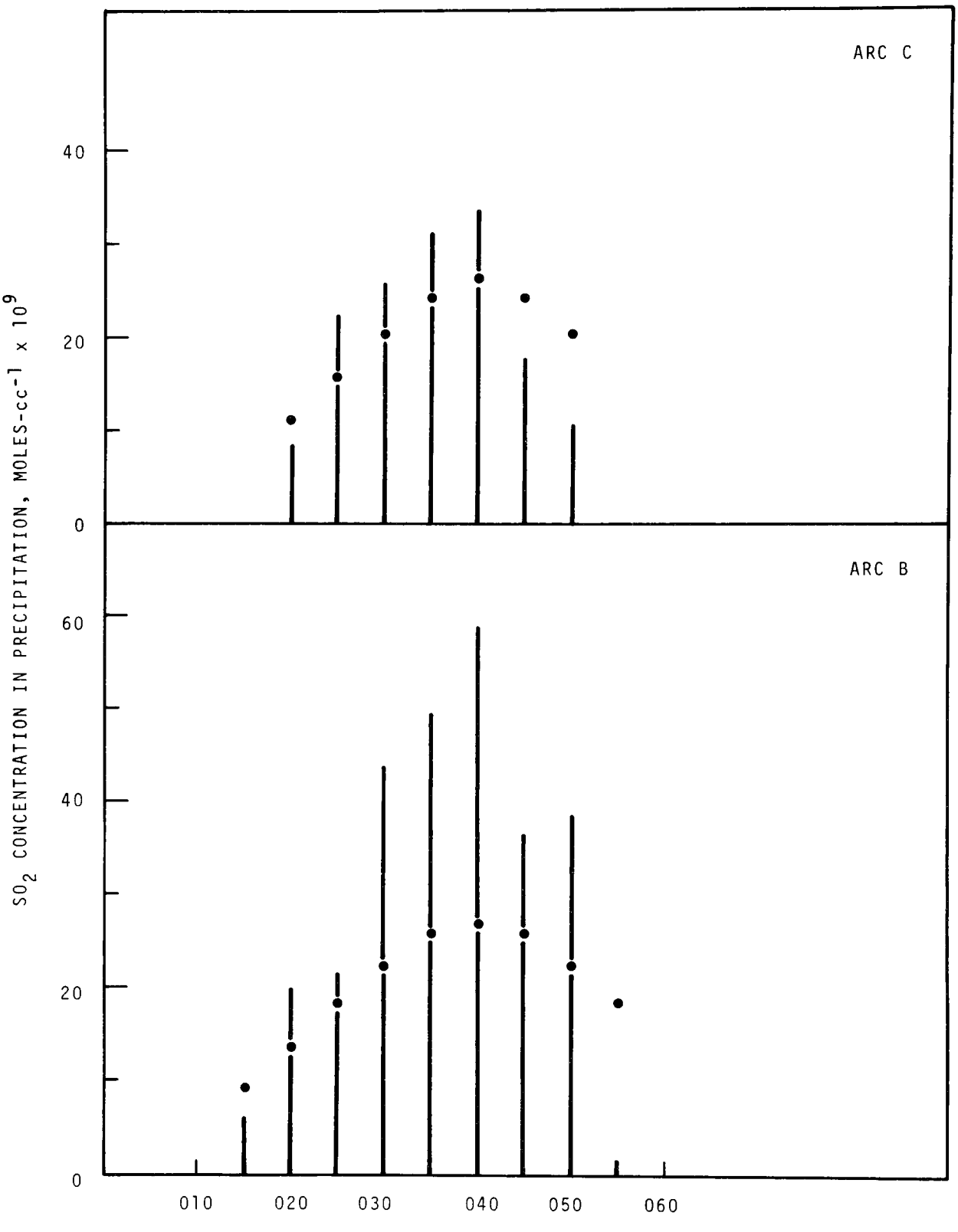

Figure B.12 Comparison of Observed Values with Those Predicted by the Peak-to-Mean Analysis Run 7W.

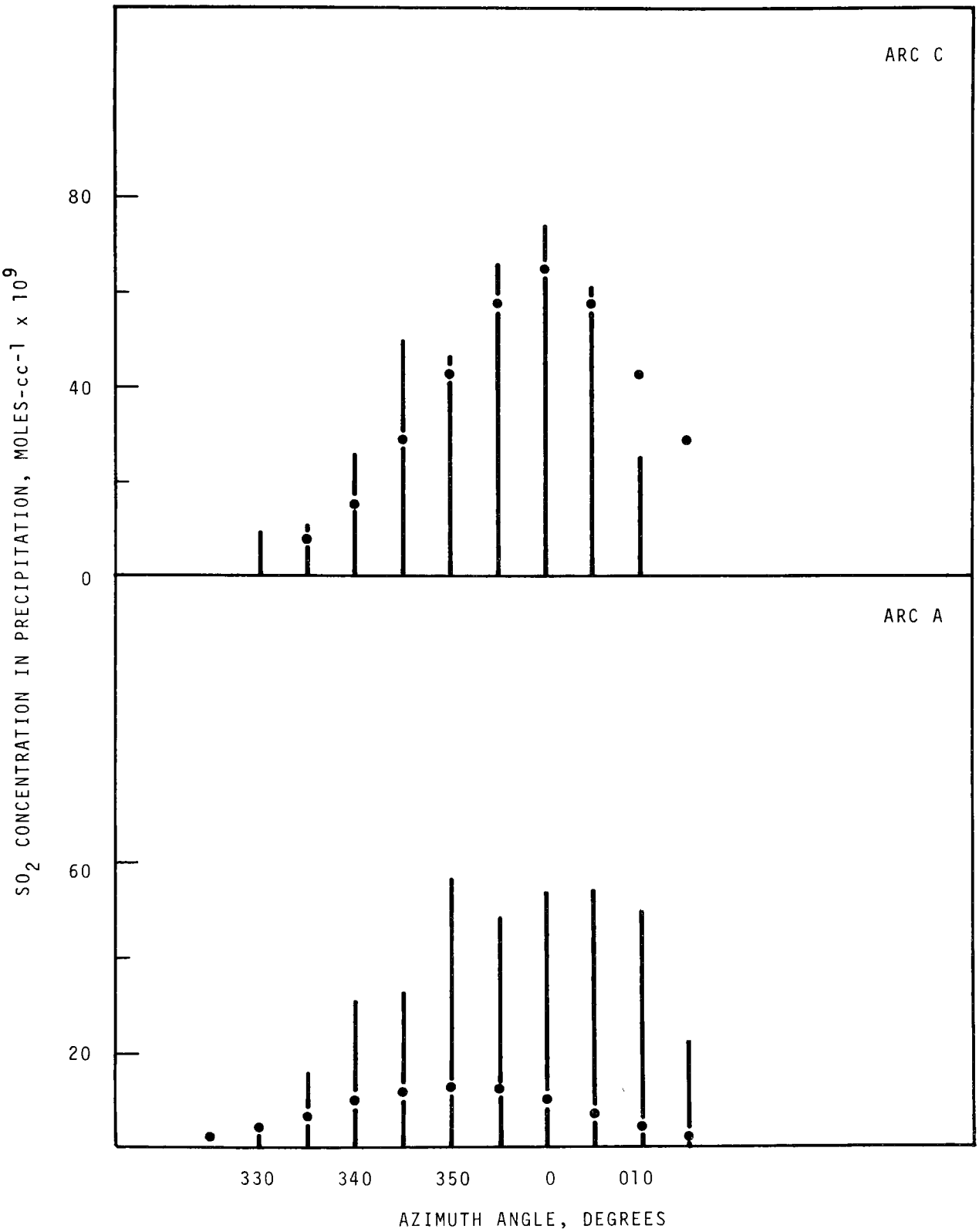

Figure B.13 Comparison of Observed Values with Those Predicted by the Peak-to-Mean Analysis Run 8E.

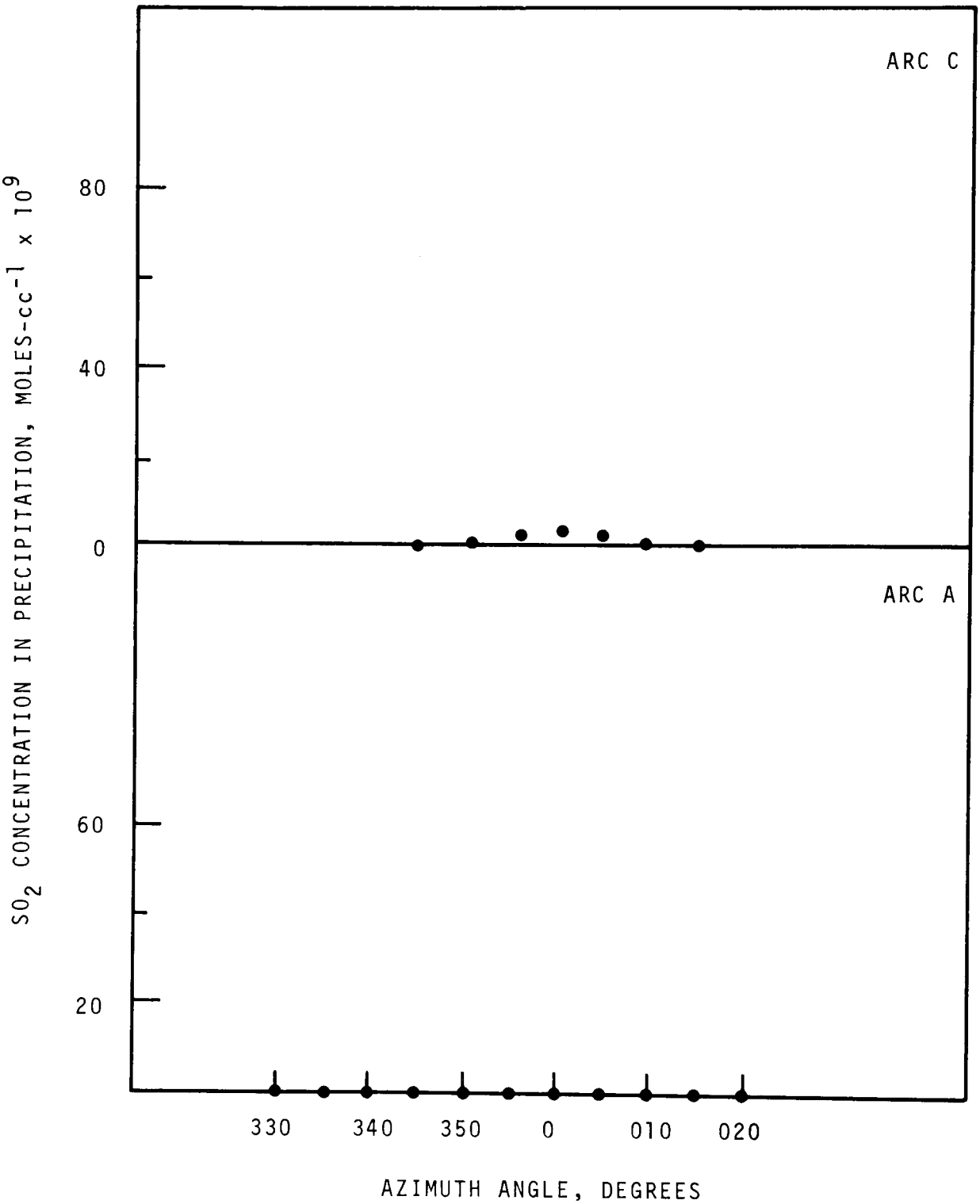

Figure B.14 Comparison of Observed Values with Those Predicted by the Peak-to-Mean Analysis Run 8W.

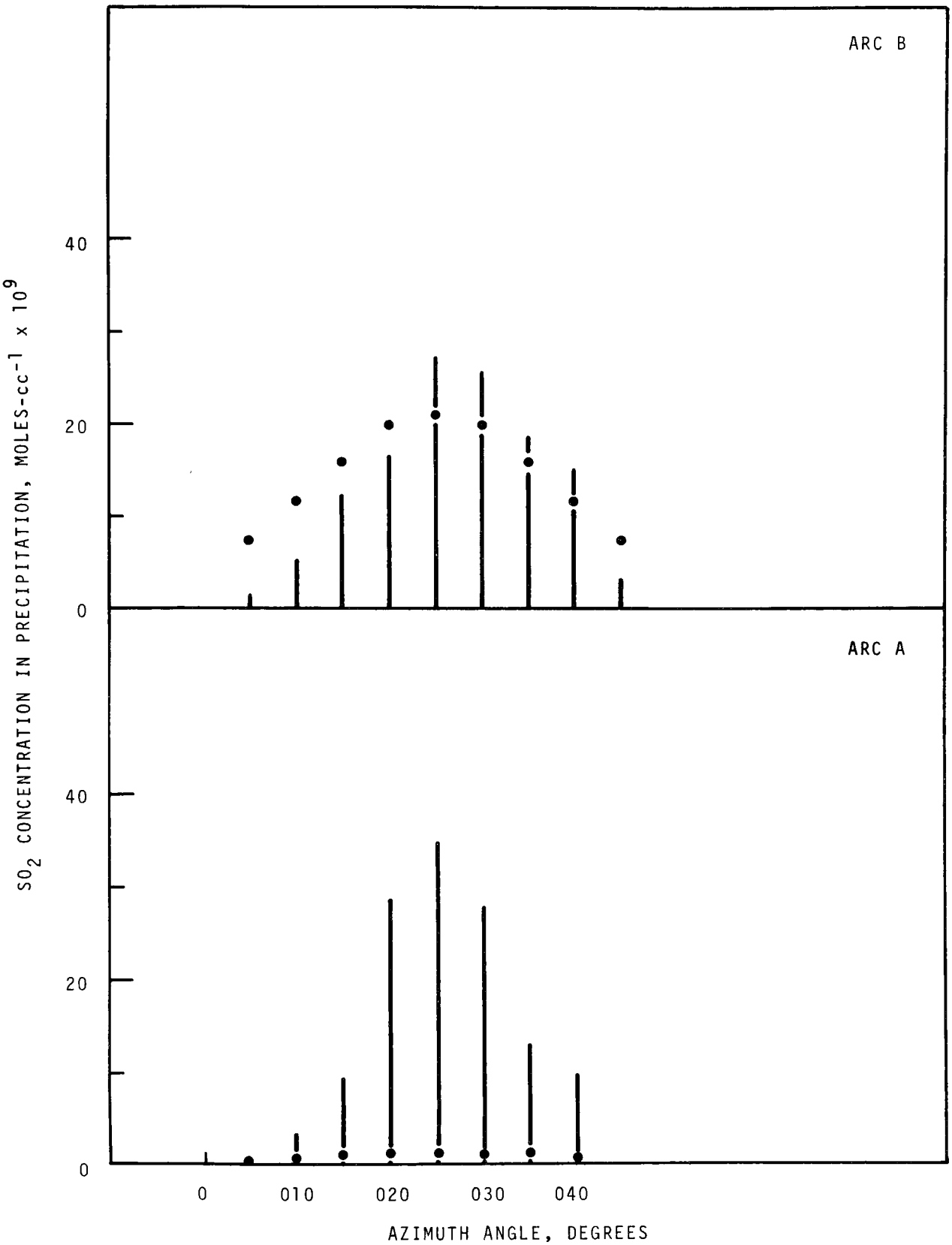

Figure B.15 Comparison of Observed Values with Those Predicted by the Peak-to-Mean Analysis Run 9E.

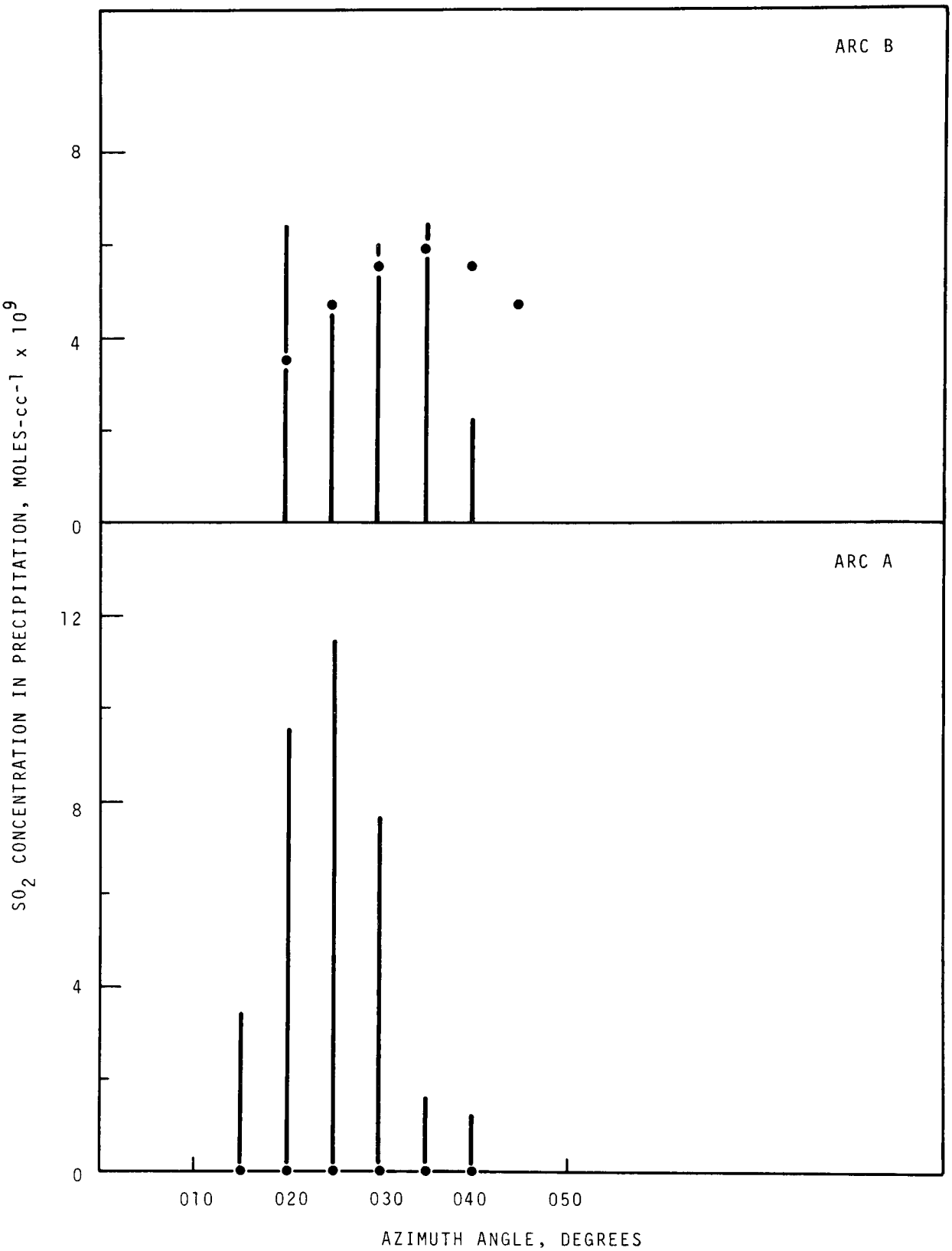

Figure B.16 Comparison of Observed Values with Those Predicted by the Peak-to-Mean Analysis Run 9W.

APPENDIX C

COMPARISONS OF MEASURED WASHOUT CONCENTRATIONS WITH PREDICTIONS BY THE NONLINEAR, NONFEEDBACK MODEL

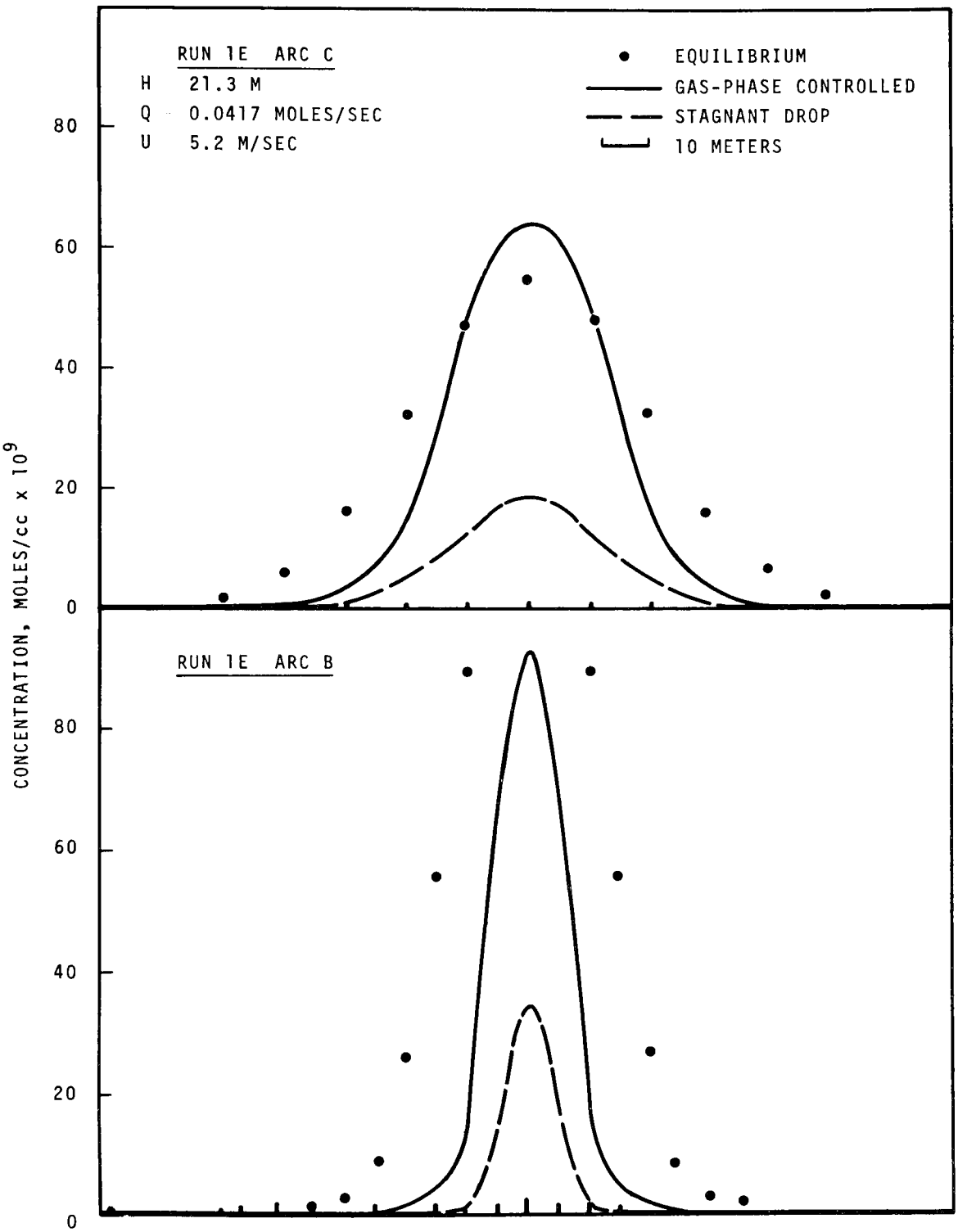

Figure C.1 Predictions of Nonlinear Model for Run 1E

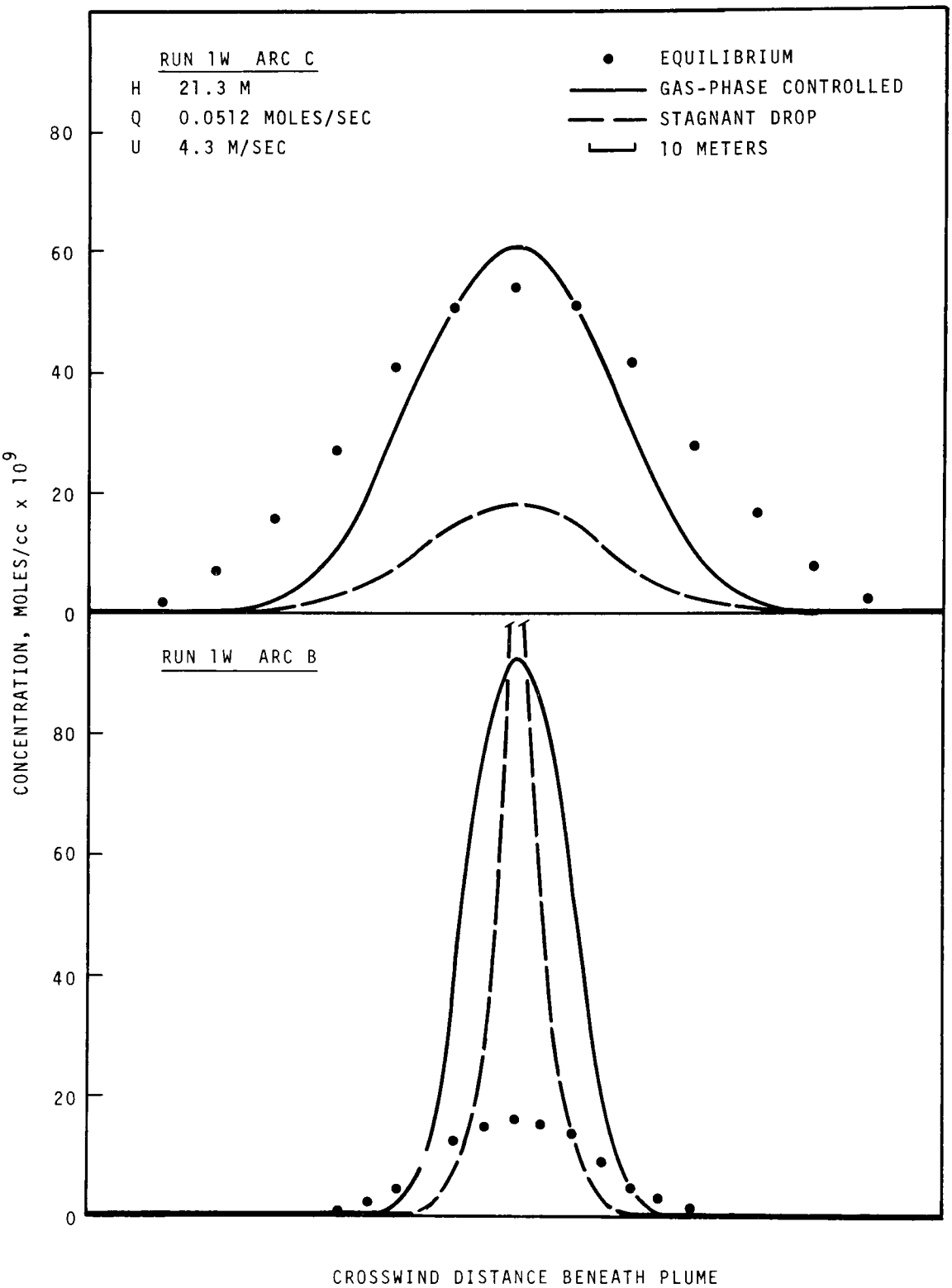

Figure C.2 Predictions of Nonlinear Model for Run 1W

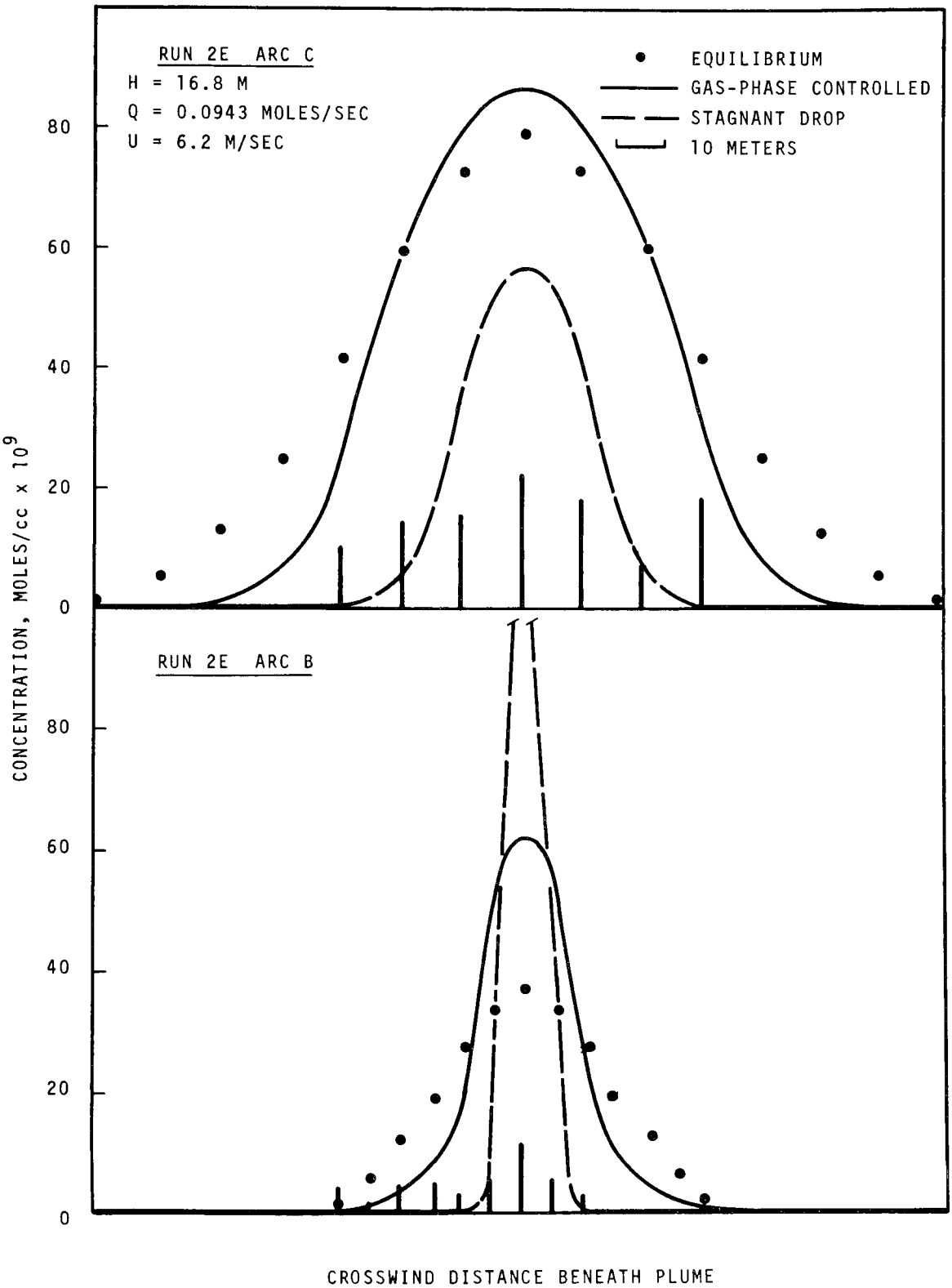

Figure C.3 Predictions of Nonlinear Model for Run 2E

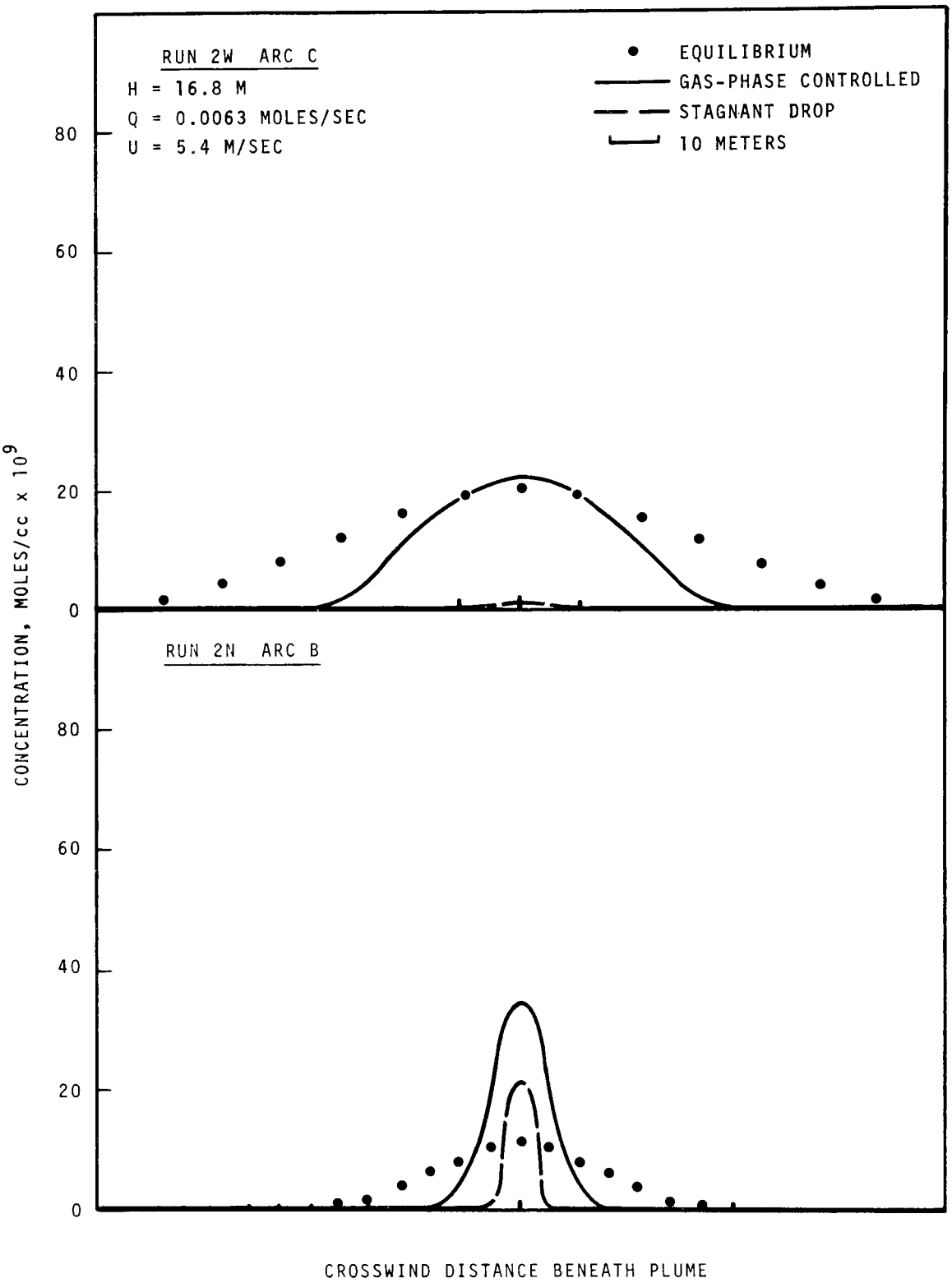

Figure C.4 Predictions of Nonlinear Model for Run 2W

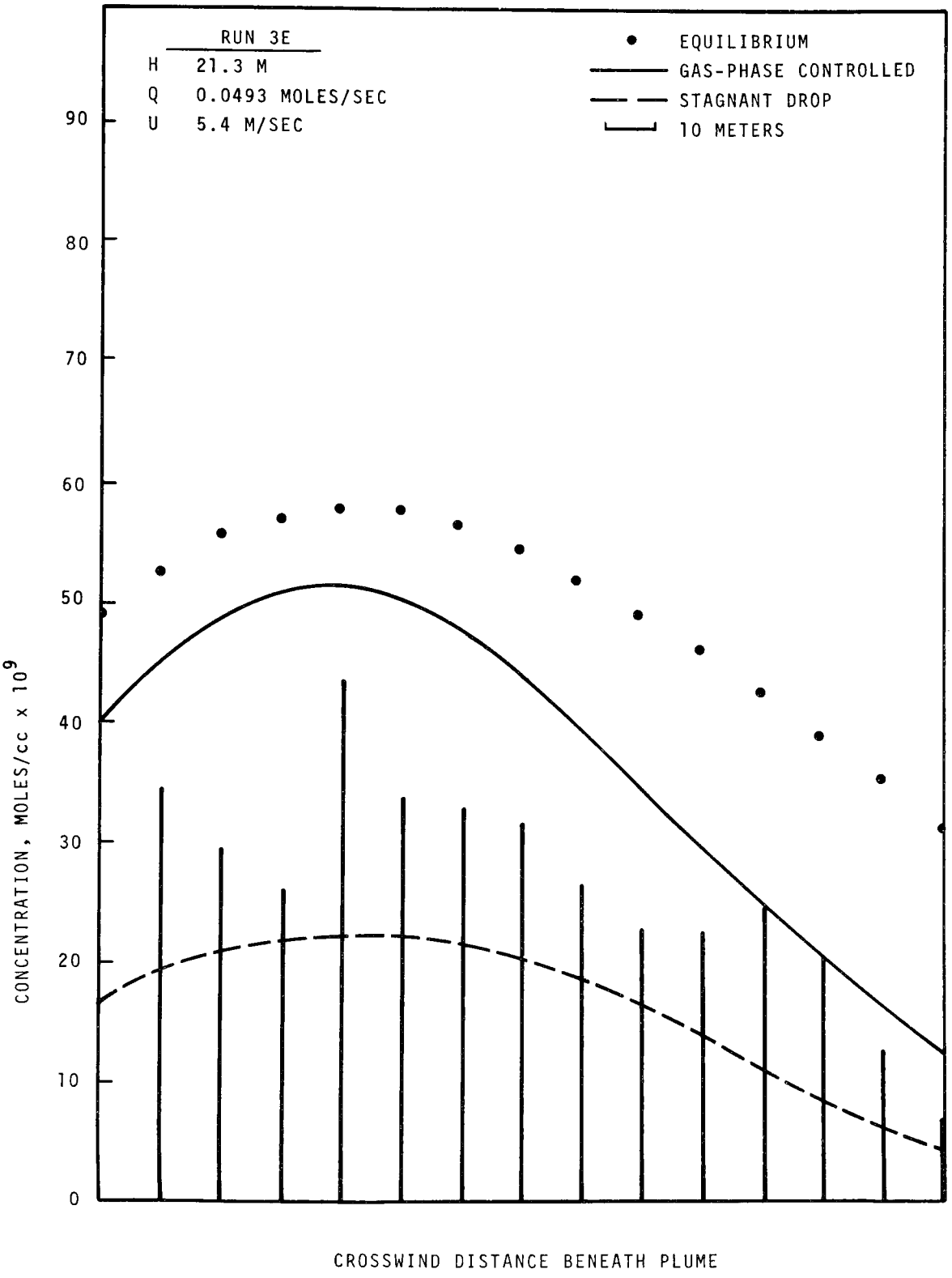

Figure C.5 Predictions of Nonlinear Model for Run 3E

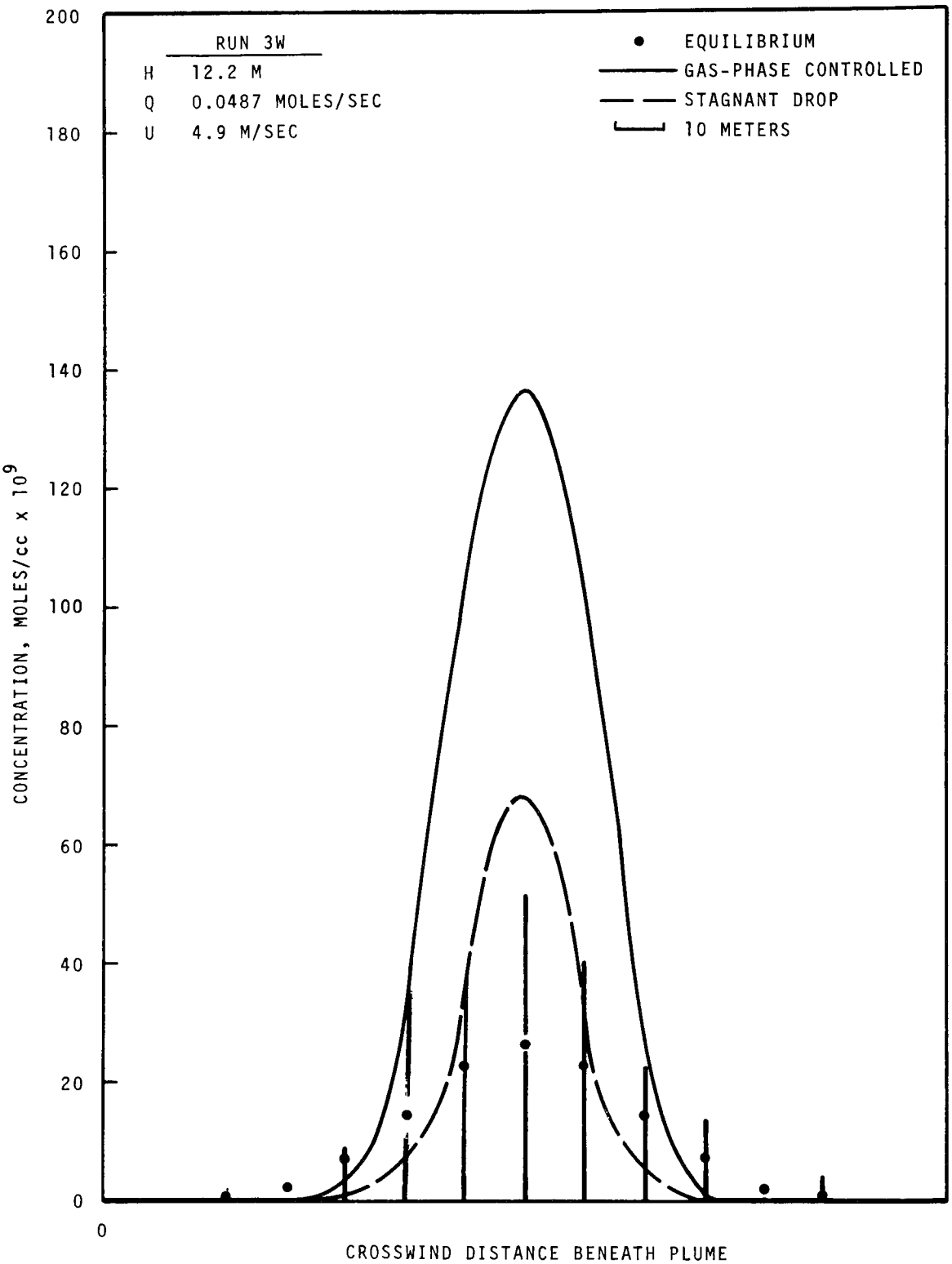

Figure C.6 Predictions of Nonlinear Model for Run 3W

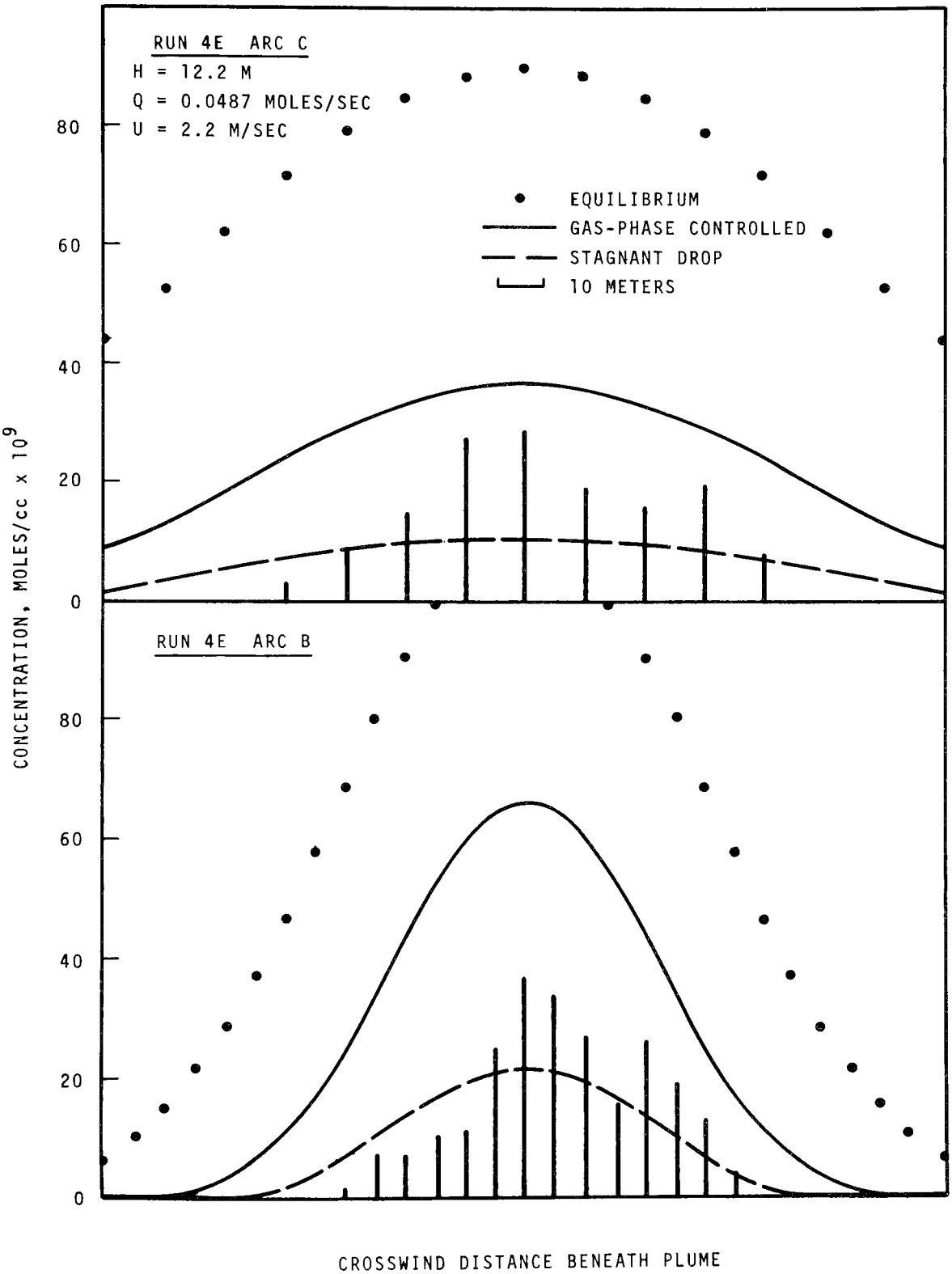

Figure C.7 Predictions of Nonlinear Model for Run 4E

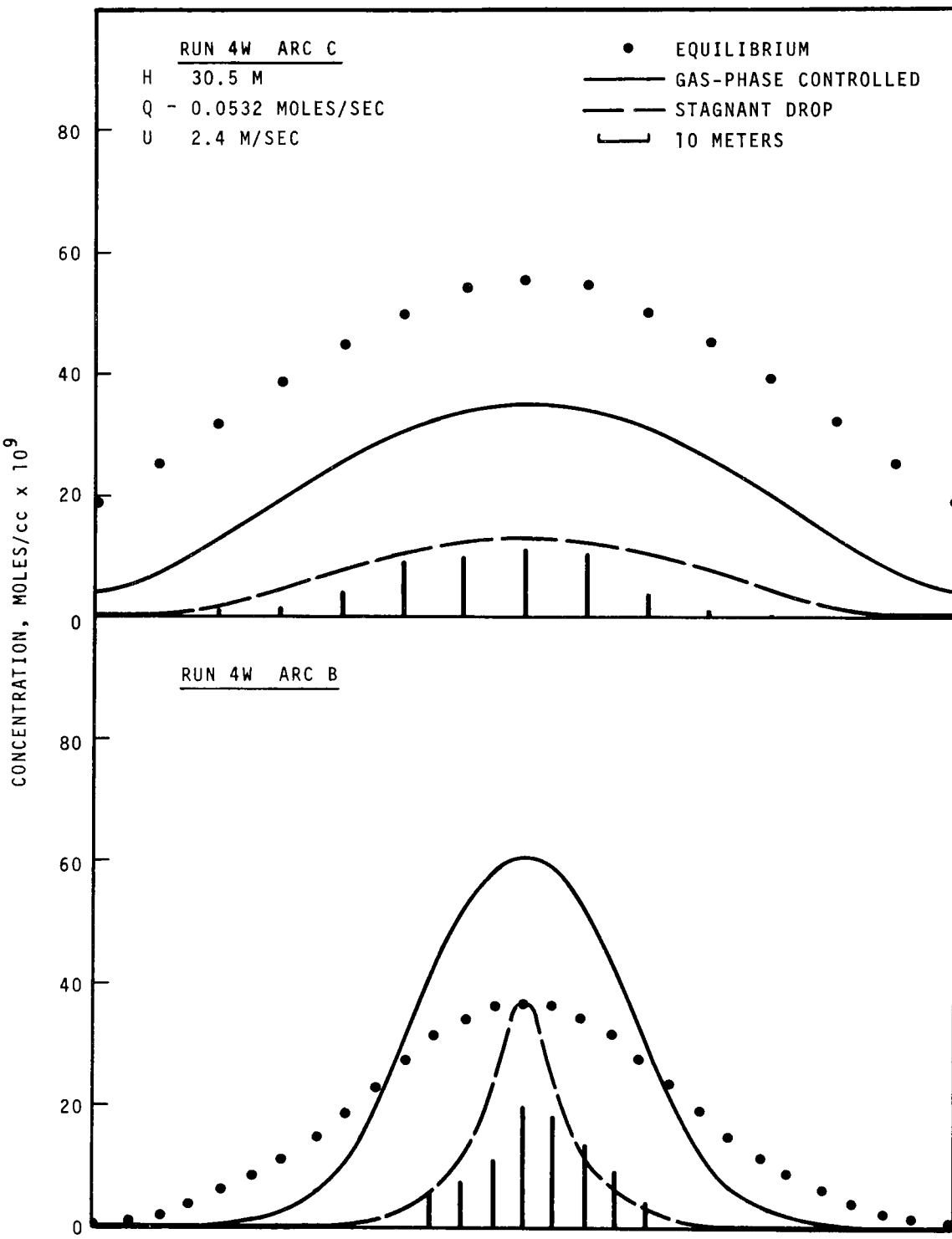

Figure C.8 Predictions of Nonlinear Model for Run 4W

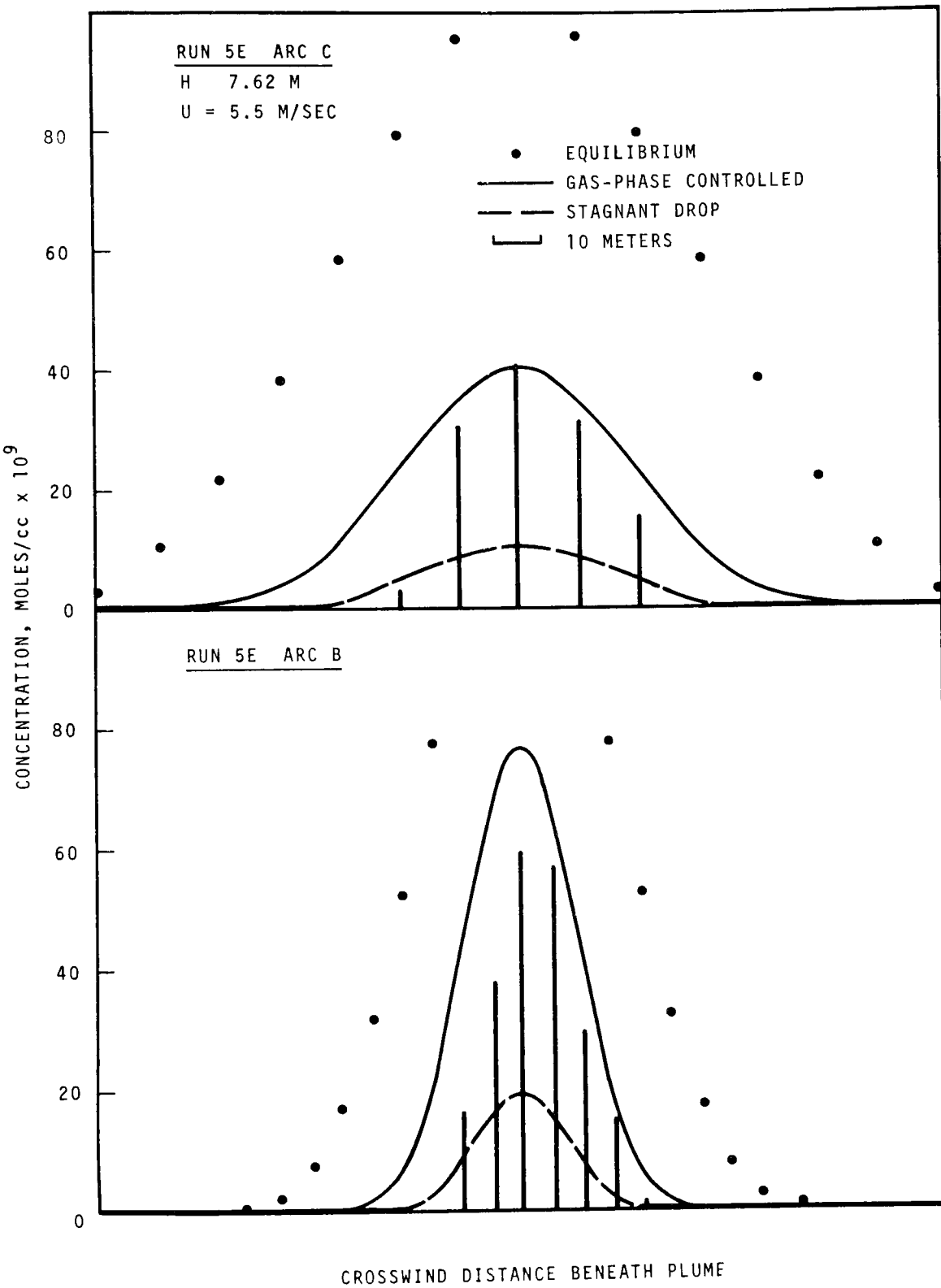

Figure C.9 Predictions of Nonlinear Model for Run 5E

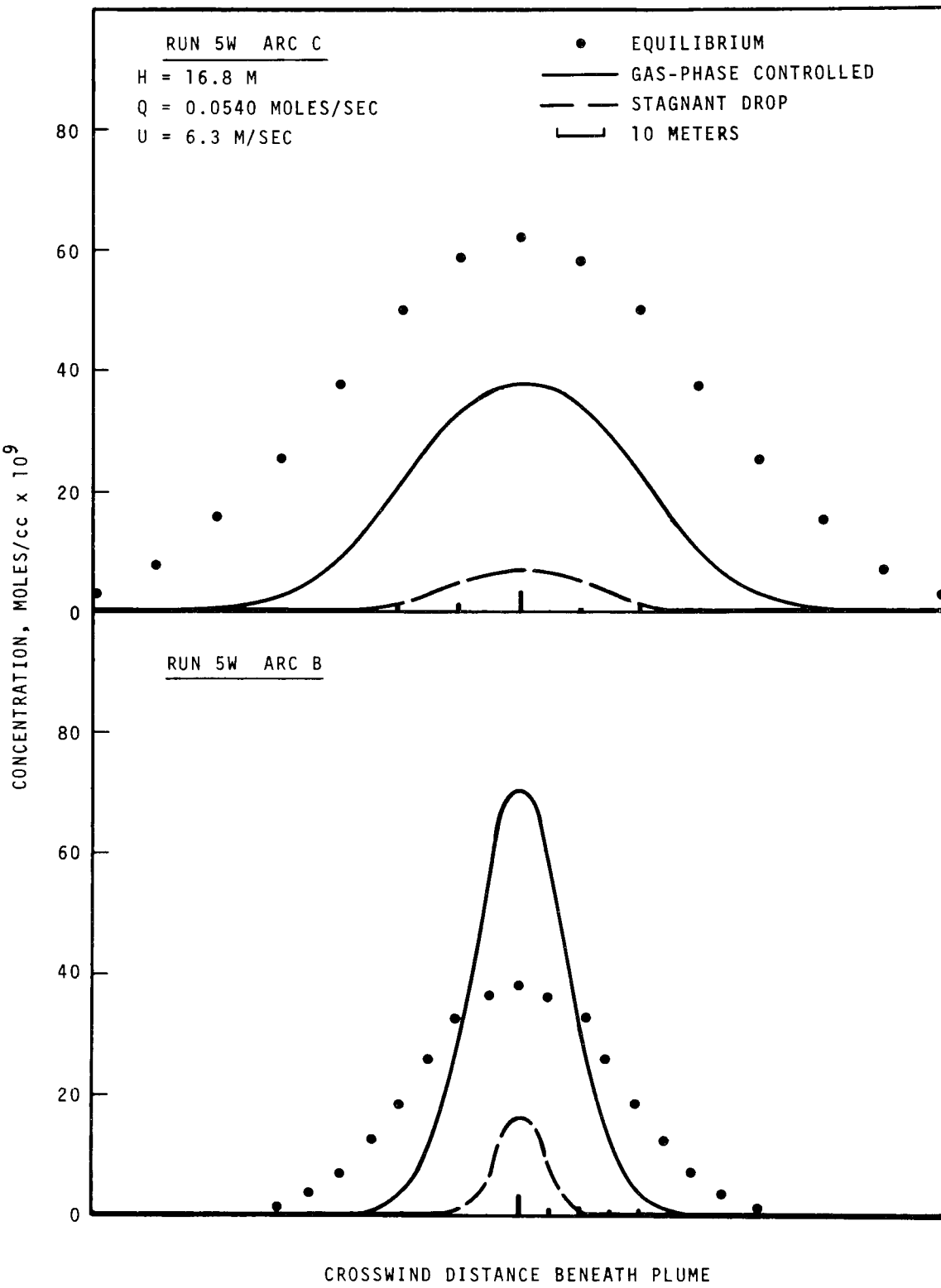

Figure C.10 Predictions of Nonlinear Model for Run 5W

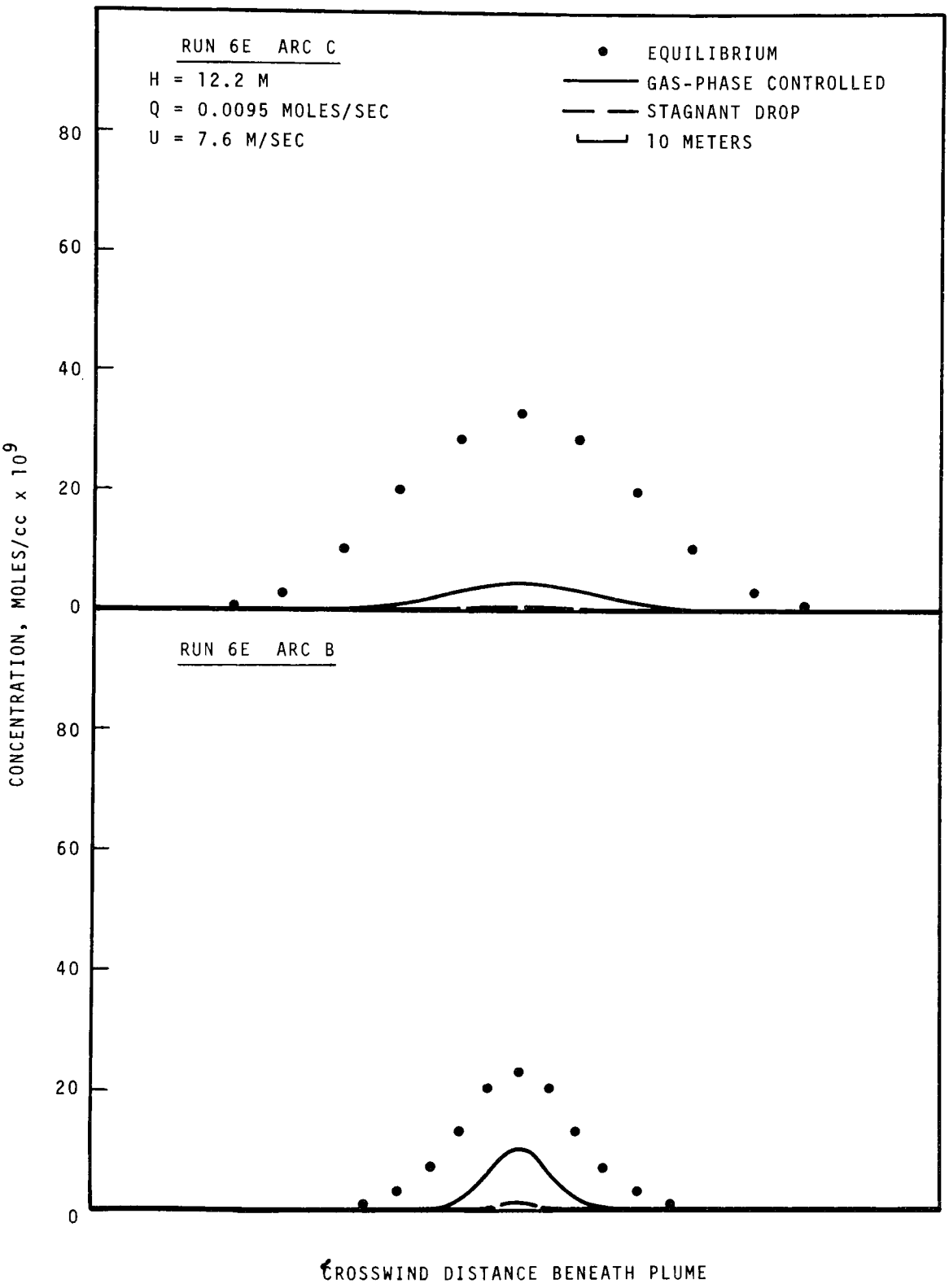

Figure C.11 Predictions of Nonlinear Model for Run 6E

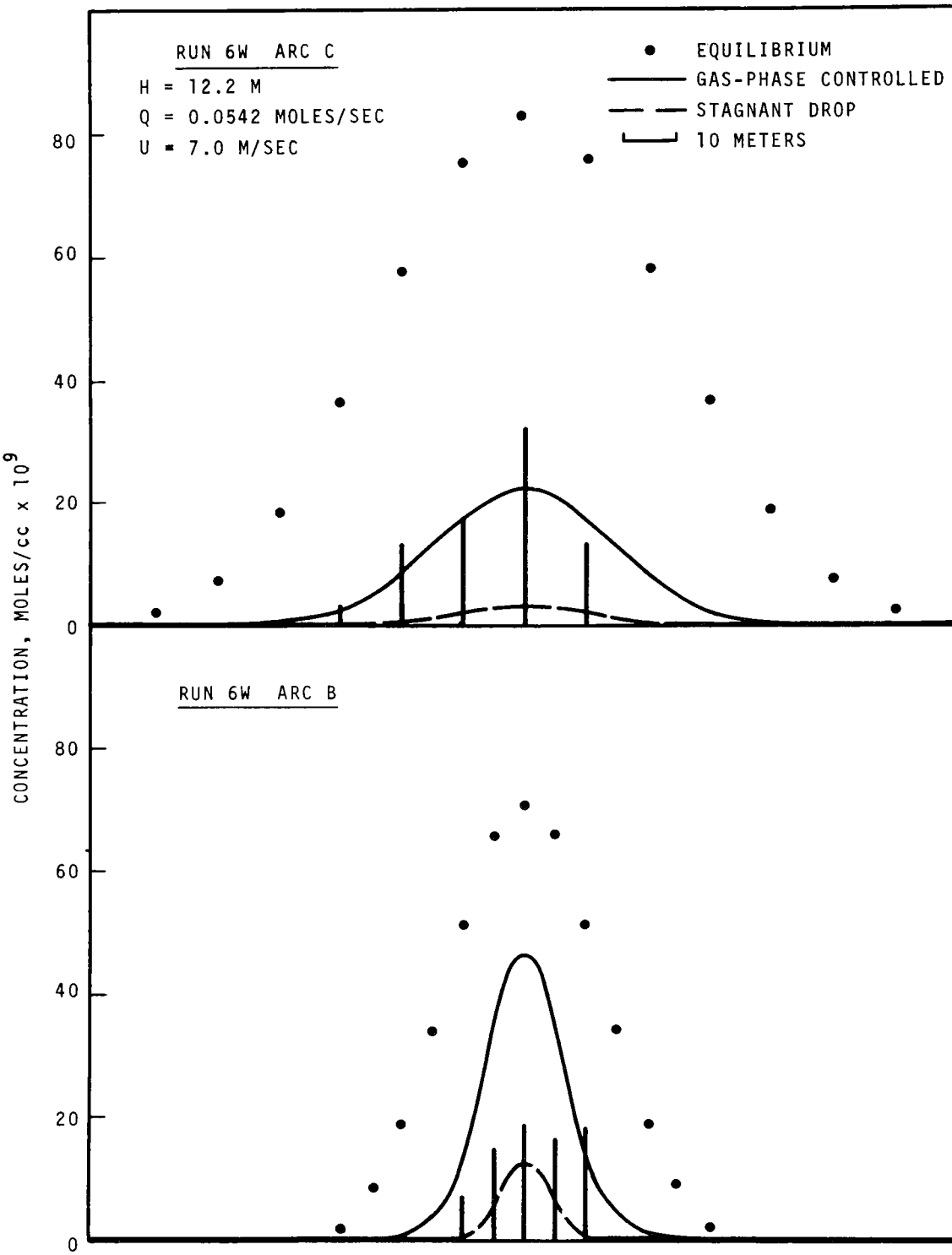

Figure C.12 Predictions of Nonlinear Model for Run 6W

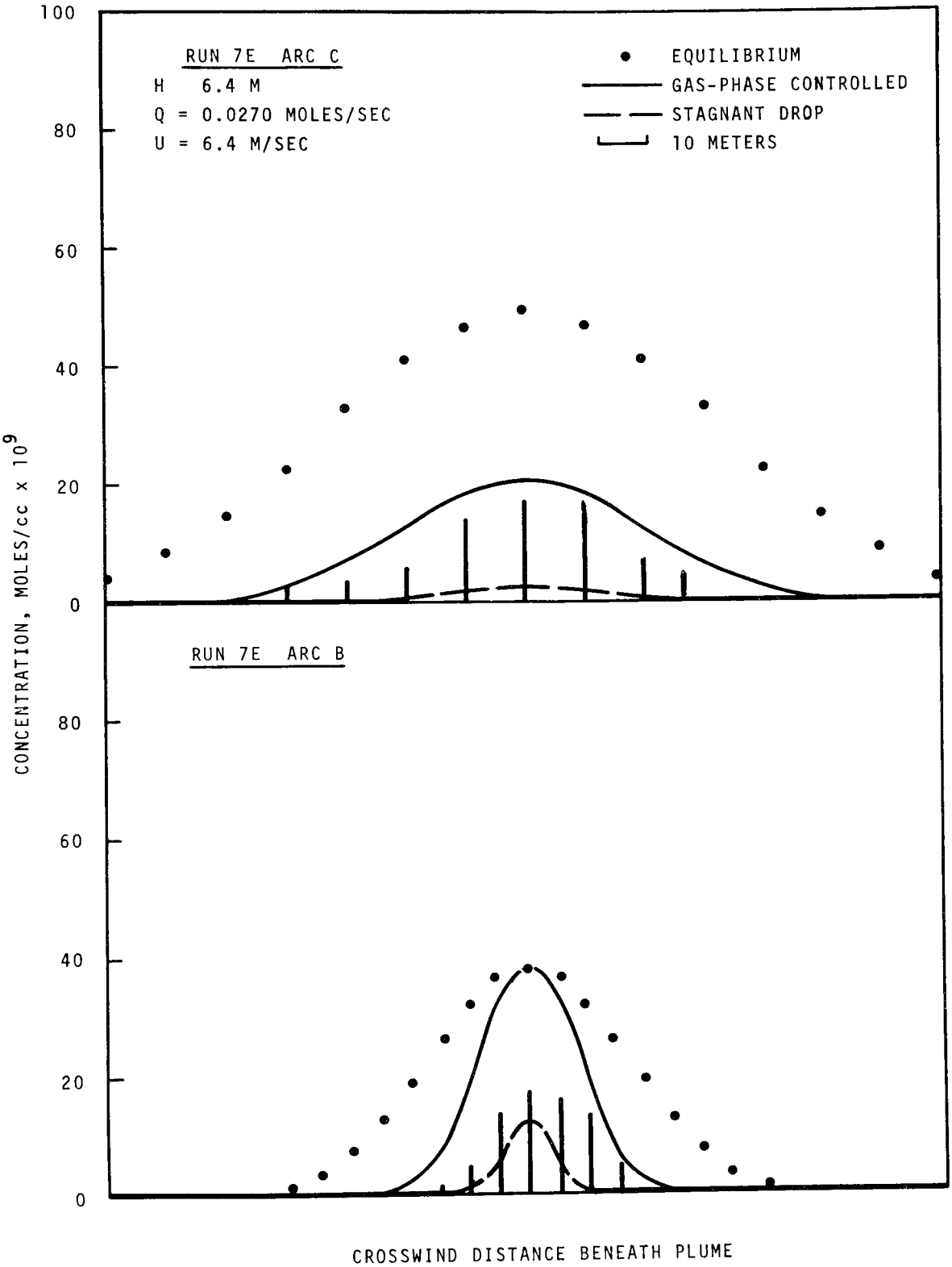

Figure C.13 Predictions of Nonlinear Model for Run 7E

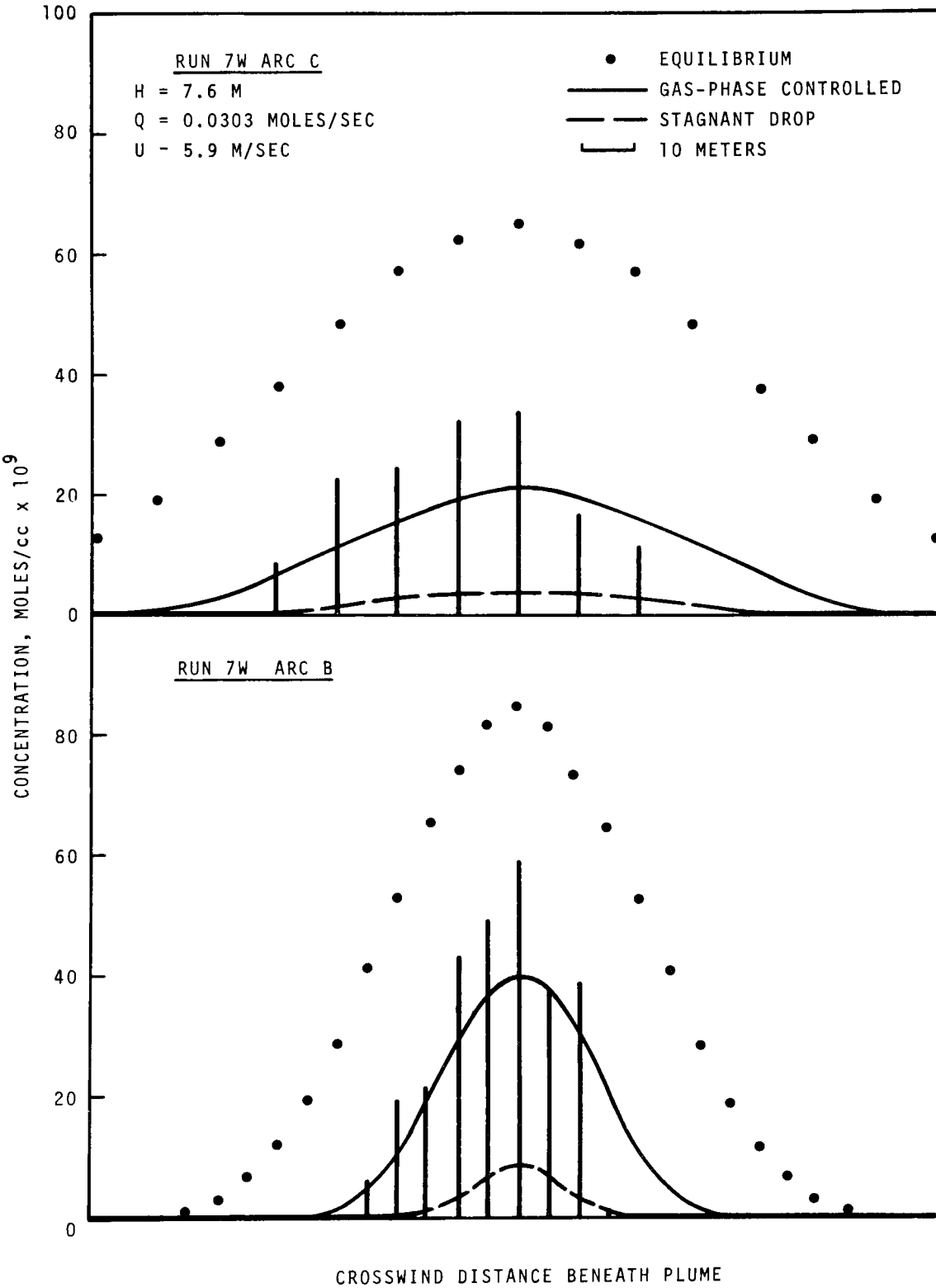

Figure C.14 Predictions of Nonlinear Model for Run 7W

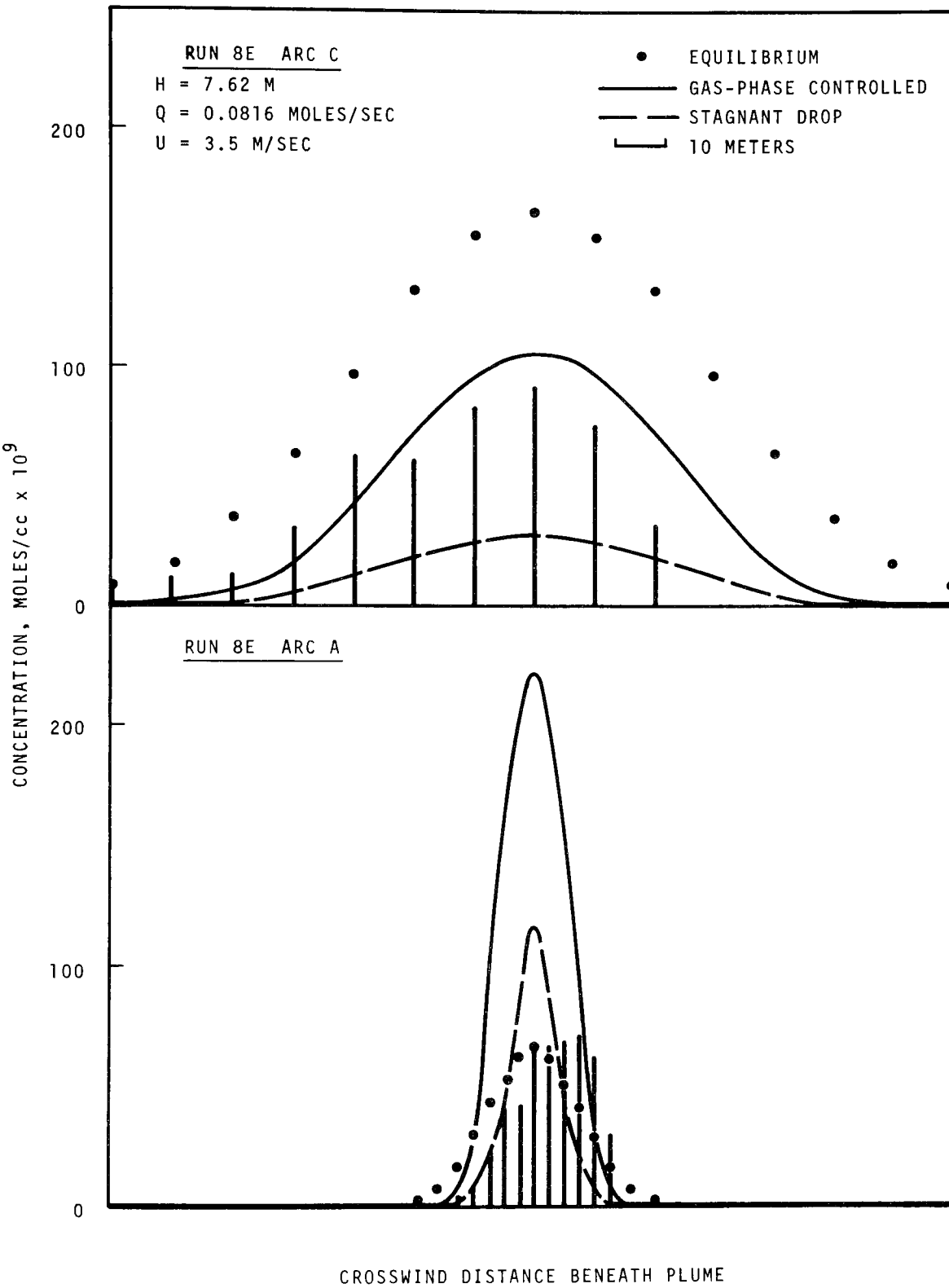

Figure C.15 Predictions of Nonlinear Model for Run 8E

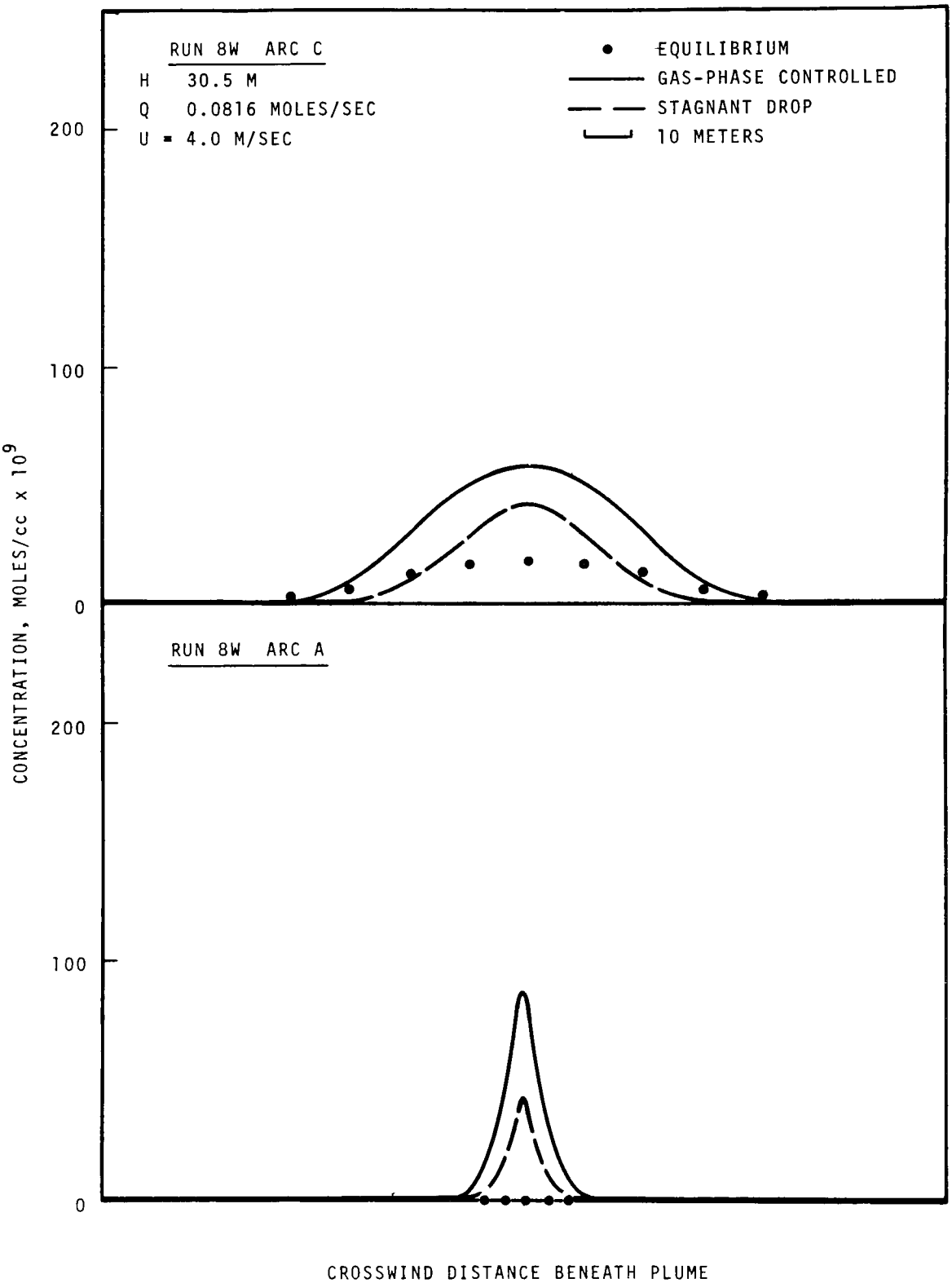

Figure C.16 Predictions of Nonlinear Model for Run 8W

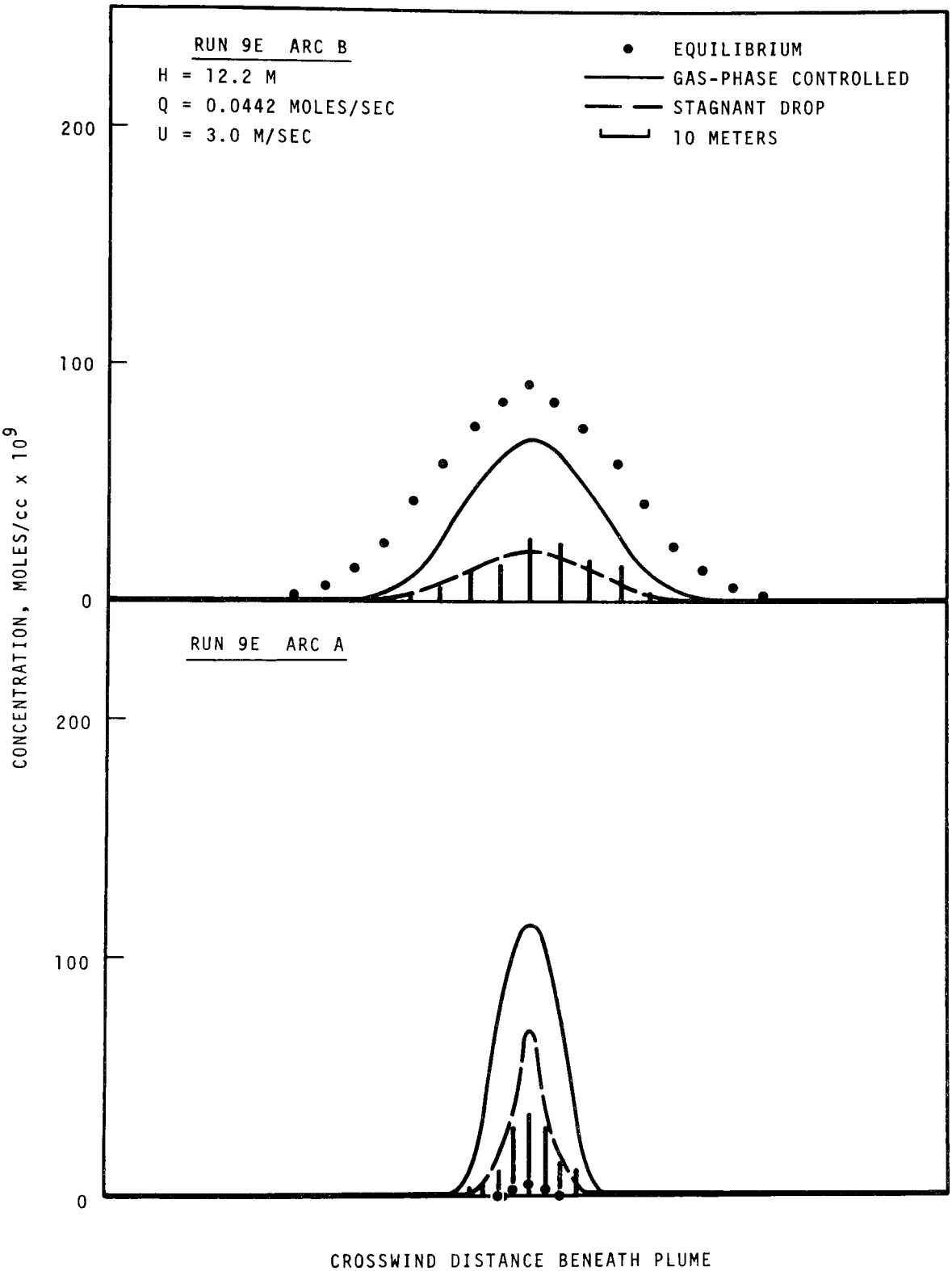

Figure C.17 Predictions of Nonlinear Model for Run 9E

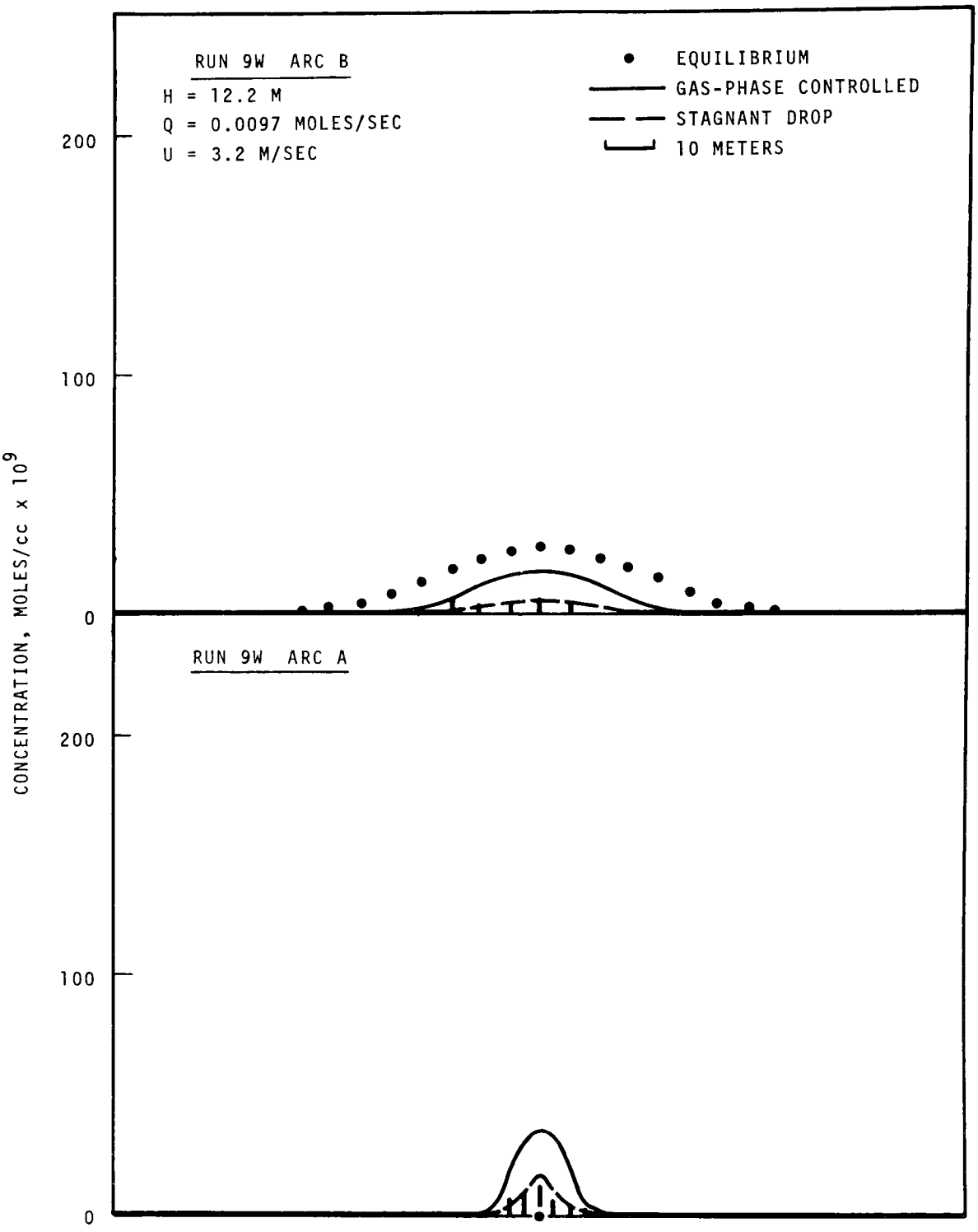

Figure C.18 Predictions of Nonlinear Model for Run 9W